Oklahoma Department of Transportation
200 NE 21st Street, Oklahoma City, OK 73105-3204

FINAL REPORT ~ FHWA-OK-14-14

3D LASER IMAGING FOR ODOT INTERSTATE NETWORK AT TRUE 1-MM RESOLUTION

Kelvin C.P. Wang, Ph.D., P.E.
Joshua Q. Li, Ph.D.
School of Civil and Environmental Engineering
College of Engineering, Architecture and Technology
Oklahoma State University

December 2014

Oklahoma Department of Transportation

3D LASER IMAGING FOR ODOT INTERSTATE NETWORK AT TRUE1-MM RESOLUTION

FINAL REPORT ~ FHWA-OK-14-14
ODOT SP&R ITEM NUMBER 2251

Submitted to:
John R. Bowman, P.E.
Director of Capital Programs
Oklahoma Department of Transportation

Submitted by:

Kelvin C.P. Wang, Ph.D., P.E.
Joshua Q. Li, Ph.D.
School of Civil and Environmental Engineering
Oklahoma State University

TECHNICAL REPORT DOCUMENTATION PAGE

1. REPORT NO.	2. GOVERNMENT ACCESSION NO.	3. RECIPIENT'S CATALOG NO.
FHWA-OK-14-14		

4. TITLE AND SUBTITLE	5. REPORT DATE
3D Laser Imaging for ODOT Interstate Network at True 1-MM Resolution	Dec 2014
	6. PERFORMING ORGANIZATION CODE
7. AUTHOR(S)	8. PERFORMING ORGANIZATION REPORT
Kelvin C.P. Wang and Joshua Q. Li	
9. PERFORMING ORGANIZATION NAME AND ADDRESS	10. WORK UNIT NO.
Oklahoma State University; 207 Engineering South, Stillwater OK 74078	
	11. CONTRACT OR GRANT NO.
	ODOT SP&R Item Number 2251
12. SPONSORING AGENCY NAME AND ADDRESS	13. TYPE OF REPORT AND PERIOD COVERED
Oklahoma Department of Transportation Materials and Research Division 200 N.E. 21st Street, Room 3A7 Oklahoma City, OK 73105	Final Report Oct 2012 - Sep 2014
	14. SPONSORING AGENCY CODE

15. SUPPLEMENTARY NOTES

16. ABSTRACT

With the development of 3D laser imaging technology, the latest iteration of PaveVision3D Ultra can obtain true 1mm resolution 3D data at full-lane coverage in all three directions at highway speed up to 60MPH. This project provides rapid survey using PaveVision3D Ultra for the ODOT interstate highways and SH-51 from I-35 to Sand Springs with approximately 1,280 center miles of pavement. With sophisticated Automated Distress Analyzer 3D (ADA-3D) software interface, the collected 1mm 3D data provide ODOT solutions for automated evaluation of pavement surface including longitudinal profile for roughness, transverse profile for rutting, predicted hydroplaning speed for safety analysis, and cracking and various surface defects for distresses. The Pruned Exact Linear Time (PELT) method, an optimal partitioning algorithm, is implemented to identify change points and dynamically determine homogeneous segments so as to assist DOT effectively using the available 1mm 3D pavement surface condition data for decision-making. The application of 3D 1mm laser imaging technology for network survey is unprecedented. This innovative technology allows highway agencies to use the 1mm 3D system for design and management purposes, particularly to meet the data needs for pavement management system (PMS), bridge deck evaluation without requiring field visits to individual bridges, Pavement ME Design and Highway Performance Monitoring System (HPMS).

17. KEY WORDS	18. DISTRIBUTION STATEMENT		
Laser imaging; 1MM 3D;	No restrictions. This publication is available from the Materials & Research Div., Oklahoma DOT.		
19. SECURITY CLASSIF. (OF THIS REPORT)	20. SECURITY CLASSIF. (OF THIS PAGE)	21. NO. OF PAGES	22. PRICE
Unclassified	Unclassified	151	N/A

SI* (MODERN METRIC) CONVERSION FACTORS

APPROXIMATE CONVERSIONS TO SI UNITS				
SYMBOL	**WHEN YOU KNOW**	**MULTIPLY BY**	**TO FIND**	**SYMBOL**
LENGTH				
in	inches	25.4	millimeters	mm
ft	feet	0.305	meters	m
yd	yards	0.914	meters	m
mi	miles	1.61	kilometers	km
AREA				
in^2	square inches	645.2	square millimeters	mm^2
ft^2	square feet	0.093	square meters	m^2
yd^2	square yard	0.836	square meters	m^2
ac	acres	0.405	hectares	ha
mi^2	square miles	2.59	square kilometers	km^2
VOLUME				
fl oz	fluid ounces	29.57	milliliters	mL
gal	gallons	3.785	liters	L
ft^3	cubic feet	0.028	cubic meters	m^3
yd^3	cubic yards	0.765	cubic meters	m^3
NOTE: volumes greater than 1000 L shall be shown in m^3				
MASS				
oz	ounces	28.35	grams	g
lb	pounds	0.454	kilograms	kg
T	short tons (2000 lb)	0.907	megagrams (or "metric ton")	Mg (or "t")
TEMPERATURE (exact degrees)				
^oF	Fahrenheit	5 (F-32)/9 or (F-32)/1.8	Celsius	^oC
ILLUMINATION				
fc	foot-candles	10.76	lux	lx
fl	foot-Lamberts	3.426	candela/m^2	cd/m^2
FORCE and PRESSURE or STRESS				
lbf	poundforce	4.45	newtons	N
lbf/in^2	poundforce per square inch	6.89	kilopascals	kPa

APPROXIMATE CONVERSIONS FROM SI UNITS				
SYMBOL	**WHEN YOU KNOW**	**MULTIPLY BY**	**TO FIND**	**SYMBOL**
LENGTH				
mm	millimeters	0.039	inches	in
m	meters	3.28	feet	ft
m	meters	1.09	yards	yd
km	kilometers	0.621	miles	mi
AREA				
mm^2	square millimeters	0.0016	square inches	in^2
m^2	square meters	10.764	square feet	ft^2
m^2	square meters	1.195	square yards	yd^2
ha	hectares	2.47	acres	ac
km^2	square kilometers	0.386	square miles	mi^2
VOLUME				
mL	milliliters	0.034	fluid ounces	fl oz
L	liters	0.264	gallons	gal
m^3	cubic meters	35.314	cubic feet	ft^3
m^3	cubic meters	1.307	cubic yards	yd^3
MASS				
g	grams	0.035	ounces	oz
kg	kilograms	2.202	pounds	lb
Mg (or "t")	megagrams (or "metric ton")	1.103	short tons (2000 lb)	T
TEMPERATURE (exact degrees)				
^oC	Celsius	1.8C+32	Fahrenheit	^oF
ILLUMINATION				
lx	lux	0.0929	foot-candles	fc
cd/m^2	candela/m^2	0.2919	foot-Lamberts	fl
FORCE and PRESSURE or STRESS				
N	newtons	0.225	poundforce	lbf
kPa	kilopascals	0.145	poundforce per square inch	lbf/in^2

*SI is the symbol for the International System of Units. Appropriate rounding should be made to comply with Section 4 of ASTM E380. (Revised March 2003)

Table of Contents

List of Figures

List of Tables

CHAPTER 1 INTRODUCTION

1.1 Background

Accurate and timely information on pavement surface characteristics are critical for evaluating the performance, condition, and safety of pavement infrastructure. Both pavement design and pavement management rely on these and other information for comprehensive pavement evaluation. Data collection on pavement surfaces include longitudinal profile for roughness, transverse profile for rutting, macro-texture for safety, and cracking and various surface defects for distresses. Pavement data collection technologies have improved gradually in the last few decades. Particularly after steady R&D investments in pavement profile measurements since the 1980's, roughness, rutting, and macro-texture data can be inexpensively obtained at acceptable accuracy levels. However, due to sensor and computing limitations, limited research funding, and inherent difficulties to meet stringent requirements of precision and bias, the hardware and software necessary to automatically obtain pavement cracking and other distress data have not been realized. In addition, roughness, rutting, and macro-texture data are currently obtained through separate instrumentation on a relatively small area within a pavement lane.

Pavement engineering as an area of study has suffered from inadequate and poor quality distress data. High quality pavement distress data for the next-generation pavement design system, Pavement ME Design (DARWin-ME), is critically needed to facilitate the calibration of prediction models, and further

validation of relevant mechanistic models. Further, many state highway agencies have been collecting pavement distress data, particularly cracking data, for years through manual, automated, or semi-automated means. However, it is believed that such data sets are of poor quality due to problems associated with consistency, repeatability, and accuracy of collected data and subsequent analyses. Despite the need to obtain pavement distress data for both management and design purposes, progress on delivering true automated survey technology for pavement distresses has been minimal.

In addition to being slow and unsafe when conducted in the field, manual survey results show wide variability. Therefore, automation technology for pavement survey has long been sought and tested for precision and bias (Wang 2004, 2011a, and 2011b; McGhee, 2004). However, the existing operating system is based on 1-mm 2D laser images of pavement surface, which poses challenges in terms of further improving its accuracy and consistency. Cracking, along with many other pavement surface defects, all have unique and distinctive characteristics in the 3rd dimension, which are lost in 2D images. Therefore, developing new technology that can capture realistic pavement surface characteristics in the digital domain at sufficiently high resolution, or actual surface models of pavements, is a necessary step. New algorithms and software can be subsequently developed on the surface models to produce consistent, repeatable, and accurate pavement survey data.

The research team at Oklahoma State University, previously with the University of Arkansas, is recognized internationally as a leader in the automated survey of pavement infrastructure. The team has conducted research and delivered

solutions to the industry for over 15 years. In particular, the most significant development occurred in the last three years during which the team developed and implemented a 3D laser imaging sensor for pavement condition survey. With the latest PaveVision3D Ultra technology, the resolution of surface texture data in vertical direction is about 0.3 mm and in the longitudinal direction is approximately 1 mm at 60MPH data collection speed. With the high power line laser projection system and custom optic filters, the 3D system can work at highway speed during daytime and nighttime and maintain image quality and consistency. Pavement surface data gathered at this speed and 1mm resolution provide engineers advantages in both visualization and analysis, and this capability is not available anywhere else.

1.2 Proposal Tasks

The primary objectives of this research project are:

- generating geographically true and complete pavement surfaces or virtual pavement surfaces with an Inertial Measurement Unit (IMU) at 1mm resolution for the ODOT interstate network and SH 51 from I-35 to Sand Springs (about 70 centerline miles);
- providing ODOT solutions for automated evaluation of pavement surface including cracking, rutting, and pavement macro-texture, cross-slope, and roadway geometric data for safety analysis;
- providing ODOT workstation with multiple monitors and software programs for providing the solutions.

1.3 Report Organization

Chapter 1 provides an introduction to automatic distress data collection systems and outlines the project tasks to be completed.

Chapter 2 overviews current 3D data collection techniques. In particular, the PaveVision3D Ultra system which is capable of collecting pavement surface data at 1mm resolution at highway speeds for various surface data analysis. PaveVision3D Ultra is used to collect and analyze data for this project.

Chapter 3 presents the provisional approved AASHTO Designation PP67-10 *Quantifying Cracks in Asphalt Pavement Surfaces from Collected Images Utilizing Automated Methods* (PP67-10 for short) for quantifying cracking distress at the network level and the Automated Distress Analyzer 3D (ADA-3D) software, one of the software tools equipped with PaveVision3D Ultra, for data analysis and report.

Chapter 4 introduces the inertial profiling system using the implemented 1mm 3D sensors and high accuracy digital accelerometers. Filtering algorithms and analytical results are provided.

Chapter 5 integrates the real-time 1mm PaveVision3D Ultra surface data and high precision IMU data into potential hydroplaning speed prediction model. Hydroplaning hazardous locations can be therefore identified so that pavement engineers may take remedy measures to increase the potential hydroplaning speed and minimize potential traffic accident.

Chapter 6 presents the usage of PaveVision3D Ultra for in-production highway network survey in ODOT. Pavement surface cracking, rutting, roughness in

term of IRI, and predicted hydroplaning speed for each 0.1-mile section are generated with ADA-3D. The Pruned Exact Linear Time (PELT) method, an optimal partitioning algorithm with a pruning step to reduce the computational cost, is applied to identify change points and determine homogeneous segments based on the calculated performance indicators.

Chapter 7 outlines other potential applications of PaveVision3D in bridge deck surface evaluation, Pavement ME Design and Highway Performance Monitoring Systems (HPMS).

Chapter 8 presents the conclusions and future research recommendations.

CHAPTER 2 PAVEVISION3D ULTRA SYSTEM

2.1 3D Data Collection Techniques

3D surface features of pavements have been studied closely for years for various data analysis needs. However, true 3D surface measurements of pavements obtained for computer analysis at high resolution and at highway speed were difficult to obtain. Rather, 2D images have been used by pavement engineers to estimate pavement distress, with less than desirable results. Therefore it is critical to better understand the pavement surface in its original format, or a 3D representation.

There are several techniques to collect 3D surface data. A conventional method is based on the photogrammetric principle, widely used in highway engineering dating to the use of analog film. The NCHRP IDEA program funded the team to use photogrammetric principle to establish 3D pavement surfaces in the project “Automated Pavement Distress Survey through Stereovision” (Wang, 2004). The research produced good results. However, a limitation of this technique is the lighting requirement for the pavement surface. The illumination of a pavement surface to the required intensity level under direct sunlight is nearly impossible, which is required for photogrammetric image acquisition. Figure 2.1 illustrates the photogrammetric principle used in the NCHRP research and the resulting software to match a pair of 2D images with common points to generate a 3D surface model of pavement.

Another technique for 3D surface modeling is Light Detection And Ranging (LIDAR), which was initially used to geo-reference terrain features. In some literature LIDAR is referred to as laser altimetry. A LIDAR system shown in Figure 2.2(a) is

composed of a laser scanning system, global positioning system (GPS), and an inertial measuring unit (IMU). The laser scan data is collected using a scanning mirror that rotates transverse to the direction of motion. LIDAR signal is not a point but rather is an area beam. The beam is very narrow, but it does get larger as it moves away from the source. Moreover, it also becomes distorted, taking on an ellipsoidal shape, as it travels along the scan (Burtch, 2002). Based on LIDAR principle, Figure 2.2(b) shows a rotating laser system for pavement survey developed in the 1990's by Phoenix Scientific (Herr, 2001 and 2009). Due to difficulties in making significant improvements to the resolution of the system, its usage has been limited.

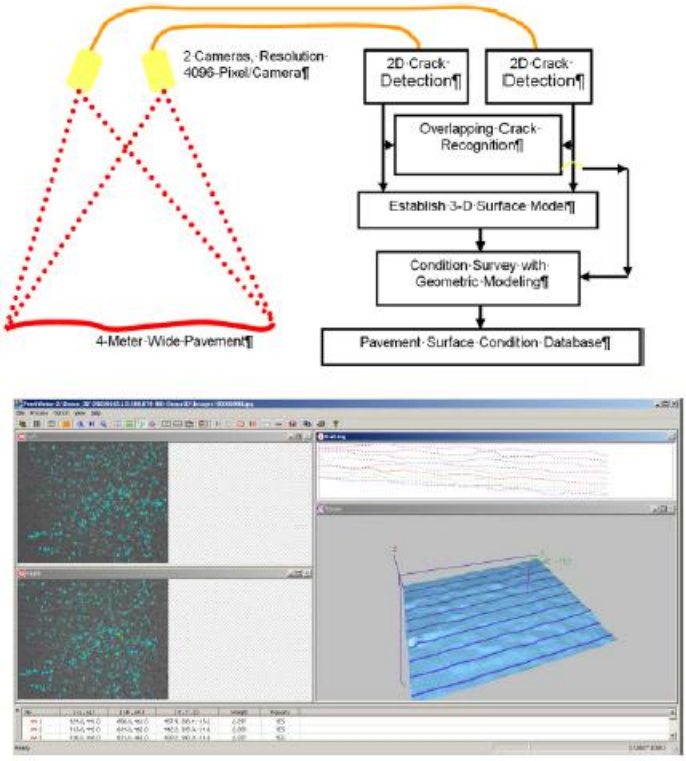

Figure 2.1 Stereovision and 3-D reconstruction (Wang, 2004)

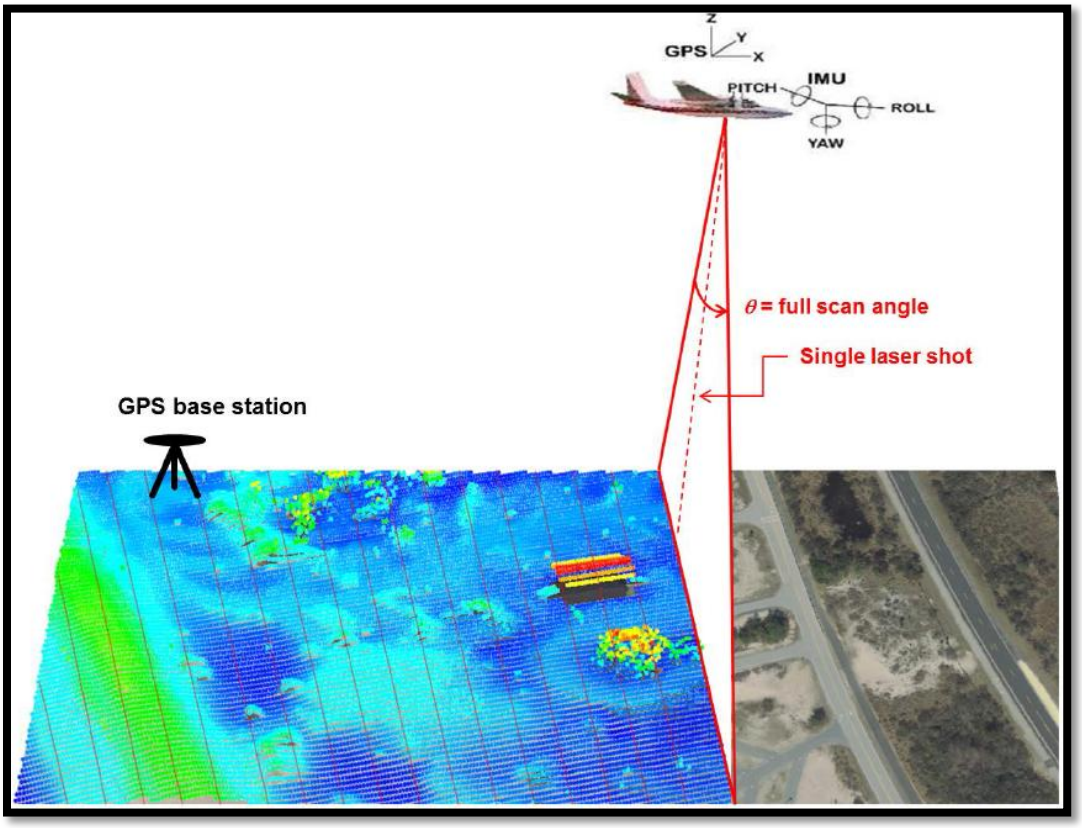

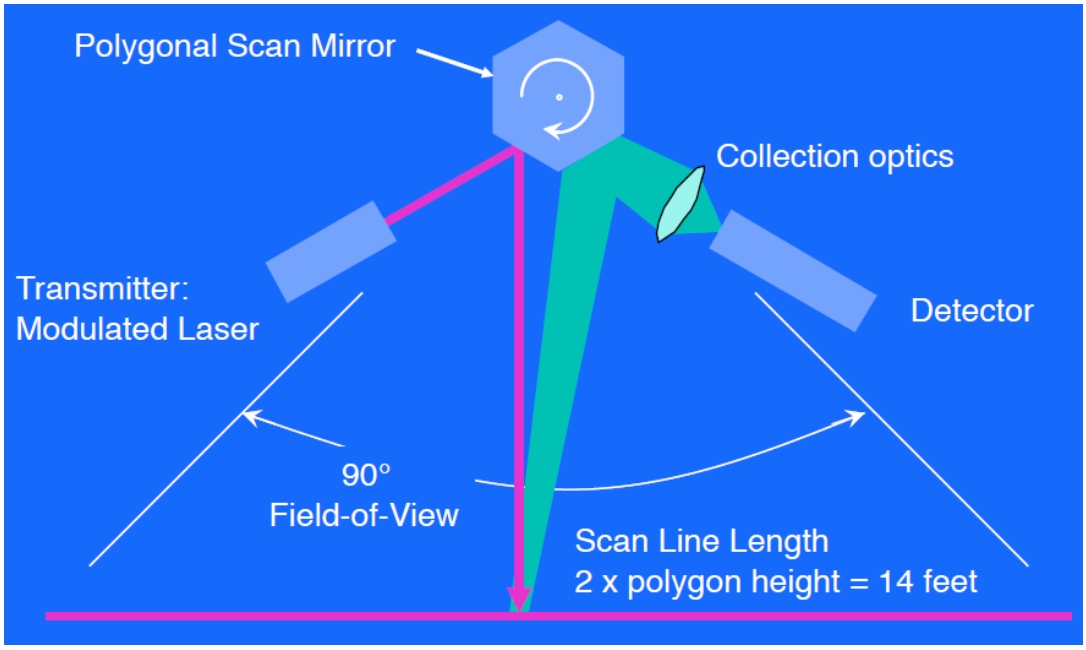

Figure 2.2 LIDAR (NOAA 2012) and Rotating Laser System (Herr 2001)

2.2 PaveVision3D Ultra System

2.2.1 Overview

The PaveVision3D Ultra (3D Ultra for short) laser imaging system has been evolved into a sophisticated system to conduct full lane data collection on roadways at highway speed up to 60mph (about 100 km/h) (Wang 2011a). The resolution of surface texture data in the vertical direction is about 0.3 mm and in the longitudinal direction is approximately 1 mm at data collection speed of 60 mph. 3D Ultra is able to acquire both 3D laser imaging intensity and range data from pavement surface through two separate sets of sensors. Recently, two 3D high resolution digital accelerometers have been installed on the system, capable of reporting compensated pavement surface profile and generating roughness indices. The collected data are saved by image frames with the dimension of 2, 048 mm in length and 4, 096 mm in width. In summary, the 1mm 3D pavement surface data can be used for:

- Comprehensive evaluation of surface distresses: automatic and interactive cracking detection and classification based on various cracking protocols;
- Profiling: transverse for rutting and longitudinal for roughness (Boeing Bump Index and IRI);
- Safety analysis including macro-texture in term of mean profile depth (MPD) and mean texture depth (MTD), hydroplaning prediction, and grooving identification and evaluation;

- Roadway geometry including horizontal curve, longitudinal grade and cross slope.

Figure 2.3 Digital Highway Data Vehicle (DHDV) with PaveVision3D Ultra

2.2.2 Hardware System

With the high power line laser projection system and custom optic filters, DHDV can work at highway speed during daytime and nighttime and maintain image quality and consistency. 3D Ultra is the latest imaging sensor technology that is able to acquire both 2D and 3D laser imaging data from pavement surface through two separate left and right sensors. Each sensor in the rear of the vehicle consists of two lasers and five special-function cameras. For the two lasers, one is for providing 2D visual illumination and the other one is for providing the 3D data illumination. For the five cameras, four cameras are for capturing 3D laser illumination and the other one is for capturing 2D laser illumination. The camera and laser working principle is shown in Figure 2.4.

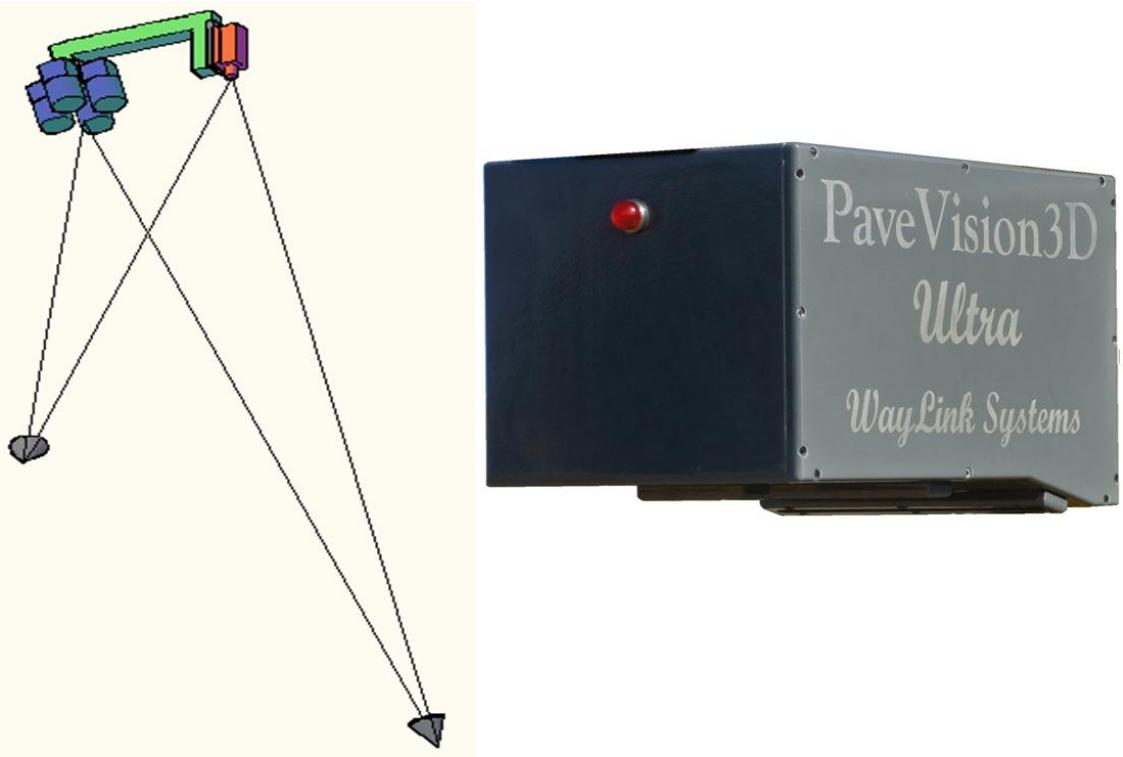

Figure 2.4 Laser Imaging Principle

In addition to the 3D camera sensors, the positioning data collections including precision gyro, high-frequency differential GPS receiver, Distance Measurement Instrument, and Inertial Measurement Unit (IMU) are incorporated into the 3D Ultra to ensure high geographic accuracy. An IMU is an electronic device that measures and reports on velocity, orientation, and gravitational forces, using a combination of accelerometers and gyroscopes. An IMU allows a GPS to work when GPS-signals are unavailable, such as in tunnels, inside buildings, or when electronic interference is present. IMUs work, in part, by detecting changes in pitch, roll, and yaw (as shown in Figure 2.5), which can be used to determine pavement geometric parameters such as horizontal curves, longitudinal grade, and cross slope. The IMU can provide a refresh rate of 100Hz.

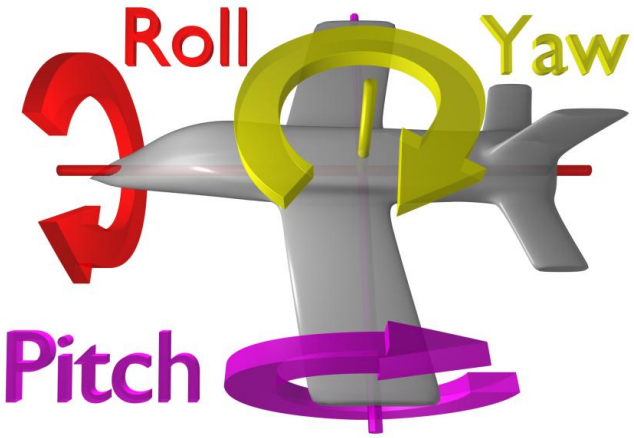

Figure 2.5 IMU Working Principle

2.2.3 Software System

The 3D Ultra system installs two key software applications: the 3D Automated Distress Analyzer (ADA-3D) and the Multimedia based Highway Information System (MHIS).

ADA-3D is the automatic cracking analyzing tool. By implanting the sophisticated algorithms, ADA-3D is currently capable of conducting automated cracking, rutting, roughness, and texture analyses at 1 mm resolution at highway speed. ADA3D also allows users to perform semi-automated distress analysis. Different protocols are coded in ADA-3D, whose operating interface is shown in Figure 2.6.

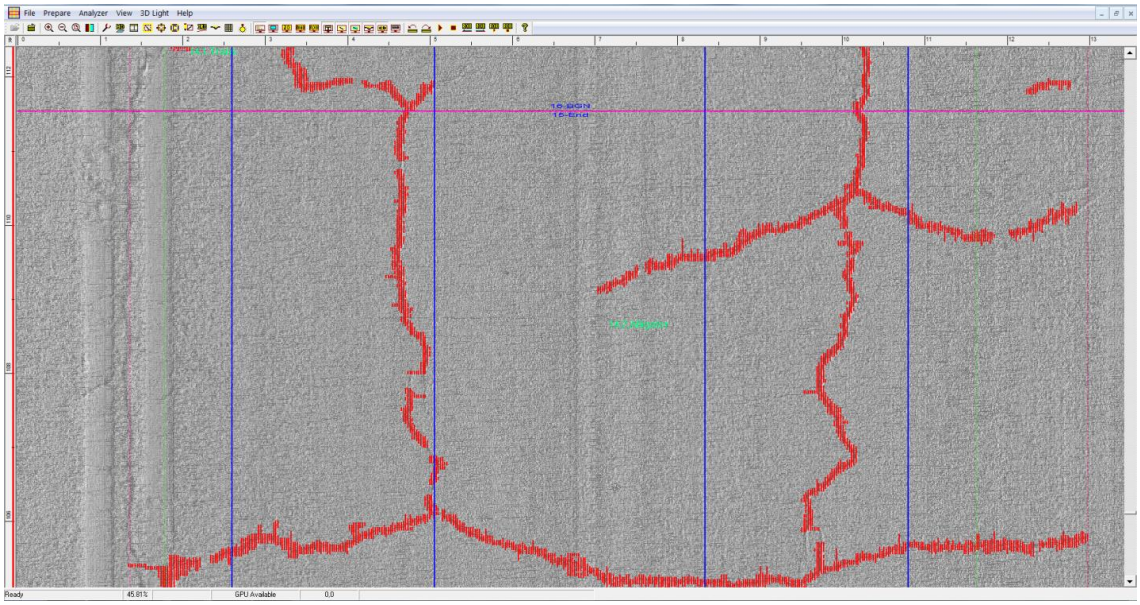

Figure 2.6 Operating Interface of ADA3D

MHIS-3D Deluxe is a comprehensive application interface to view the collected data sets collected and the automatic processed cracking data. It provides the user with a 2D and 3D graphical representation of all the data sets collected using 3D Ultra data collection vehicle. These data sets, which are accessed and organized by MHIS-3D Deluxe, include Pavement Vision 3D images, Right-of-Way images, DMI and GPS readings. MHIS-3D Deluxe provides a geo-referenced map to access multiple DHDV data collections for a certain region as shown in Figure 2.6. MHIS-3D Deluxe displays the distresses detected by ADA-2D and ADA-3D by default. The distress affected area can also be marked manually on the pavement images with provided manual rating tools. MHIS does not analyze the distress itself; instead, it is a tool to visualize and play the 3D, 2D, and ROW images. The user's markings as input are processed and integrated into the DHDV database through

MHIS-3D Deluxe. Distress indices, such as AASHTO protocol, World Bank's CI and UK SCANNER can also be produced in the MHIS-3D.

Figure 2.7 shows the overall user interface of MHIS-3D Deluxe. Each sub-window in MHIS-3D Deluxe is an MHIS Frame. An example of 3D pavement surface image from MHIS is illustrated in Figure 2.8.

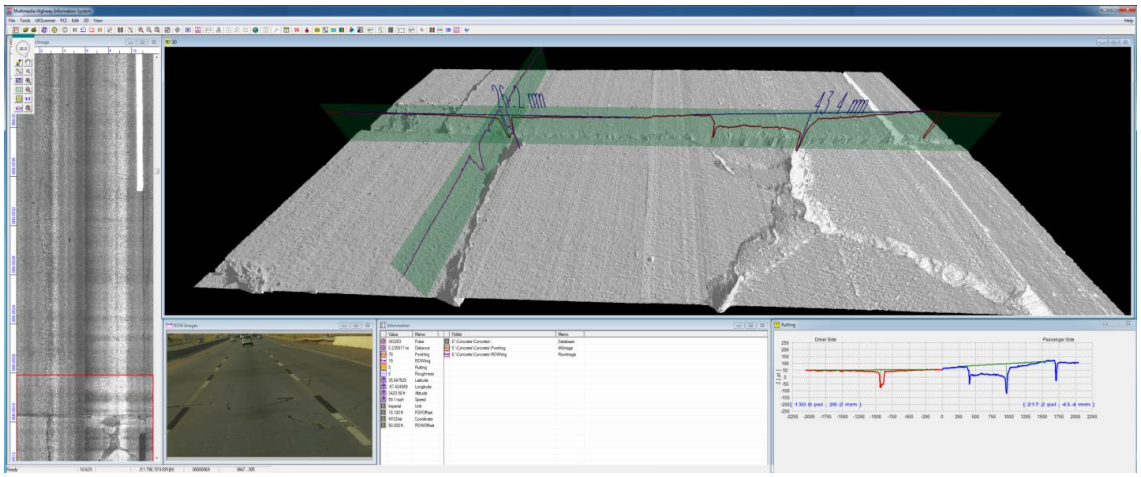

Figure 2.7 MHIS-3D Interface

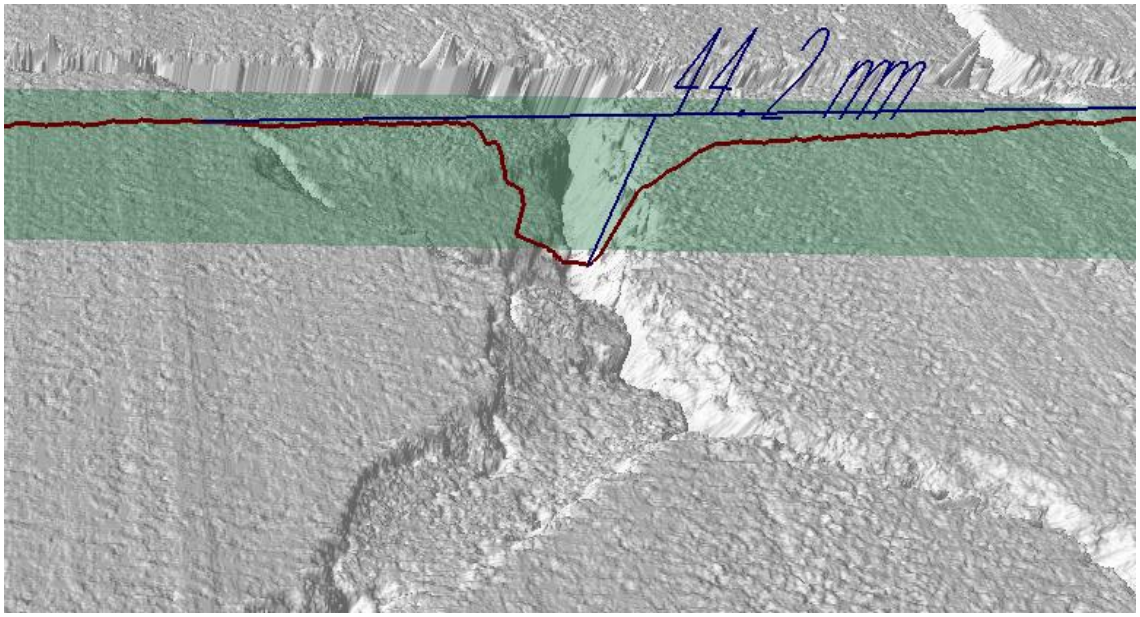

Figure 2.8 Example 1mm 3D Data at 60mph on I-35

2.2.4 3D Ultra System Calibration

To obtain high quality accurate data, the 3D Ultra system must be calibrated if it is running for the first time or the positions of one or more cameras are changed. 3D height and flatness calibration, 3D sensor alignment, 2D and 3D offset adjustment should be performed in sequences before running the system.

2.3 PaveVision3D Ultra Data

3D Ultra system simultaneously takes 2D, 3D, and ROW images at 1mm resolution. Both 2D and 3D images have 4,096 pixels transversely and 2,048 pixels longitudinally at 1mm resolution. Mathematically, each image is a matrix with 2,048 rows and 4,096 columns.

2.3.1 3D Data

For 3D images, the values of the elements in the matrix can be used to express two different types of information. The first type is the relative elevations or namely, heights of the pavement surface. Each value represents the height of a point on the surface. The values are pavement information on the vertical direction. Each pixel represents 0.3 mm. This information is used for roughness, texture, and rutting analysis.

2.3.2 2D Data

2D images were the predominant approach to analyze cracking before the emerging of 3D technology. However, as the values of the elements in the 2D image matrix only represent the intensity information of the pavement surface, it is barely

useful for pavement rutting and roughness analysis. However, it is useful for lane marking detection.

2.3.3 Right of Way Data

Right of Way (ROW) data are recorded by a video camera mounted at the front of the van, which may include the traveled lane, lane marking, and the shoulder, the guardrail, the median, the signage, the drainage systems, and landscapes within the right of way limit. The ROW data do not directly use for pavement distress analysis. However, it is an effective tool to rapidly and intuitively view the pavement section that is being inspected. An overall condition can be obtained from the ROW data. In addition, the configurations of the traveled lanes as well as other transportation assets such as signage can be obtained via the ROW data.

2.3.4 Data Structure

The PaveVision3D Ultra data for each pavement section are stored in one folder. Inside of each folder, the same data structures are used including the following files:

- Sub-file folder “3DData”: used for 3-D images storage;
- Sub-file folder “PvmtImg”: used for 2-D images storage;
- Sub-file folder “ROWImg”: used for 2-D Right-Of-Way images storage;
- Sub-file folder "Result": used for automated distress analyzing results;
- “Alignment.seq”: the alignment file used for camera alignment;
- “Calibration.cal": used for camera calibration; and

- “WisInfoIdx”: the access database file which contains the data collection information. This database file will be used for the data viewing software MHIS.

CHAPTER 3 NEW AASHTO RUTTING AND CRACKING PROTOCOLS

3.1 Relevant Terminologies

Recently, AASHTO published the provisional approved AASHTO Designation PP67-10 (2013a) *Quantifying Cracks in Asphalt Pavement Surfaces from Collected Images Utilizing Automated Methods* (PP67-10 for short) for quantifying cracking distress at the network level and Designation PP69-10 (2013b) *Standard Practice for Determining Pavement Deformation Parameters and Cross Slope from Collected Transverse Profiles* (PP69-10 for short) for rutting characterization and cross slope measurements. To develop cracking and deformation parameters from the collected pavement images and transverse profiles, basic and relevant terminologies are defined in the protocols.

- Lane: The pavement surface between inside edges of inside (left) and outside (right) lane markings. If the lane marking is absent, an equivalent portion of the surface is accounted.
- Centerline: The centerline is a fictive line located at the middle of the lane which is parallel to the lane markings.
- Wheel-path: There are two wheel-paths on each lane. A wheel-path is a longitudinal strip of the pavement 0.75 m (30 in.) wide. The inside (left) wheel-path is centered 0.875m (35 in.) from the centerline towards the adjacent lane (left) and outside wheel-path is centered 0.875m (35 in.) from the centerline towards the should (right).

The identification of the wheel-path is the foundation of data process using the protocols. The generation of many parameters is based on the location of wheel-path.

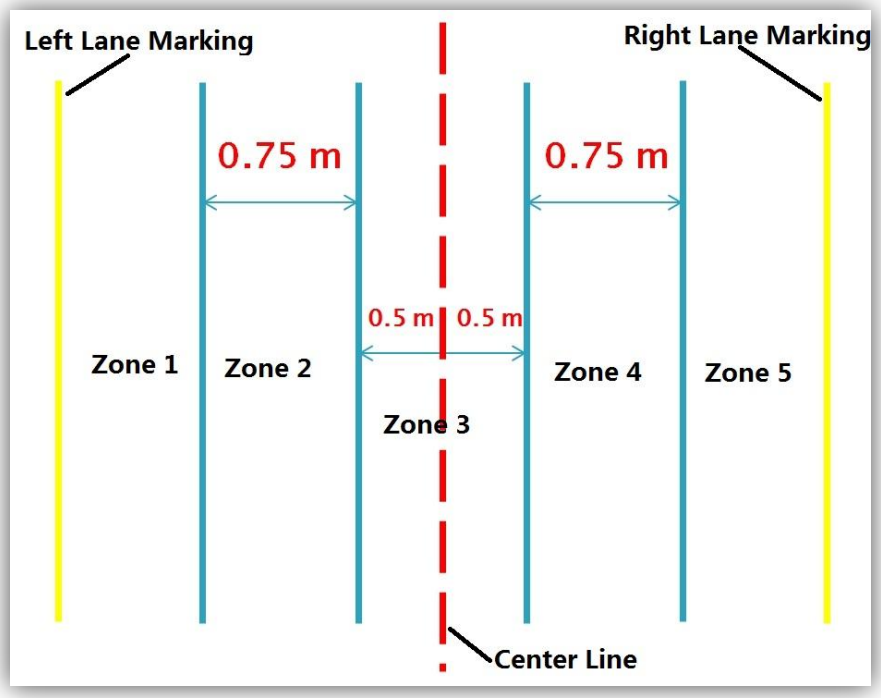

Figure 3.1 Wheelpath Definition in AASHTO PP67-10

3.2 Rutting Protocol PP69-10

To characterize pavement permanent deformation, three types of indicators are developed in PP69-10: surface deformation condition, rut related attributes and water entrapment condition. These attributes are interconnected and mutually affected but with different emphases (Simpson, 2001).

Since investigating an array of rutting indicators is not the focus of this project, PP69-10 is not discussed with details. Only rut depths in the left and right wheelpath are reported for this project.

3.3 AASHTO Cracking Protocol PP67-10

The AASHTO Designation PP67-10 (AASHTO 2013a): *Quantifying Cracks in Asphalt Pavement Surfaces from Collected Images Utilizing Automated Methods* outlines the procedures for quantifying cracking distress at the network level. The image data for analysis should abide by the AASHTO Designation PP68-10 (AASHTO 2013c) *Collecting Images of Pavement Surfaces for Distress Detection*. PP67-10 protocol has the following features:

- The protocol is designed for fully automated survey. Minimal human intervention is needed in the data processing.
- Definition of cracking is addressed in detail.
- Two cracking properties are reported: the cracking length and the cracking width.
- Three cracking types are defined: the transverse cracking, the longitudinal cracking, and the pattern cracking. The classification of the cracking is based on the orientation of the cracking spanning.
- Five zones are generated for entire lane coverage. The total cracking length and average cracking width of each cracking type are reported for each zone.

PP67-10 is unique from other protocols in terms of its cracking types, measured quantities, and report format. Based on the lab and field test, the image

data collected by 3D Ultra fully meet the data collection requirements in the PP68-10 (AASHTO 2013c): *Collecting Images of Pavement Surfaces for Distress Detection* and are suitable for conducting analysis according to PP67-10.

3.4 Preliminary Evaluation of Protocol PP67-10

3.4.1 Comparison of Cracking Protocols

PP67-10 is different from other current used protocols in many aspects. Conventionally, the principal physical characteristics of cracking are type, extent, severity, and relative location. These aspects are related to the mechanism of the cracking formation, prediction of propagation, and subsequent maintenance and repair actions. Cracking type characterizes the visual pattern or orientation of the cracks, such as alligator and longitudinal cracking. Extent reflects the quantity of the cracks. Example measures are total length, extended area, and percentage of the surface. Severity usually refers to the surface-width of the cracks, while in some occasions other information such as spalling and faulting at cracks are attributed to the classification of severity level. Relative location can be used to identify different zones of a lane which is usually divided by the wheel-path.

A comparison of six widely accepted cracking survey protocols are summarized in Table 3.1. It is observed that various combinations of the abovementioned four aspects are implemented in these standards. The AASHTO cracking protocol PP67-10 and PP44-00, and LTPP manual clearly define the technical parameters for all four aspects. The cracking extent is the only characteristic that are required to report in all the six protocols.

Table 3.1 Cracking Survey Protocols

Protocol	Reporting Items	Major Types	Extent	Severity	Relative Location
MEPDG (AASHTO)	Criteria are set for distresses to determine failure. No overall evaluation.	Transverse, Longitudinal, and Alligator.	Transverse and Longitudinal: ft/mi, Alligator: %.	N/A	Wheel-path and non-wheel-path.
PP67-10 (AASHTO)	Report individual attribute	Pattern, Transverse and Longitudinal.	Actual length.	Actual widths.	5 zones are divided by the two wheel-paths.
LTPP (FHWA)	Report individual attribute.	Fatigue, Block, Longitudinal, Reflection, Transverse, and others.	Length or area according to crack type.	Low, Moderate, and High applied to different types of cracks.	Longitudinal cracks either in or out wheel-path. Fatigue only in wheel-path.
HPMS (FHWA)	Report extent for three types of cracking	Fatigue, Transverse and Longitudinal	Percentage area for fatigue and actual length for transverse in AC.	N/A	Fatigue only in wheel-path.
PCI (ASTM)	Type, extent, and severity are used to calculate PCI.	Alligator, Block, Joint reflection, Longitudinal and Transverse, and others.	Length or area (percentage) as per feature.	Low, Medium, and High. Considering other associated distresses.	N/A
PP44-00 (AASHTO)	Report individual attribute	Transverse, Longitudinal, and Interconnected Cracking	Total length of cracking per unit area (m / m^2) for 5 strips.	Level 1, 2, and 3 (least severe to the severest).	5 strips are divided by the two wheel-paths.

Survey Methods: 1 is manual, 2 is semi- automated, and 3 is fully automated.

The AASHTO protocol PP44-00, ASTM standard, and the LTPP standard are prevailing protocols in the current practice. The Highway Performance Monitoring Systems (HPMS) collects cracking data based on PP44-00 or the LTPP protocol. The Mechanistic-Empirical Pavement Design Guide (MEPDG) develops its performance models using distress data collected following the LTPP protocol.

Similar to PP67-10, PP44-00 also requires three types of cracking: longitudinal, transverse and interconnected cracking. Each cracking is classified with severity

levels. Level 1 cracking has a width less than 3 mm; Level 2 cracking has a width between 3mm and 6 mm width; and cracking width greater than 6 mm is classified into Level 3. In addition, PP44-00 requires reporting the extent of cracking using Total Length of Cracking per unit area (m/m^2). Wheel-path is also defined in PP44-00, which is the same as PP67-10. As the total length for each zone is recorded in PP67-10, it is straightforward to convert the data from PP67-10 into the format required by PP44-00.

Comparing to the three cracking types in PP 67-10, LTPP and ASTM protocols record at least five types. It is challenging to further classify the three types of AASHTO PP 67-1-0 cracking into more detailed crack types in other protocols. However, transverse cracking and longitudinal cracking in PP 67-10 could be simply recognized as the corresponding cracking types in LTPP and ASTM.

With actual crack length and width recorded based on PP67-10, severity level can be determined following the LTPP protocol definitions. Cracking with mean width less or equal to 6mm can classified as low severity level; cracking with mean width higher than 19 mm can be defined high severity level cracking; while all in-between can be classified as moderate level cracking. According to PP67-10, all the pattern cracks are recorded by length; however in LTPP fatigue and block cracks are recorded by extended area. Assumptions are needed to convert data between PP67-10 and LTPP.

In summary, the major challenge among different cracking protocols is the lack of consistency in the definition of cracking types. The intensity and extent data in PP67-10 could be converted to other data formats with assumptions. For HPMS

data report, if the cracking data are historically abides by PP44-00, the conversion is straightforward. However, if the LTPP protocol is adopted for HPMS, assumptions are needed for data conversion. In order to use cracking data from PP67-10 for Pavement ME Design, there are two difficulties (a) how to link the pattern cracking in PP67-10 to alligator cracking in the ME Design; (b) how to covert the length and width measured in PP67-10 to the percentage of lane area defined in ME Design for alligator cracking.

3.4.2 Discussions

During the extensive data processing and analysis, several vague definitions are observed and recommendations made as below:

First, pattern cracking in PP67-10 includes all cracking other than longitudinal and transverse cracking. Conventionally, pattern cracking includes alligator cracking and block cracking which are generally inter-connected crack either due to traffic load or environmental load. However, pattern cracking in PP 67-10 does not consider the interconnectivity of the cracking. In many scenarios, traditional interconnected linear cracking such as longitudinal or transverse cracking are classified as pattern cracking regardless of their zone locations because the orientation of the cracks are outside of the ±10 degree range paralleling or perpendicular to the pavement centerline.

Second, it is defined that cracking should have a minimum length of 25 mm (1 in.), and transverse and longitudinal cracking should have lengths more than 0.3 m (12 in.). However, not specific length threshold is required for pattern cracking. If the

cracking length is between 25 mm (1 in.) and 0.3 m (12 in.), and the orientation meets the criteria of transverse or longitudinal cracking, it is not clear on how to classify such type of cracking. Similar challenge is also presented in the definition of cracking width.

Third, as required in PP67-10, the amount (length) of the cracking by zones should be reported. However, it is not clear in the protocol on how to determine the crack type if a continuous cracking spans more than one zone. In the current PP67-10 practice, the continuous crack will be divided into several pieces by zones.

Fourth, the average width is one of the two attributes to report in the protocol. However, how to obtain cracking width for multiple cracking is not provided. As a surface fissure, cracking spans to a certain length with different width at different positions. For one cracking, the average width is considered the mean of the width along the cracking spanning.

Last but not least, validating automated results is challenging. The protocol is proposed for automatic cracking data analysis, however, data validation of automatic software algorithms is performed by comparing with field observations other than automatically collected pavement image data. This is unrealistic for many reasons: (1) the resolution from the field measurements cannot achieve as accurate as data from ultra high resolution digital images; (2) the line of sight measurement in the field has limitations in determining the orientation and other properties such as width of a cracking without the aid of computers. The manual survey results vary significantly due to pavement condition, ambient lighting, and traffic condition variations; (3) Manual distress survey is time and resources consuming.

3.5 Automated Distress Analyzer 3D (ADA-3D)

Due to the diversity and complexity of pavement surface environment, fully automated cracking detection is still remaining as a challenge. There is no fully automated cracking detection algorithm that has been widely used. A common problem for automated cracking detection algorithms is that consistently high detection accuracy is not guaranteed due to unpredictable uncertainties presented on diverse pavement surfaces. Although machine learning algorithms have become popular in recent years, they are still immature in predicting unlimited presences of pavement cracking with limited offline learning sources. Therefore, full - automation without manual intervention for cracking processing at network level for state DOT production does not exist yet. Moreover, the current automated cracking detection algorithms have paid insufficient attention to observer's involvement for reference. In other words, the current automated algorithms have not provided a way for users to improve the detection performance based on their experience and observations. Most importantly, no current automated algorithms can guarantee that almost all of cracks could be located.

Therefore, an interactive cracking detection system using Minimal Contrast as the primary parameter is proposed by the research team for detection improvements with high levels of flexibility and adaptability by taking advantage of observer's feedback. This interactive system employs two levels of detection to implement automated detection and semi-automated detection. Automated Detection (as

shown in Figure 3.2) which is the bottom level of interactive detection uses observer's feedback during training to improve the Minimal Contrasts for interested sections, and then applies the trained Minimal Contrasts to corresponding sections respectively for automated detection. Meanwhile, Assisted Detection (as shown in Figure 3.3) which is the top level of interactive detection is adopted to adjust the Minimal Contrast according to observer's feedback, in order to find cracks missed by Automated Detection or delete noises introduced by Automated Detection within the observer-defined region.

Based on a case study conducted by the research team (Zhang and Wang, 2014), the Automated Detection could be able to achieve high detection precision and recall with appropriate training, and the integration of Automated Detection and Assisted Detection is capable of finding almost 100 percent of cracks and eliminating almost all noises. The limitation of the proposed detection system is the increase of time when smaller section size for Automated Detection and refinement via Assisted Detection are considered for higher accuracy. However, the advantage of the proposed detection system is that it provides a flexible approach for users to obtaining desired results based on their tolerance and acceptance level. In other words, the greatest challenge for an interactive detection algorithm would be the promise: how accurate the results will be depends on how much effort that the users would like to pay. Since the Assisted Detection proposed in this paper can find almost all cracks or delete noises bit by bit but with undeterminable amount of time, future developments will be focused on higher adaptability and accuracy of Automated Detection.

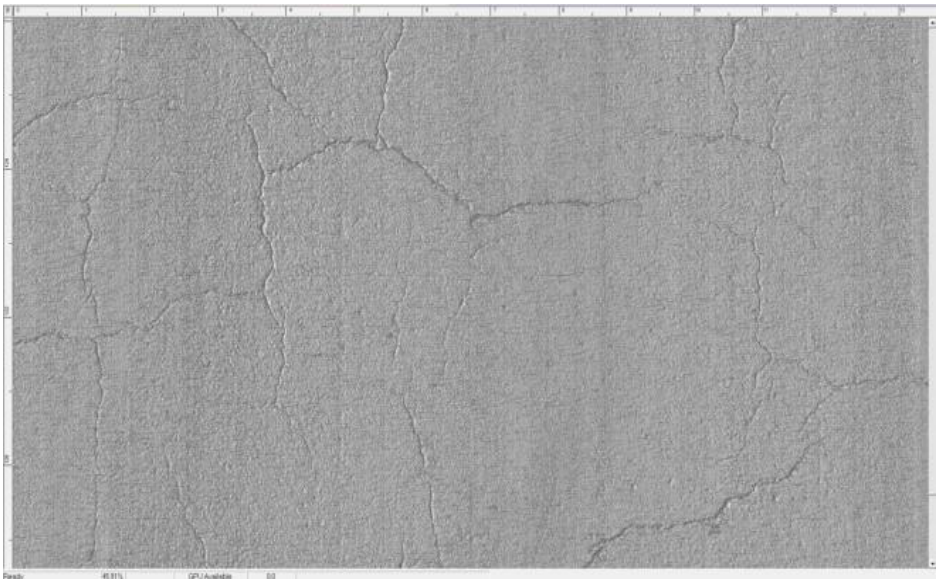

(a) Raw Image

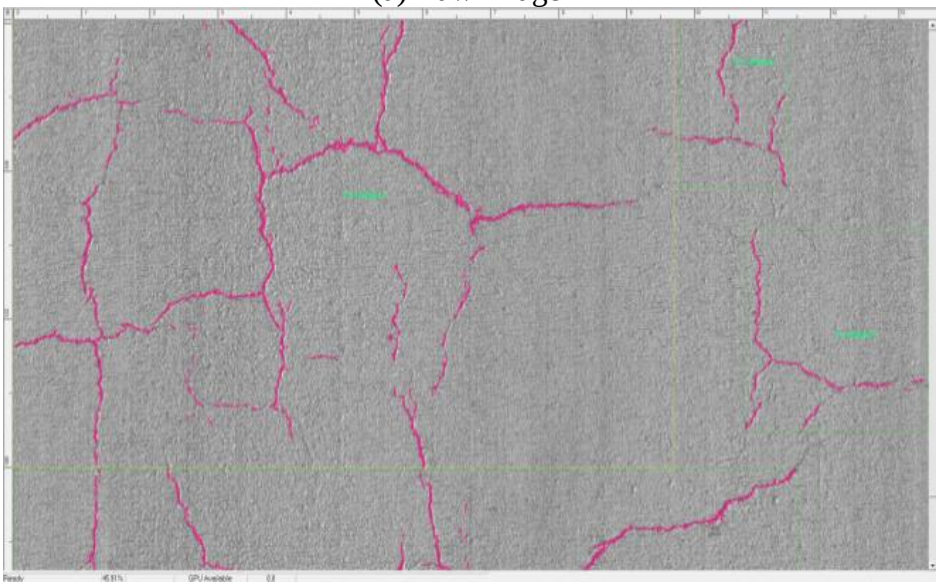

(b) Automated Detection Results

Figure 3.2 Fully Automated Crack Detection

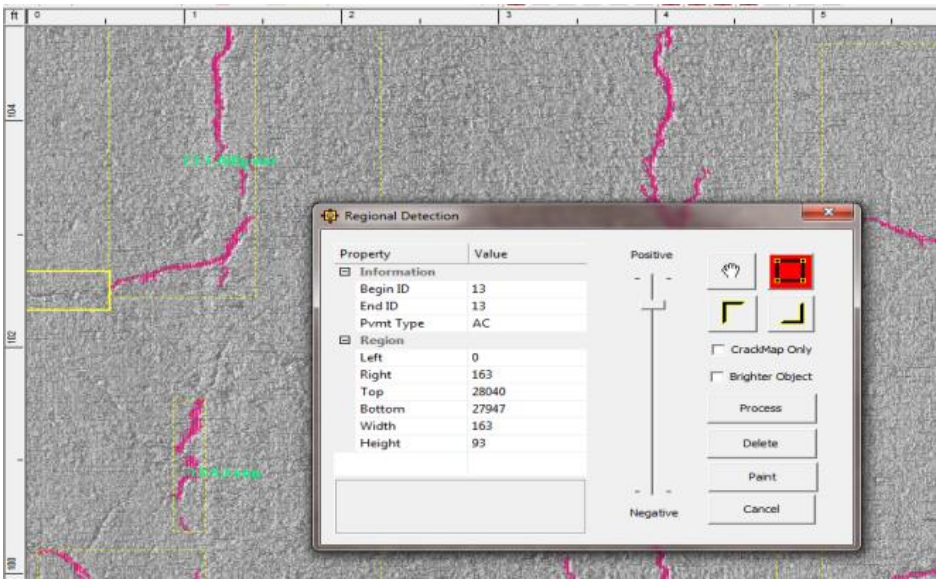

(a) Missing Cracks from Automated Crack Detection

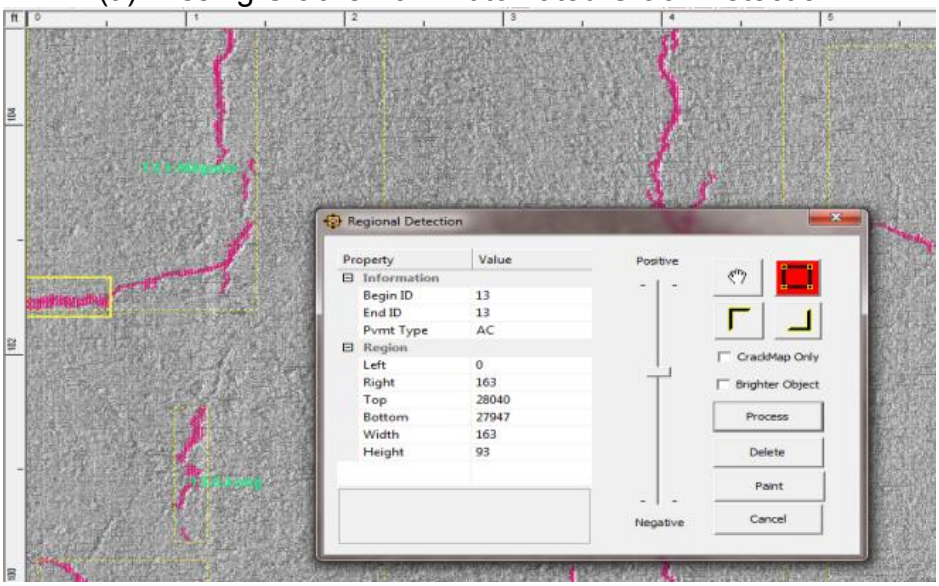

(b) Missing Crack Retrieved using Assisted Regional Detection

Figure 3.3 Assisted Crack Detection

CHAPTER 4 INERTIAL LONGITUDINAL PROFILER BASED ON 1MM 3D DATA

4.1 Introduction

With respect to pavement management and evaluation, pavement roughness is one of the most significant functional indicators for the pavement engineers. Road roughness directly affects the driving experience and it is also closely related to some hidden vehicle costs like tire wear, fuel consumption, and vehicle maintenance costs. Furthermore, it also has remarkable impacts on road safety issues. Therefore, since the 1960s, many studies on road roughness have been carried on to evaluate the road roughness, most of which measure longitudinal profiles to quantify road roughness. From the definition of American Society of Testing and Materials standard (ASTM, 2012), longitudinal profiles are “the perpendicular deviations of the pavement surface from an established reference parallel to the lane direction, usually measured in the wheel tracks.” Many devices can measure road profiles such as a rod and level (Sayers and Karamihas, 1998), walking profilers and inertial profilers. With the collected profile data, many road smoothness indices can be calculated such as International Roughness Index (IRI) and Ride Number (RN). IRI, computed based on profile measurements using a quarter-car model at a simulation speed of 50 mph (80 km/h) (ASTM, 2012), is one of the most popular smoothness indices to diagnose the road conditions.

With the advancement of the 1mm 3D sensor pavement surface data collection technology, it is feasible to construct an inertial profiling system based on

1mm 3D data. The accelerometer, height sensors and distance measuring instrument (DMI) are three essential devices for collecting road profiles. The accelerometer is a transducer that provides an output that proportional to the vertical acceleration. The height sensor is a non-contacting transducer that provides an output that proportional to the distance from the sensor to the road surface. The DMI is a distance measuring device that provides triggering for height sensors. Traditional inertial profilers used Roline sensors that mounted closely to the road surface, to measure height data. The 1mm 3D sensor based profiling system, which mounted higher than the traditional height sensors, to collect the height information of the complete pavement lane.

4.2 Equipment

The 1mm 3D based profiling system consists of full-size passenger van equipped with PaveVision3D sensor cases, in which 3D sensors and accelerometers are located (Figure 4.1). Left side sensor case and right side sensor case measure elevation profile traces in the left wheel path (LWP) and right wheel path (RWP) respectively. Inside the sensor case, accelerometers are mounted in tandem with 3D sensors. The accelerometer has very high resolution, which can sample the vertical acceleration at an average rate of 10 KHz. It needs no external trigger and is highly stable against outside noises. The DMI is mounted on the left wheel of the host vehicle. A data acquisition system is developed based on the three essential devices to collect, process, generate and store profile data for roughness analysis. The sampling interval of the profiling system is 0.5 inch.

Figure 4.1 High-Speed Inertial Profiler Based on 1mm 3D Data

4.3 Software Development

In order to build up a real time profiling system, three software programs are developed: the Control Panel program, the Pavement 3D Capture program and the Profiler program. The Control Panel program collects distance and speed information and controls the starting and ending of a data acquisition. The Pavement3D Capture program retrieves the height data from the left and right wheel paths and shares the specified elevation data with the Profiler program. The Profiler program has the capability of retrieving acceleration data from accelerometers, converting it to the vertical displacement data, displaying the integrated profile data, calculating IRI information and reporting results. The integration of the three software programs is illustrated below (Figure 4.2).

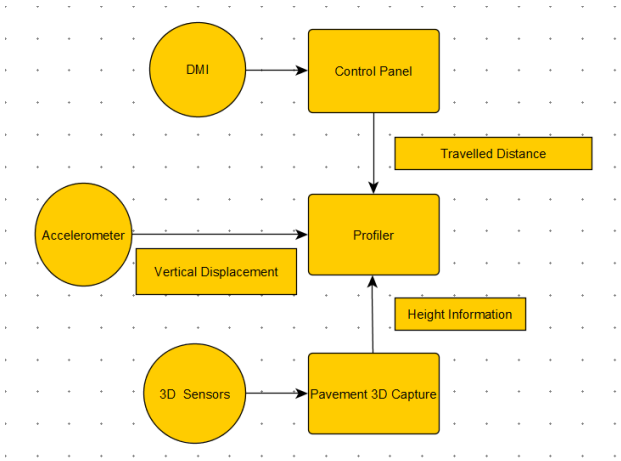

Figure 4.2 Integration of Software Programs

The profiler program consists of two major parts: Data Acquisition and Data view. Data Acquisition includes several modules and implements tasks such as collecting, processing, generating and compressing profile data. The Data Acquisition interface is shown in Figure 4.3 (a), which displays the latest generated pavement profile in real time. The IRI calculation and displaying module calculates and displays real-time IRI values for every 50-meter section.

Data View employs algorithms to decompress, display profile data (Figure 4.3 (b)), compute IRI information with any reporting interval and export profile data or IRI results to ERD file which can be used in the ProVAL software.

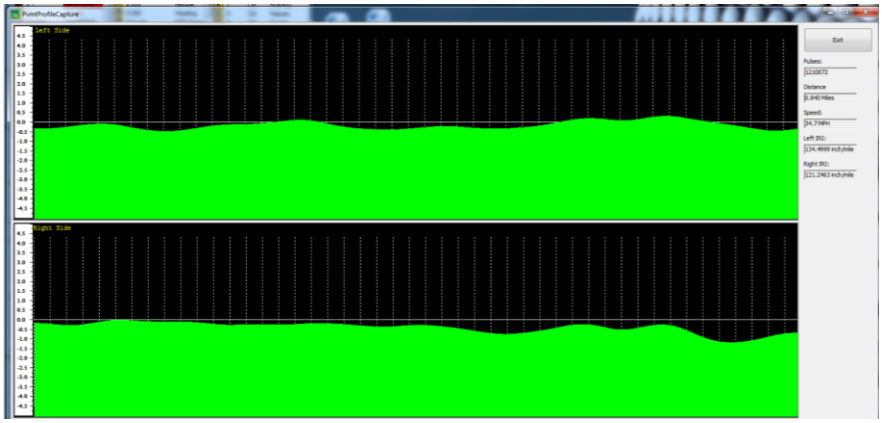

(a) Real Time Profile Data Acquisition

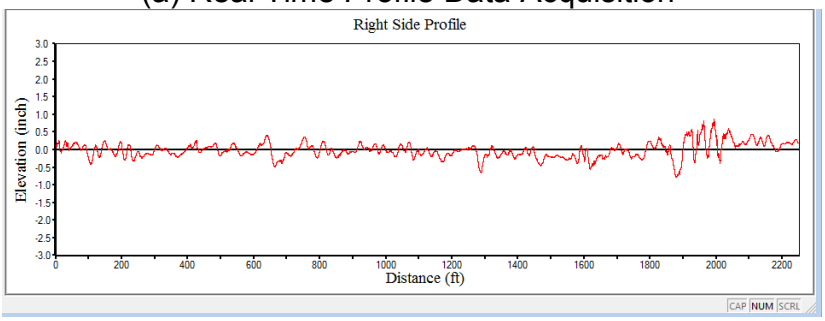

(b) Profile View

Figure 4.3 Profiler Software Interface

4.4 Field Validation

Extensive testing has been performed on three different pavements selected for field validation: two asphalt pavements and the other one PCC pavement. Two groups of field testing are conducted: the first group involves 10 repeated passes for the same site at the same speed, and the second group involves 3 different speeds for two different pavements. Each speed repeats 3 passes.

Figure 4.4 (a) shows a right-of-way view of Testing Site #1. It is an 1100-ft. tangent section with 500-ft. lead in and 500-ft. lead out distance. Two traffic cones labeled with a white reflective tape were placed at the start and end of the effective data collection section. They can provide consistent start and end for the 10 repeated passes by automatic triggering. The vehicle speed for Testing Site 1 is 30

mph. Additionally, SurPRO 3500 and Ames profiler were used to collect road profiles and provide reference IRI values. Testing Site #2 is a PCC pavement with longitudinal grade and horizontal curves. The data collection was triggered automatically by a red cone and was terminated after a distance of 1750 ft. The vehicle speed for Testing Site #2 is 40 mph. Site #3 has asphalt surface. The data collection was triggered automatically by a red cone and was terminated after a distance of 1640 ft. The vehicle collected profile data at two different speeds of 50 mph and 60 mph for this site. For Testing Site #2 and #3, AMES profiler was adopted to collect profile data and provide reference IRI values.

(a) Testing Site #1

(b) Testing Site #2

(c) Testing Site #3

Figure 4.4 Field Validation Sites

After data collection, the IRI values were computed from the raw profiles in accordance with ASTM E 1926 (ASTM, 2008). Figure 4.5 compares the IRI values

from 10 passes in Testing Site #1. The IRI values of SurPRO were computed for an average of three passes. The IRI values of Ames and proposed inertial profiler were obtained from all 10 repeated passes.

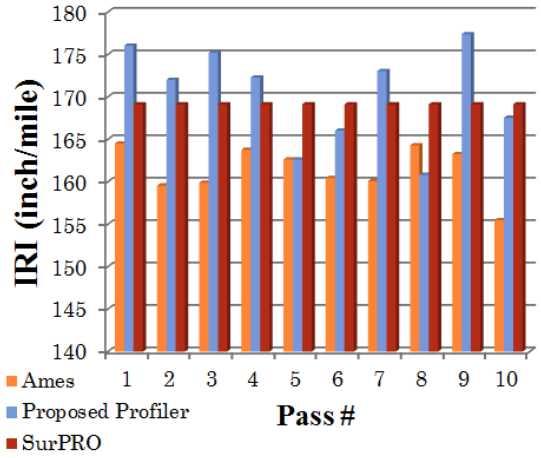

Figure 4.5 IRI Values for 10 Passes at Testing Site #1

Profile cross-correlation is a statistical metric to measure the correlation between two profiles of the same section. A large cross-correlation value indicates the profile pairs are highly correlated; otherwise, the profile pairs are negatively correlated. The cross correlation of the right wheel path profiles from the 10 passes in Testing Site #1 are computed in Table 4.1. The results indicate the 1mm 3D based profiler is able to provide repeatable and accurate profile data.

Table 4.1 Cross Correlation of 10 Repetitive Runs in Testing Site #1

Pass #	1(%)	2(%)	3(%)	4(%)	5(%)	6(%)	7(%)	8(%)	9(%)	10(%)
1(%)		81.5	80.9	82.4	83.0	84.9	75.9	77.3	82.0	83.0
2(%)	81.5		89.2	88.9	88.2	87.8	78.9	81.9	90.6	80.6
3(%)	80.9	89.2		89.3	88.6	89.0	81.6	77.7	88.2	87.5
4(%)	82.4	88.9	89.3		91.0	85.0	79.3	75.9	87.3	80.6
5(%)	83.0	88.2	88.6	91.0		91.7	79.5	79.4	87.5	85.7
6(%)	84.9	87.8	89.0	85.0	91.7		81.2	81.8	88.5	91.4
7(%)	75.9	78.9	81.6	79.3	79.5	81.2		75.6	78.9	79.4
8(%)	77.3	81.9	77.7	75.9	79.4	81.8	75.6		77.5	73.0
9(%)	82.0	90.6	88.2	87.3	87.5	88.5	78.9	77.5		86.6
10(%)	83.0	80.6	87.5	80.6	85.7	91.4	79.4	73.0	86.6	

Figure 4.6 compares the IRI results from the 1mm 3D based profiler system and those from Ames profiler for all 9 passes at Testing Site #2 and #3.

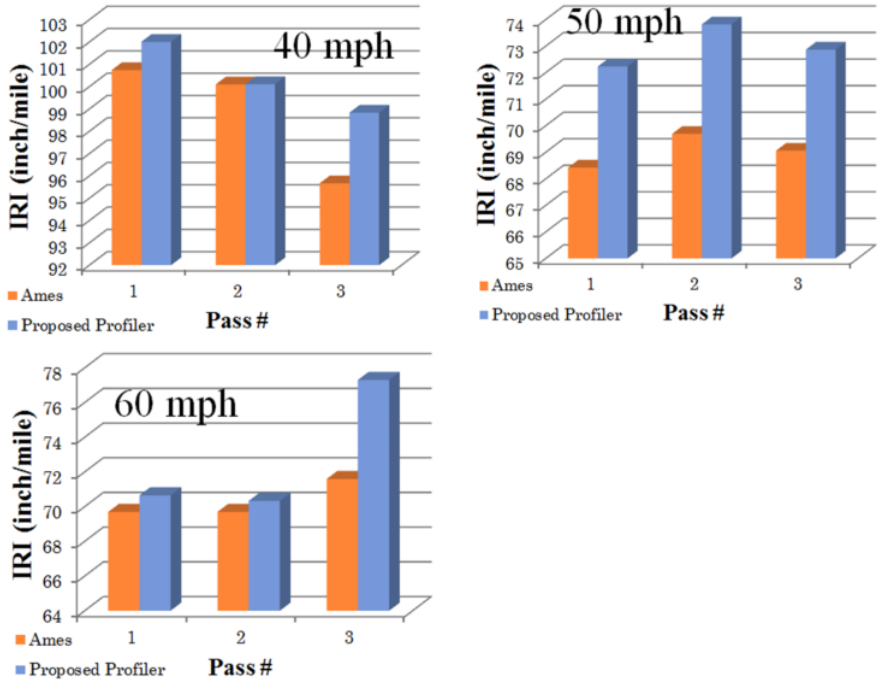

Figure 4.6 IRI Comparison Results for Testing Site #2 and #3

Based on the IRI comparison results and profile cross correlation discussed above, the 1mm 3D based profiling system which consists of stable hardware

devices and software programs is able to generate reliable profile data and produce accurate IRI values while maintaining good repeatability for multiple passes, various speeds and different road conditions and geometries. The 1mm 3D based profiling system is used to obtain IRI data for ODOT interstate highways in this project.

CHAPTER 5 HYDROPLANING SPEED BASED SAFETY EVALUATION

5.1 Introduction

Hydroplaning occurs when water pressures build up in front of a moving tire resulting in an uplift force sufficient to separate the tire from the pavement. During high intensity rainfall events, a water film builds up on the surface of a road. The risk of vehicle hydroplaning increases as the depth of this film increases. The loss of steering and drag force produced during hydroplaning may then cause the vehicle to lose control, especially when a steering tire is involved (Kumar and FWA, 2009).

Therefore, hydroplaning is a critical evaluation index for pavement safety management, and it is highly associated with the pavement drainage capacity. However, little research was conducted to identify hazardous locations with hydroplaning due to the fact that it was difficult to collect complete pavement surface data with geometric and geographical accuracies which are required to conduct texture, profiling, and cross slope analyses. With the emerging 1mm 3D PaveVision3D Ultra technology, texture data are continuously collected at high speeds. Cross slope and longitudinal grade with high accuracy are acquired with an Inertial Measurement Unit (IMU) system and 3D transverse profiling.

Highway with high speed limit and heavy traffic can lead to higher risk of hydroplaning accidents than other types of road. Therefore, hydroplaning evaluation for interstate network and national highway systems (NHS) is of great importance for pavement safety management. Gallaway model is implemented to identify the

segments with potential hydroplaning so that pavement engineers can take further measures to improve pavement safety.

5.2 Factors Contributing to Hydroplaning

5.2.1 Rainfall Intensity

Rainfall intensity is the most important environmental factor in hydroplaning. The depth of water on the road is directly proportional to the rainfall intensity.

5.2.2 Road Geometry

The road geometric design, such as cross slope and longitudinal grade, must consider pavement drainage. The length of time water is able to stay on the road will influence the depth it achieves. Longer flow paths mean more time to accumulate rainfall and results in higher film depth. Changes in cross slope and longitudinal grade can help to shorten the flow path length and reduce the time of water running off the pavement surface (Chesterton et al., 2006).

5.2.3 Pavement Texture

The pavement texture depth affects the water accumulation and water dispersion. Well textured pavement can provide flow paths to allow water in front of the tire to be forced out under pressure.

5.2.4 Tire Characteristics

Tire grooves help in expulsion of water from the tire pavement contact region by providing escape channels, thus reducing the risk of hydroplaning. Deeper tire

groove depth, lesser tire groove spacing and larger tire groove width offer a more effective channel for water flow, and as such hydroplaning takes place at a higher speed due to a lower rate of development of the hydroplaning uplift force. (Kumar et al., 2009)

5.3 Data Preparation

5.3.1 Estimated Mean Texture Depth (EMTD)

The methodologies for texture measurements can be grouped into two categories: static and high-speed methods. Static test methods include Sand Patch Method commonly used for determining MTD (ASTM, 2006), Circular Track Meter (ASTM, 2005), and Outflow Meter (ASTM, 2009). The measurements using static methods are normally conducted on marked small areas, and are not suitable for network level applications. As for the high-speed test techniques such as the laser based data acquisition systems, their measurements are conducted on one longitudinal profile or line-of-sight, and the produced texture index is termed as the Mean Profile Depth (MPD), which is a two dimensional measure and cannot represent pavement texture for the entire lane. However, water film depth (WFD) is related to pavement texture of the entire lane. Therefore, in this study the calculation of estimated MTD (EMTD) is conducted based on the volumetric Sand Patch measuring method using texture data for the entire lane, as shown in Equation 5.1 in 3D domain (Wang et al., 2014):

$$\mathrm{EMTD} = \frac{1}{\mathrm{K}} \times \sum_{\mathrm{i}=1}^{\mathrm{K}} \frac{\iint_0^{\mathrm{D}} [\mathrm{F}_0 - \mathrm{F}(\mathrm{x},\mathrm{y})]\,\mathrm{dxdy}}{\mathrm{D}} = \frac{1}{\mathrm{K}} \times \sum_{\mathrm{i}=1}^{\mathrm{K}} \frac{\sum_{\mathrm{x}=1}^{\mathrm{x}=\mathrm{N}} \sum_{\mathrm{y}=1}^{\mathrm{y}=\mathrm{M}} [\mathrm{F}_0 - \mathrm{F}(\mathrm{x},\mathrm{y})]}{\mathrm{D}} \qquad (5\text{-}1)$$

Where: $F(x, y)$ The pixel depth at point (x, y); D: The integral or gridded area containing of M×N pixels; F_0: The maximum peak in each area D; K: The number of grids within the test sample.

5.3.2 Cross Slope Calibration

The capability to measure transverse slope is important since a properly designed and constructed cross slope allows water to drain off the pavement quickly and reduce hydroplaning and accidents. Too little slope can cause low efficiency of drainage, while too much slope may cause vehicle handling problems. IMU mounted on the data vehicle can measure the Euler angles, which are called as roll (Euler angle about x-axis), pitch (Euler angle about y-axis) and yaw (Euler angle about z-axis). The roll angle is widely accepted to represent pavement cross slope, and pitch angle is widely used to represent the pavement longitudinal grade, which are based on the assumption that the vehicle floor is parallel with the pavement during the travelling.

However, in real word the vehicle floor is unparalleled with the pavement during traveling (Figure 5.1) with the following reasons: 1) the uneven gravity distribution of vehicle; 2) the vibration of the vehicle during the traveling; 3) surface condition of pavement.

The angle of vehicle relative to the pavement (angle γ) can be measured using collected 3D data. In PaveVision3D Ultra, the instruments used in measuring the cross slope include IMU system and the 3D Ultra sensors. The IMU is mounted in the middle of the vehicle, and the two sensors are overhung on the rear end of the

vehicle. These two sensors cover the entire lane, and the 3D range data from the two 3D sensors are directly related to the distance between the pavement surface and the two sensors. As Figure 5.1 shows, the IMU provides angle of the vehicle relative to a level datum, as shown by angle θ, and the difference in laser measured height y_1 and y_2 over distance L is equal to the slope of the vehicle relative to the pavement (γ as shown in Equation 5.2). Due to the irregularity and distress on pavement, the road surface does not appear as straight line in transverse direction. A least square regression straight line is introduced to approximate the transverse profile. Therefore, the "true" cross slope of the roadway can be approximately determined based on two values: the tilt of the vehicle floor (γ) and the slope of the road surface (θ) using Equation 5.3 (Wang et al., 2014).

$$\gamma = \operatorname{act}\tan\left(\frac{y_2 - y_1}{L}\right) \qquad (5\text{-}2)$$

$$= \tan(\theta - \gamma) \qquad (5\text{-}2)$$

Since the angle θ and γ are very small, the cross slope equals to the slope of IMU roll angle minus the slope of vehicle relative to the pavement.

$$= \tan(\theta) - \tan(\gamma) \qquad (5\text{-}4)$$

Where: – Cross slope of pavement; γ – angle measured by the laser sensors with respect to the roadway surface; θ – Roll angle measured by the IMU; L – The distance between left and right laser; y_1 – The vertical distance from left sensor to the least-square approximation line of pavement; y_2 – The vertical distance from right sensor to the least-square approximation line of pavement.

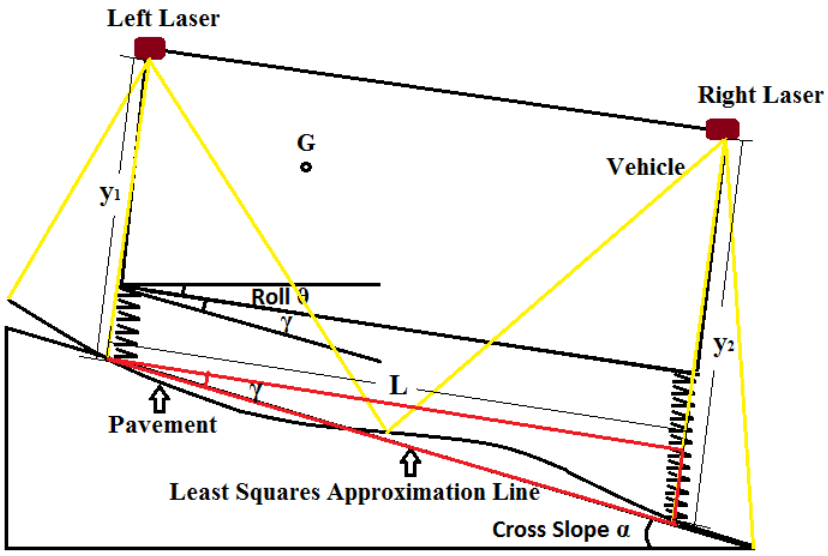

Figure 5.1 Estimation of Cross Slope based on IMU and 1mm 3D Data

5.3.3 Sample Size

The 3D texture data collected using PaveVision3D Ultra is stored on computer hard disk in the form of raw images with the size of 4096 pixel wide by 2048 pixel long. The raw images are used as the basic sample elements. Afterwards, data processing and analysis can be conducted on each sample. In this study one raw image is considered as a sample. The same sample length is also used to record the IMU data including roll and pitch angles, and 3D transverse profile data.

5.4 Hydroplaning Prediction Model

Gallaway B. M. et al (1979) developed an empirical method on hydroplaning prediction for the US Department of Transportation. The method as shown below was adopted in the Texas Department of Transportation Hydraulic Design Manual. Local rainfall intensity and road geometry is used to obtain the water film depth. This

depth is then used to predict hydroplaning velocity (Equation 5.6). This model can be used to determine the relationship between driving speed and hydroplaning occurrence on a pavement (Gallaway, 1979).

$$V = 0.9143SD^{0.04}P^{0.3}(TD + 0.794)^{0.06}A \quad (5\text{-}6)$$

$$SD = \left(\frac{W_d - W_w}{W_d}\right)100 \quad (5\text{-}7)$$

$$A = \frac{12.639}{WFD^{0.06}} + 3.50 \quad (5\text{-}8)$$

$$A = \left[\frac{22.351}{WFD^{0.06}} - 4.97\right] \cdot TXD^{0.14} \quad (5\text{-}9)$$

$$WFD = z\left\{\frac{TXD^{0.11}L_f{}^{0.43}I^{0.59}}{S_c{}^{0.42}}\right\} - TXD \quad (5\text{-}10)$$

$$S_f = \left(S_l{}^2 + S_c{}^2\right)^{\frac{1}{2}} \quad (5\text{-}11)$$

$$L_f = W\frac{S_f}{S_c} \quad (5\text{-}12)$$

Where, V: Vehicle speed (km/hr) at which aquaplaning occurs; SD: Spin down speed (10% at initiation of aquaplaning); W_d: Rotational velocity of wheel on dry surface; W_w: Rotational velocity of wheel after spindown due to contact with flooded surfaces; P: Tire pressure (Kpa) (165Kpa recommended design value); TD: Tire tread depth (mm) (0.5mm recommended design value); A: The greater of the equation 5.7 and 5.8; TXD: Pavement texture depth (mm) (0.5mm recommended); WFD: Water film depth in mm on pavement surface from Equation 8; z: 0.01485 (Constant); L_f: Pavement flow path length (m); I: Rainfall intensity (mm/hr); S_c: Pavement cross slope (m/m); S_f: Flow path slope (m/m); S_l: Longitudinal grade (m/m); W: Pavement width (m). In this study, the TXD in the Gallaway model is

substituted by EMTD derived from the volumetric measuring method using 3D texture data.

5.5 Hydroplaning for Safety Evaluation

The current research activities on hydroplaning focus on pavement drainage design and tire pattern design. However, they are not helpful for evaluating the hydroplaning risk of existing road. In this project, predicted pavement hydroplaning speed is used to identify pavement segments with potential hydroplaning safety risks. A software interface has been developed as shown in Figure 5.2, which is able to read both 1mm 3D data and IMU data and predict hydroplaning speed

Figure 5.3 shows the predicted hydroplaning speeds at one testing site located in Stillwater Oklahoma. The speed limit is 45 mph. Hydroplaning might occur within the segment ranging from 1080ft to 1185ft, as shown in Figure 5.2 (a) where the predicted hydroplaning speed is lower than 45 MPH. The pavement segment with potential hydroplaning risk is marked with a yellow circle in Figure 5.2 (b). Highway agency may post a reduced speed traffic sign at that location to minimize the traffic accident caused by hydroplaning. In addition, pavement engineers may also take other measures such as constructing superior grooving texture to increase the potential hydroplaning speed.

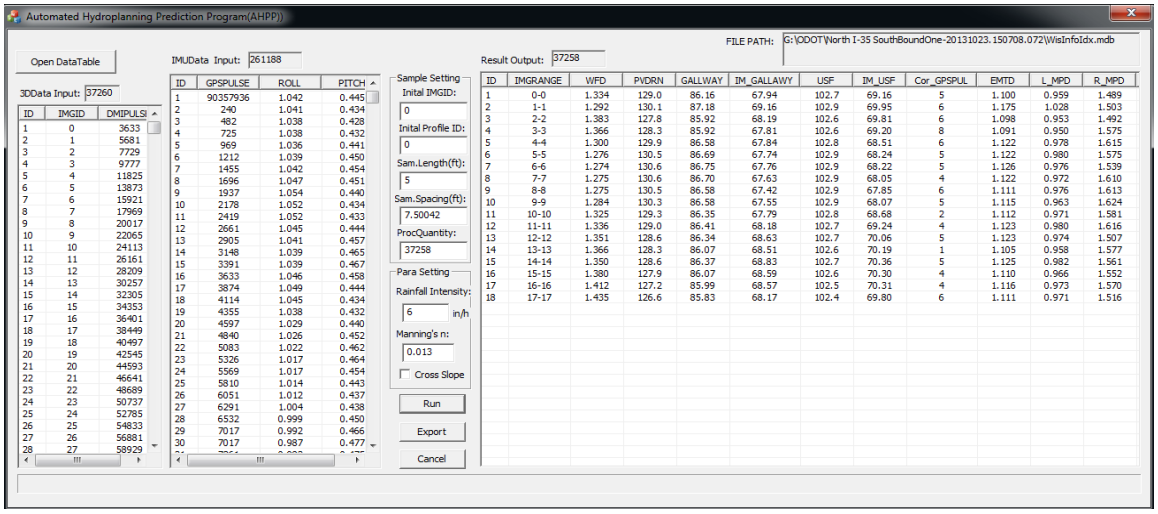

Figure 5.2 Hydroplaning Software Interface

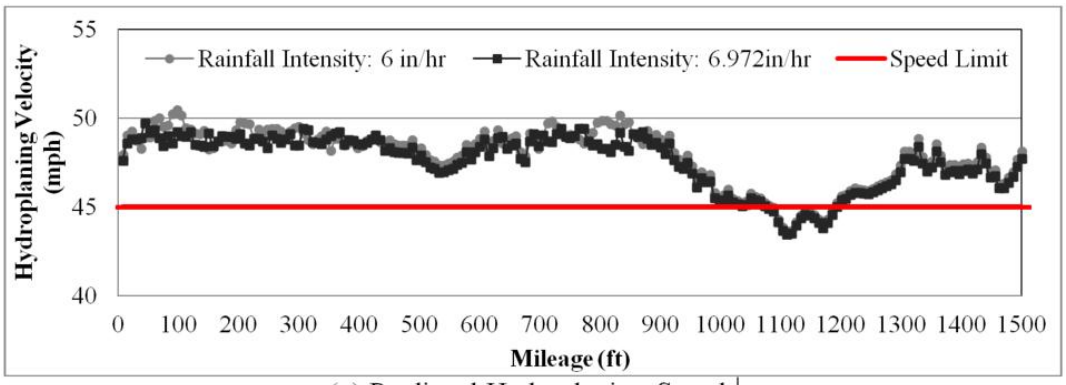

(a) Predicted Hydroplaning Speeds

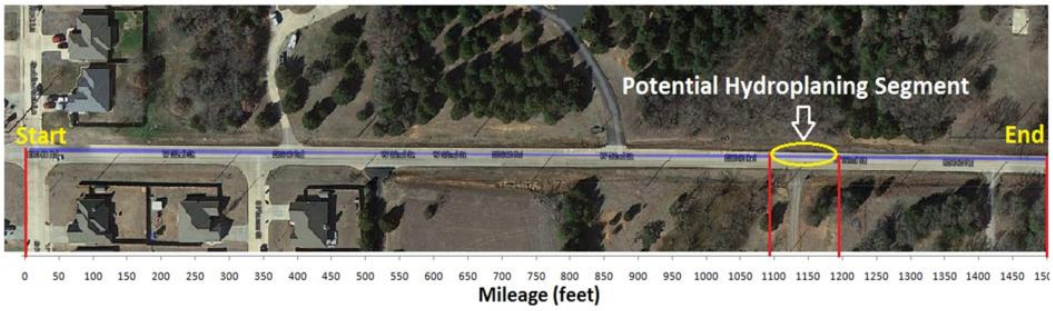

(b) Testing Site

Figure 5.3 Testing Site with Potential Hydroplaning Hazard

CHAPTER 6 IN-PRODUCTION NETWORK SURVEY

6.1 PaveVision3D Ultra for ODOT Network Survey

The data collection for this project includes ODOT interstate network (I-35 and I-40) and State Highway 51 from I-35 to Sand Springs with a total of approximately 1280 center miles, as shown in Figure 6.1 and Table 6.1. Two data collection trips were made to acquire 1mm 3D data collected at highway speed using the PaveVision3D system. The first data collection trip was executed in the beginning of March 2013 and the second in later May 2014. Since all the highways are divided, the data for both directions are collected. As can be seen in Table 6.1, the section lengths calculated based on Google Map and PaveVision3D Ultra system are approximately identical. Recognizing that the pavement surface types (AC or PCC) are constantly changing, the collected data sets for each highway are manually divided into sections based on surface type, subsequently each section is dynamically segmented into uniform segments.

Figure 6.1 Highway Network Survey for ODOT

Table 6.1 In-Production ODOT Network Survey

Folder Name	# Segment (by surface type)	Distance (mile)		Starting GPS		Ending GPS	
		ADA3D	Google	Lat	Long	Lat	Long
I-35 NB #1	11	174.7	175.0	33.7247	-97.1612	36.1155	-97.3411
I-35 NB #2	4	61.5	61.4	36.1181	-97.3447	36.9998	-97.3423
I-35 SB #1	5	52.9	52.8	37.0299	-97.3383	36.2695	-97.3278
I-35 SB #2	7	56.6	56.7	36.2703	-97.3278	35.4750	-97.4661
I-35 SB #3	5	129.1	129.0	35.4750	-97.4661	33.7259	-97.1609
I-40 EB #01	4	70.3	70.2	35.2267	-100.0065	35.5161	-98.9040
I-40 EB #02	4	84.5	84.2	35.5160	-98.9088	35.4585	-97.4560
I-40 EB #03	15	178.8	178.2	35.4759	-97.4660	35.4524	-94.4402
I-40 WB #01	14	179	178.0	35.4599	-94.4316	35.4731	-97.4662
I-40 WB #02	6	154.8	154.0	35.4577	-97.4542	35.2271	-100.0027
US-51 EB	3	70.9	70.6	36.1157	-97.3497	36.1193	-96.1172
US-51 WB #1	1	15.1	15.1	36.1159	-97.0896	36.1157	-97.3497
US-51 WB #2	4	55.9	55.7	36.1194	-96.1169	36.1159	-97.0921
Total	**83**	**1284.1**	**1280.9**				

The collected data are analyzed using the automated distress analyzer 3D (ADA-3D), and the following surface characteristics are reported:

- IRI values in the left and right wheel path at every 0.1 miles;
- Rut depth in the left and right wheel path at every 0.1 miles. The rut depth is calculated based on the first profile of each 0.1-mile section;
- Cracking data in the wheel-path and non-wheel-path zones at every 0.1 miles. The cracking data are obtained based on the AASHTO cracking protocol PP67-10;
- Predicted hydroplaning speed at every 0.1 miles.

For each indicator, the data are plotted at the interval of 0.1-mile and the detailed histograms are provided in the appendices (Appendix A to Appendix F) of this report.

6.2 PELT Method Based Dynamic Segmentation

6.2.1 Introduction

Segmenting pavement network into homogenous sections is important for road maintenance scheduling and management systems. Three types of segmentation approaches are used by highway agencies: fixed-length segments, variable-length segments, and dynamic segmentation. Fixed-length static method breaks highway routes into pre-defined lengths (such as every 0.1 miles) and are insensitive to changes in pavement attributes, which can result in significant data redundancy and problems to provide recommendations for project prioritization (Thomas 2003). Variable-length static method, on-the-other-hand, can break pavement into any length, but may be too sensitive to attribute changes and result in a large number of fine segments within a highway network (Thomas 2003). A well-known example of this method is the cumulative difference approach (CDA) proposed by AASHTO (AASHTO 1986).

Dynamic segmentation (DS) can accommodate the integration of both fixed and variable-length methods and provide more flexible data management. Two classical DS algorithms, binary segmentation and neighborhood segmentation, are widely used to estimate the locations of multiple change points of a data set. Binary segmentation (Scott and Knott 1974) first identifies a single change point for the entire data, and the procedure is repeated for the split data sets until no change points are found in any parts of the data. The binary segmentation search method is computationally efficient. However this method does not search the entire solution

space and is an approximate algorithm (Killick et al 2012). The neighborhood segmentation algorithm (Auger and Lawrence 1989) minimizes the objective using a dynamic programming technique to obtain the optimal segmentation change points. Whilst this algorithm is exact (Killick et al 2012), the computational complexity is considerably higher than that of binary segmentation.

In this project, the newly developed Pruned Exact Linear Time (PELT) method (Killick et al. 2012) is implemented to dynamically segment pavement sections into uniform subsections using 1mm 3D pavement surface data, which can be further used by decision makers for project prioritization and maintenance scheduling. Similar to the neighborhood segmentation method, the PELT algorithm conducts an exact search, but is significantly more computationally efficient by removing solution paths that are known not to lead to optimality (called as "prune" process).

6.2.2 PELT Methodology

Assuming an ordered sequence of data, $y_{1:n}$= (y_1, ..., y_n) has m change points with their positions at τ=(τ_1, ...,τ_m). Consequently the m change points split the data into m + 1 segments, with the i^{th} segment containing $y_{(\tau_{i-1}+1):\tau_i}$. The objective to identify multiple changepoints can be formulated to minimize (Killick et al., 2012):

$$\sum_{i=1}^{m+1}[C(y_{(\tau_{i-1}+1):\tau_i})] + \beta_f(m) \quad (6.1)$$

Where C is the cost function and $\beta_f(m)$ is the penalty to guard against over fitting. The PELT method considers the data sequentially and searches the solution space exhaustively. Computational efficiency is achieved by removing solution paths that are known not to lead to optimality. The assumptions and theorems which allow removal of solution paths are explained further in Killick et al. (2011). Pseudo-code for the PELT method is given in Table 6.2.

Table 6.2 Pseudo-code for the PELT method (Killick et al. 2012)

Input:	A time series of the form, ($y1, y2, \ldots, yn$) where $y_i \in$ R. A measure of fit $C(.)$ dependent on the data. A penalty β which does not depend on the number or location of changepoints. A constant K that satisfies equation.
Initialize:	Let n = length of time series and set $F(0) = -\beta$, $cp(0) = 0$, $R1 = \{0\}$
Iterate:	For $\tau^* = 1, \ldots, n$

1. Calculate $F(\tau^*) = \min_{\tau \in R_{\tau^*}} [F(\tau) + C(y_{(\tau+1):\tau^*}) + \beta]$

2. Let $\tau^1 = \arg\{\min_{\tau \in R_{\tau^*}} [F(\tau) + C(y_{(\tau+1):\tau^*}) + \beta]\}$

3. Set $cp(\tau^*) = [cp(\tau^1), \tau^1]$

4. Set $R_{\tau^*+1} = \{\tau \in R_{\tau^*} \cup \{\tau^*\}: F(\tau) + C(y_{(\tau+1):\tau^*}) + K \leq F(\tau^*)$

Output: The change points recorded in $cp(n)$.

6.3 IRI Analysis

IRI values in the left and right wheelpaths are calculated in inches per mile for each 0.1-mile pavement segment for the six roadways (three highways for both directions), as shown from Figure 6.2 to Figure 6.7. PELT changepoints are determined for each roadway. The IRI values in the left and right wheelpath shown

similar trend. For example, both wheelpaths between Mile 60 to Mile 85 on I-35 North Bound demonstrate worse pavement smoothness comparing to those at adjacent sections. In addition, the two directions of a highway show comparable IRI results. For example, on Interstate 40, from around Mile 300 to Mile 335.8 that is approaching to the border of Arkansas, the pavements have greater IRI values in both directions.

Assuming IRI values of 95 in/mi and 170 in/mi are the thresholds to classify pavement into "good", "moderate", and "poor" conditions, most majority of the highways are in “good” and "moderate" smoothness conditions. I-35 North Bound in the left wheelpath as the example, only 1.17% of the pavement are segmented as "poor" condition that have IRI values greater than 170 in/mi, 18.66% as "moderate" condition with IRI between 95 in/mi and 170 in/mi, while the remaining 80.17% have IRI values lower than 95 in/mi.

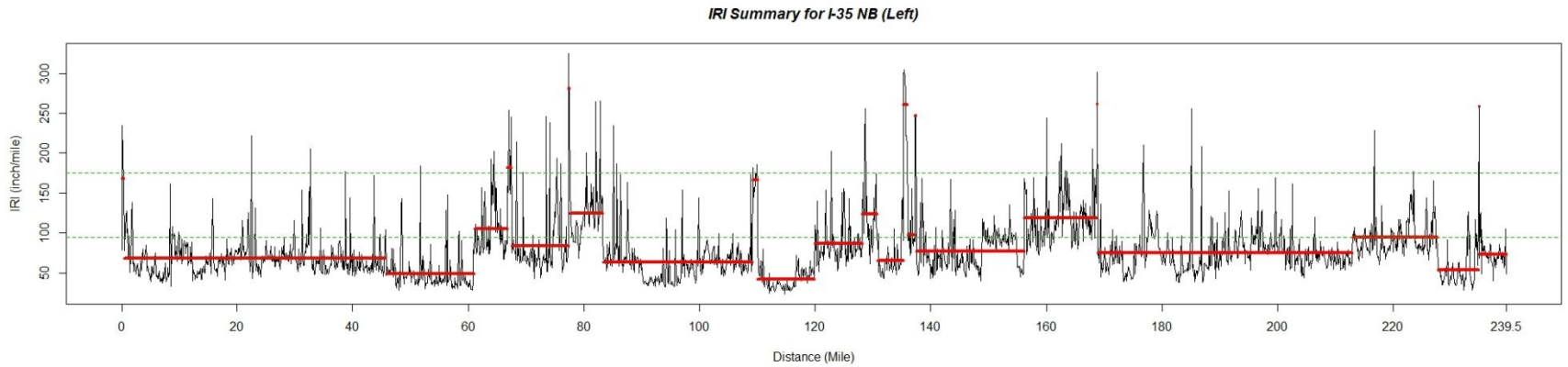

(a) Left Wheelpath

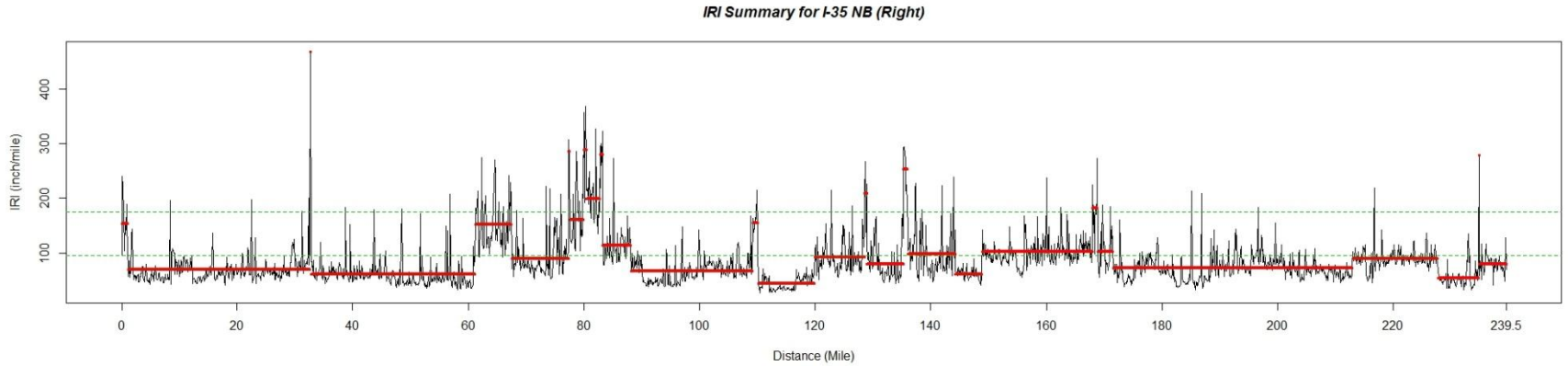

(b) Right Wheelpath

Figure 6.2 IRI and PELT Segmentation for I-35 North Bound

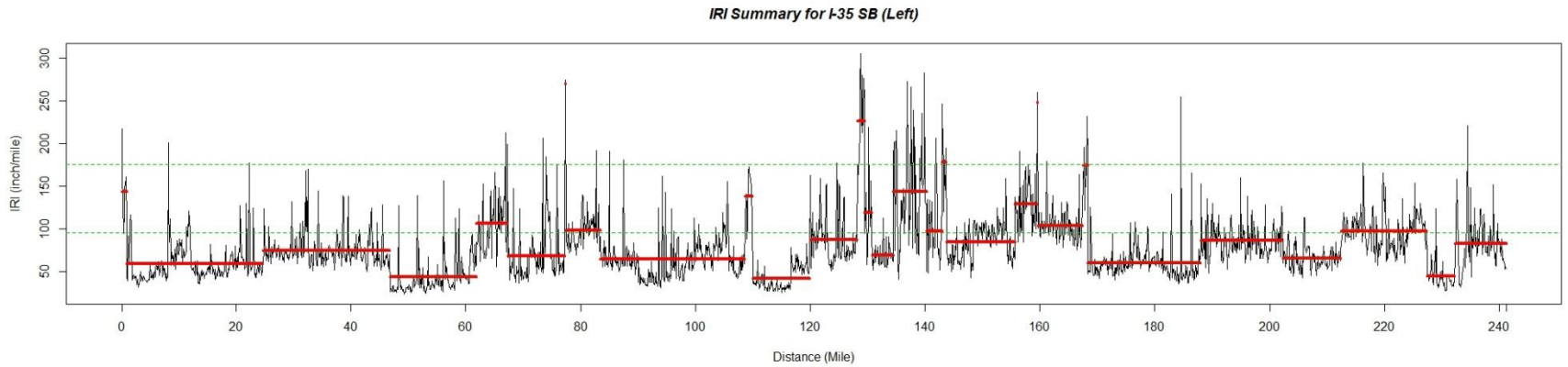

(a) Left Wheelpath

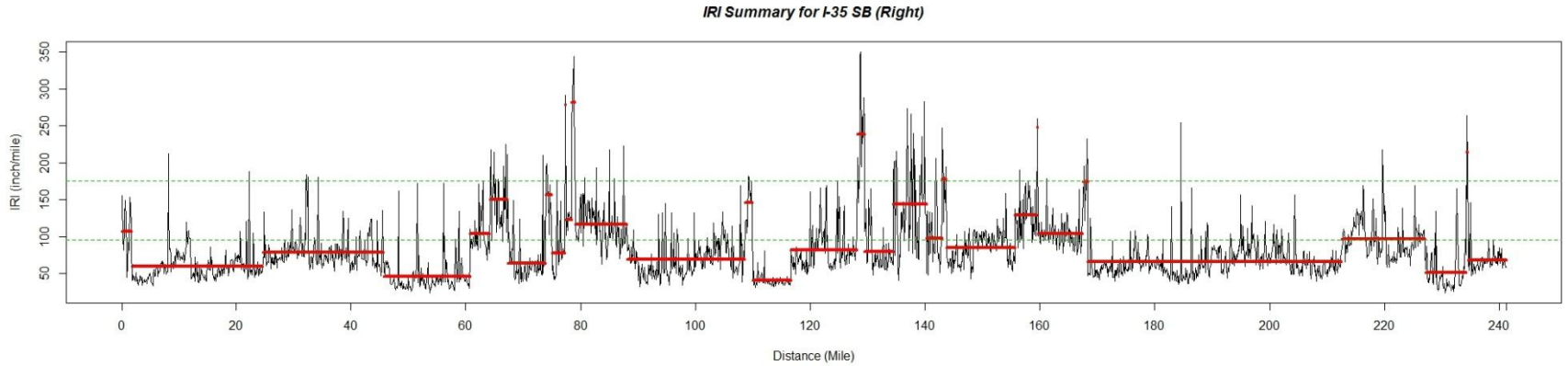

(b) Right Wheelpath

Figure 6.3 IRI and PELT Segmentation for I-35 South Bound

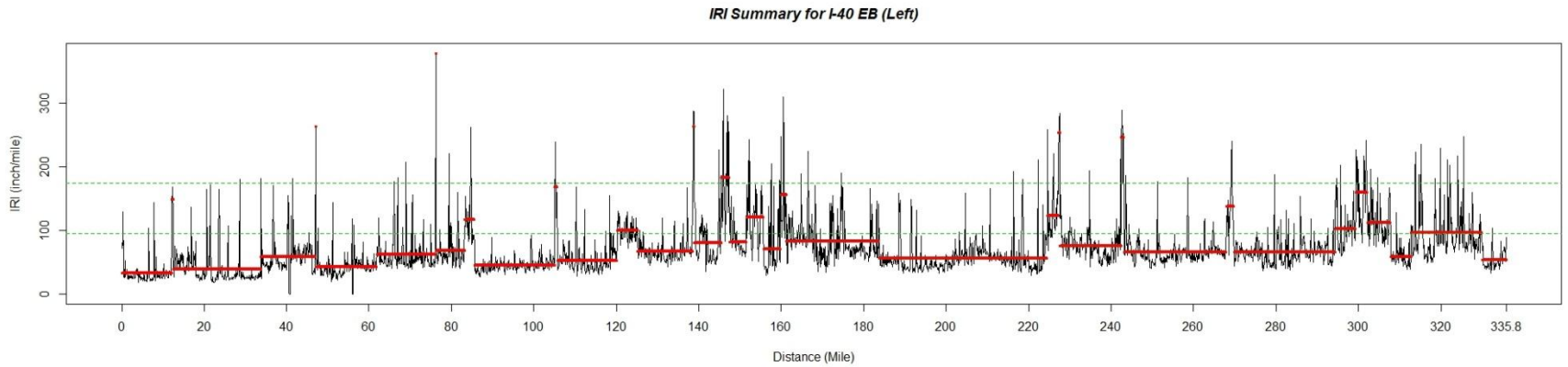

(a) Left Wheelpath

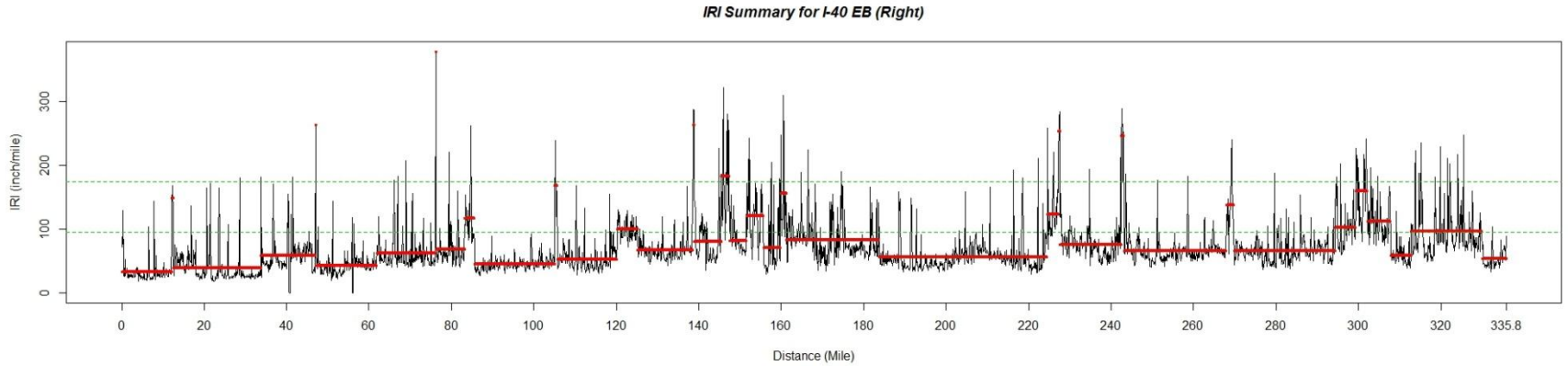

(b) Right Wheelpath

Figure 6.4 IRI and PELT Segmentation for I-40 East Bound

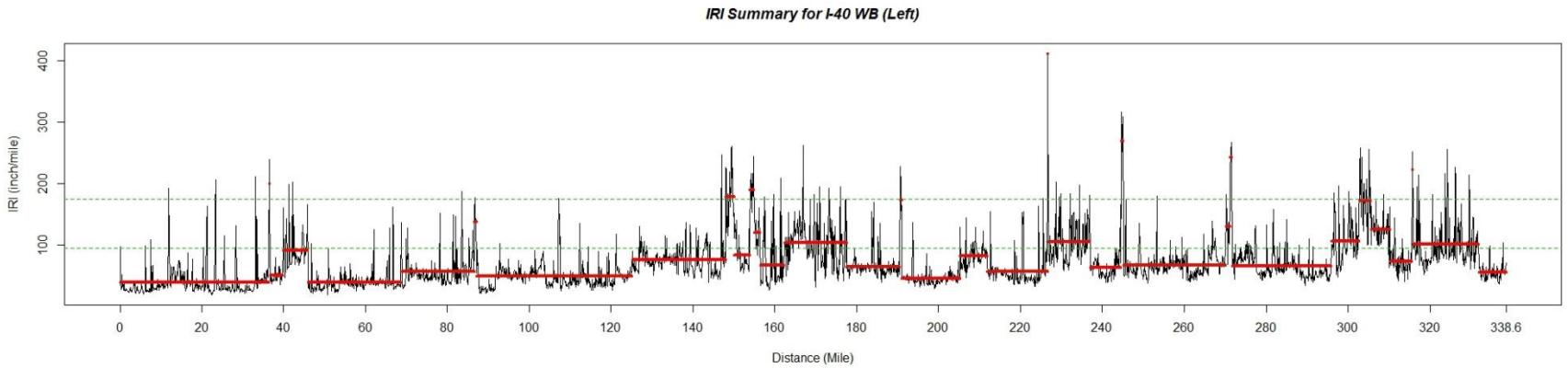

(a) Left Wheelpath

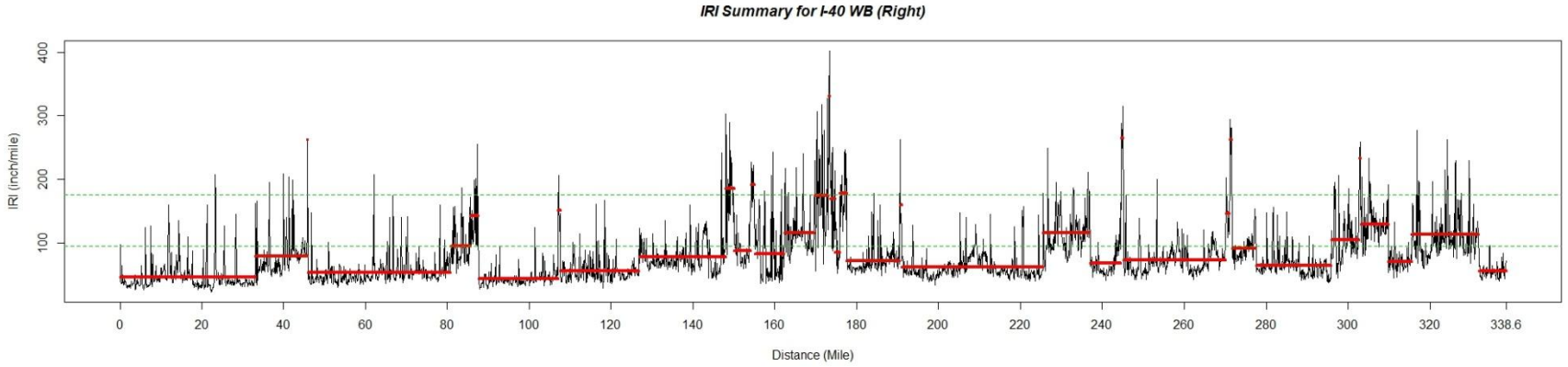

(b) Right Wheelpath

Figure 6.5 IRI and PELT Segmentation for I-40 West Bound

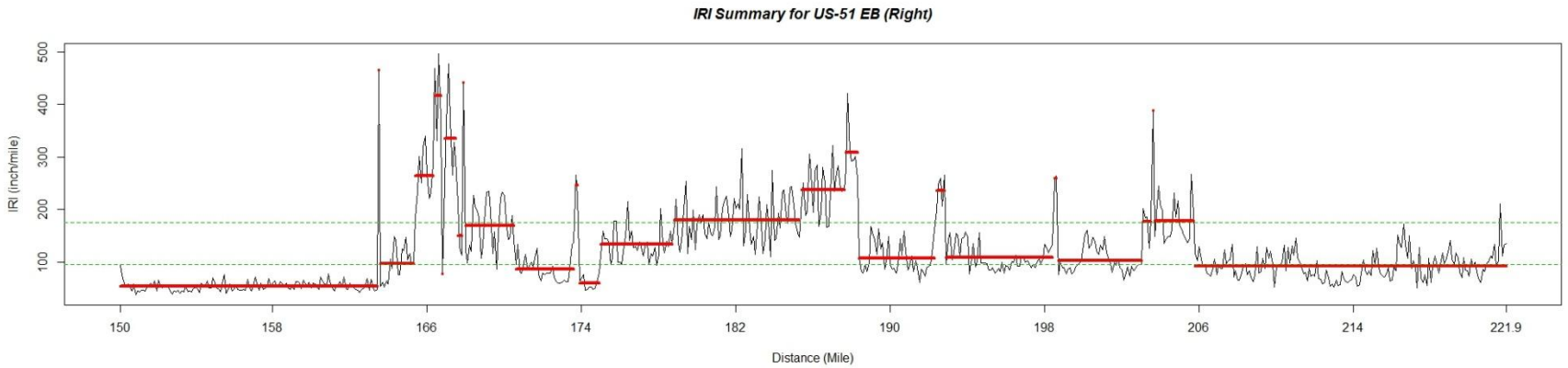

Figure 6.6 IRI and PELT Segmentation for US-51 East Bound

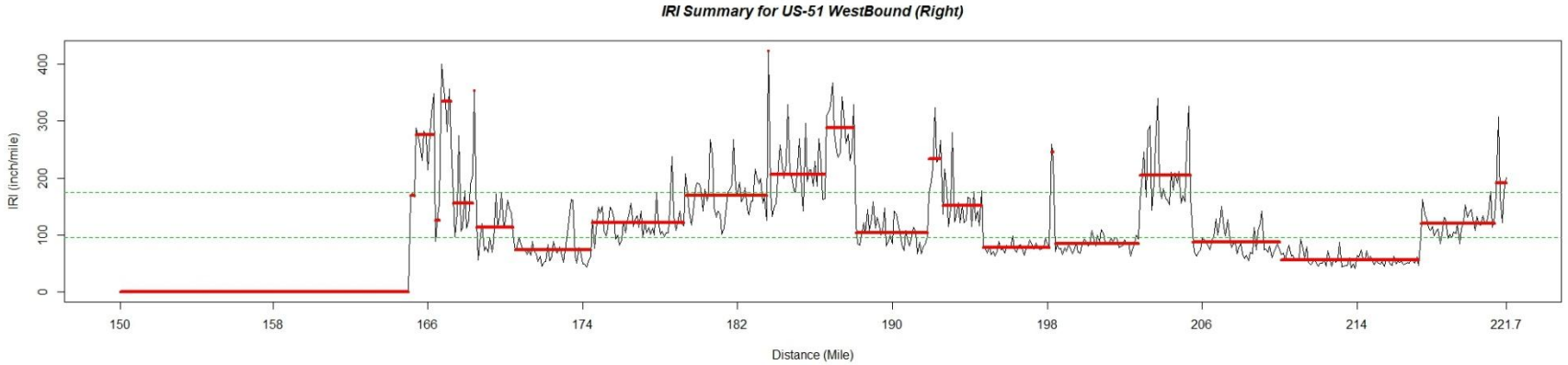

Figure 6.7 IRI and PELT Segmentation for US-51 West Bound

6.4 Rutting Analysis

Similarly, rutting in the left and right wheelpaths are calculated in inches for each 0.1-mile pavement segment for the six roadways (three highways for both directions), as shown from Figure 6.8 to Figure 6.13. PELT changepoints are determined for each roadway. Rutting data are not included for rigid PCC pavement sections in the figures, which are represented with zero rutting values.

Assuming rutting depths of 0.25 inches and 0.75 inches are the thresholds to classify pavement into "good", "moderate", and "poor" rutting conditions, most majority of the highways have rutting less than 0.25 inches, which are classified as “good” rutting condition. It is also observed that the rutting in the left and right wheelpaths and in two directions of the same roadway show similar trend.

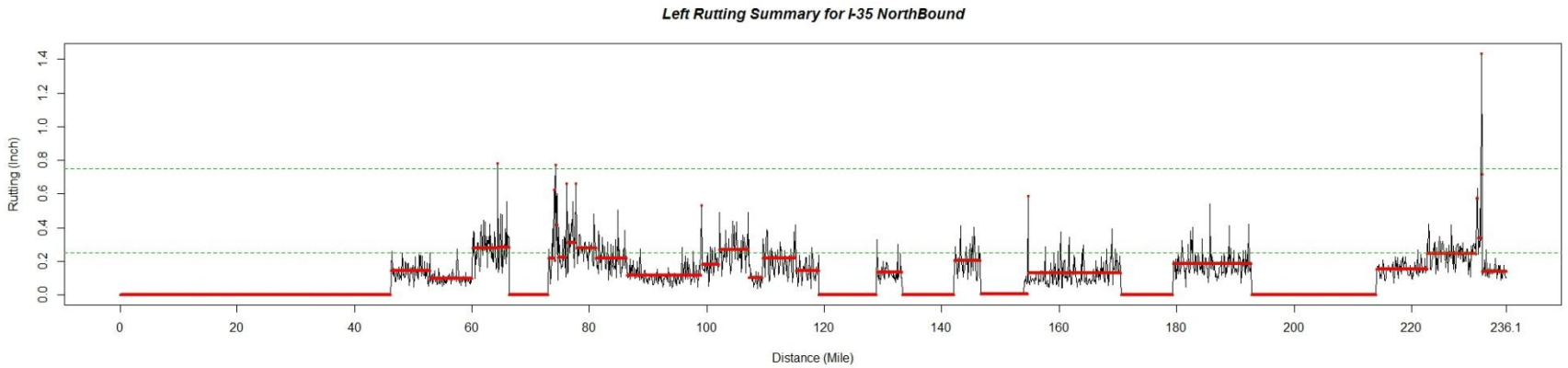

(a) Left Wheelpath

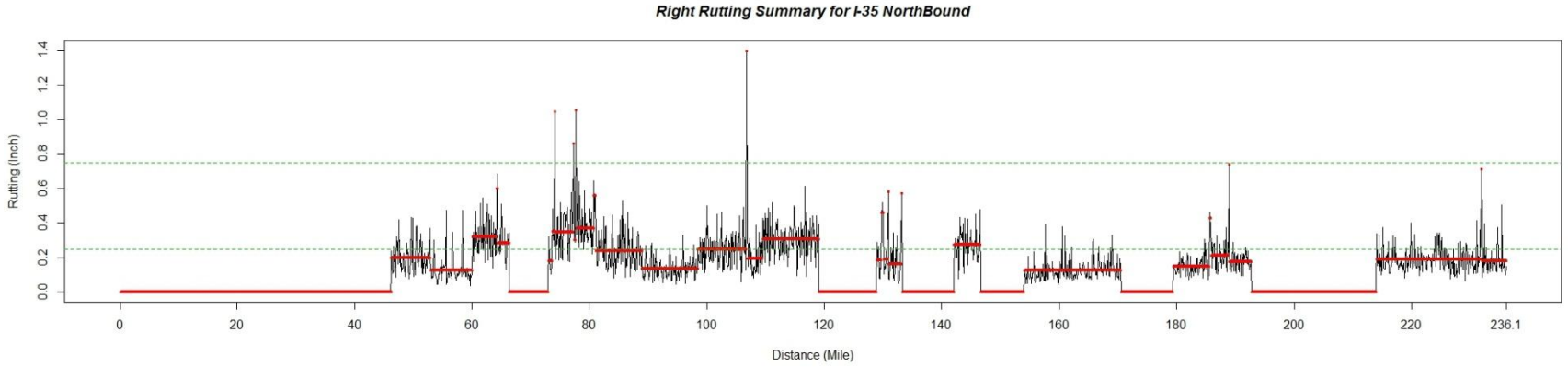

(b) Right Wheelpath

Figure 6.8 Rutting and PELT Segmentation for I-35 North Bound

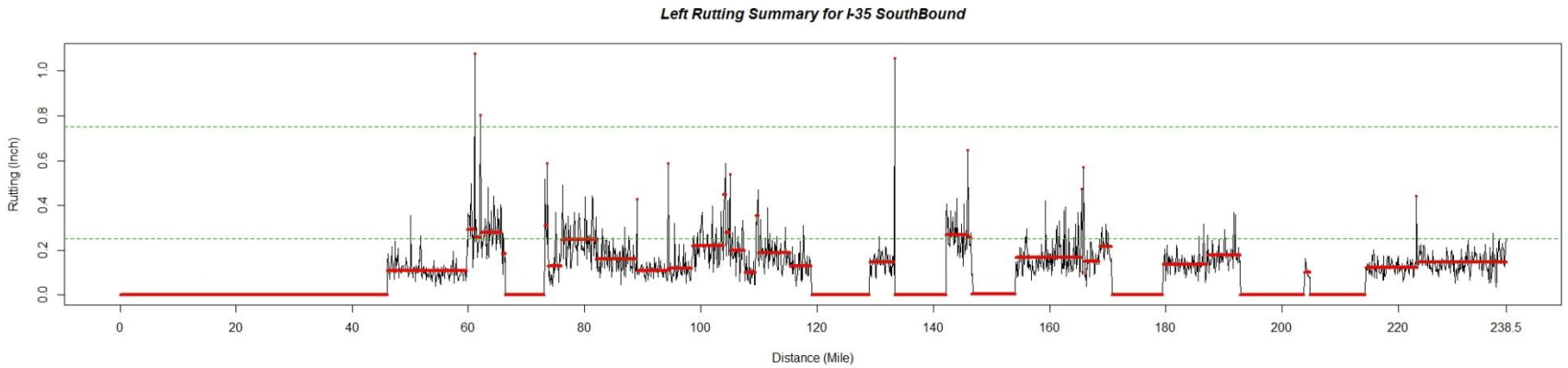

(a) Left Wheelpath

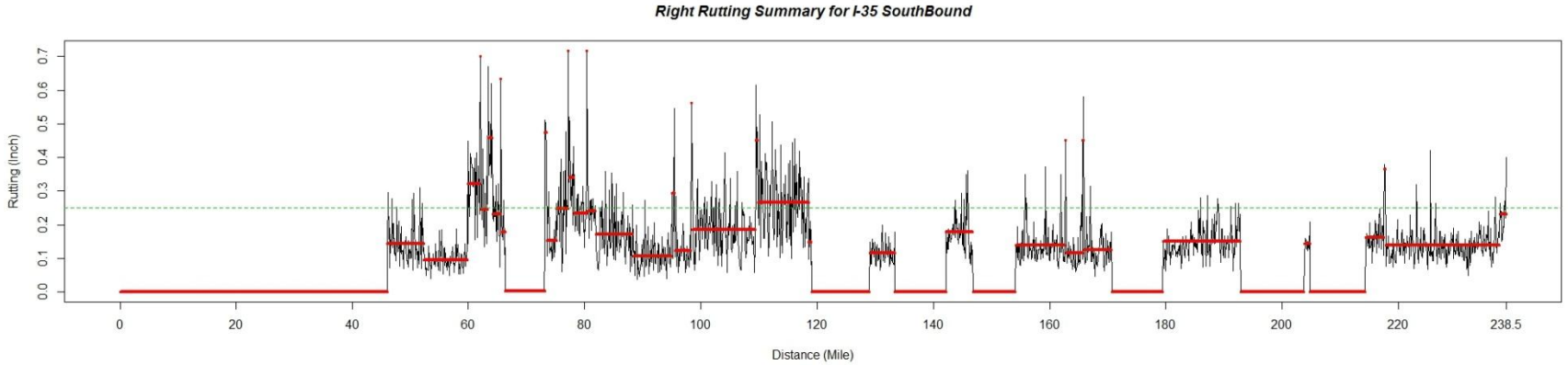

(b) Right Wheelpath

Figure 6.9 Rutting and PELT Segmentation for I-35 South Bound

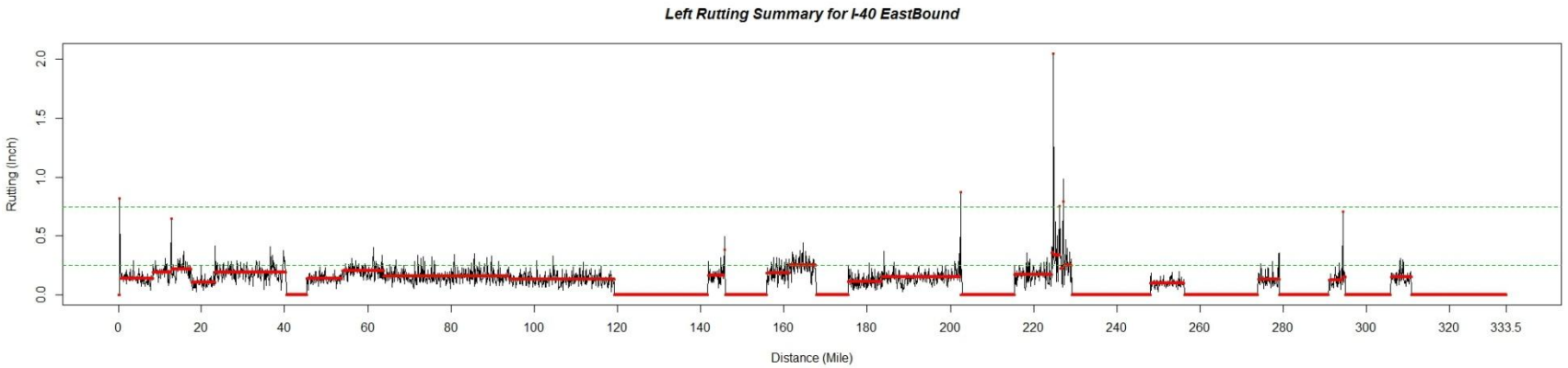

(a) Left Wheelpath

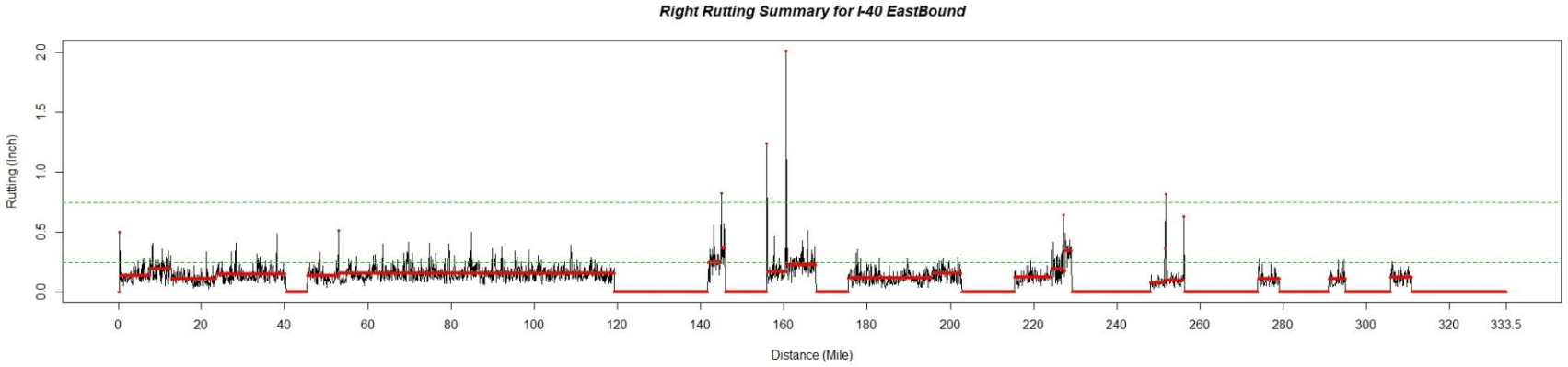

(b) Right Wheelpath

Figure 6.10 Rutting and PELT Segmentation for I-40 East Bound

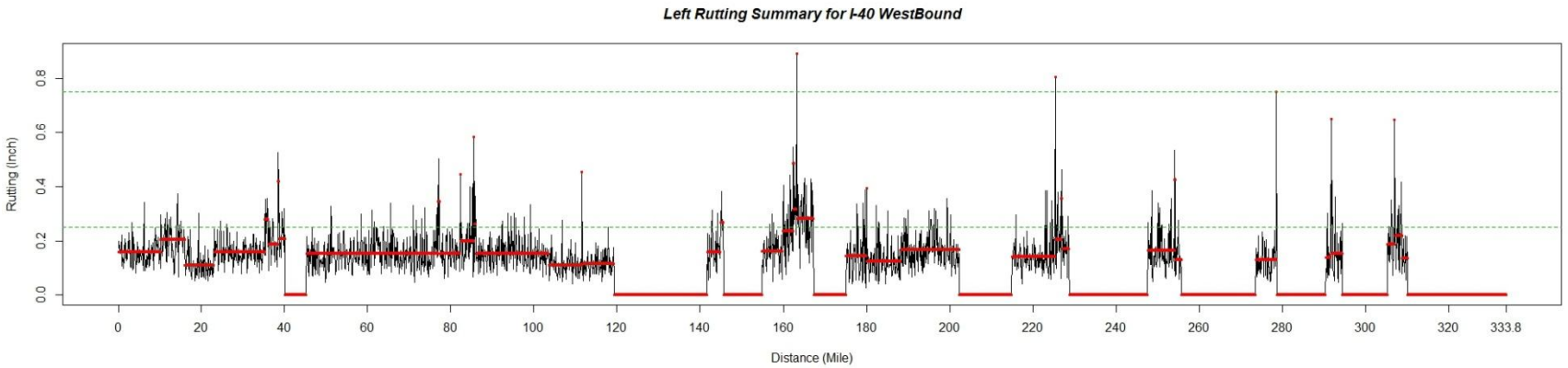

(a) Left Wheelpath

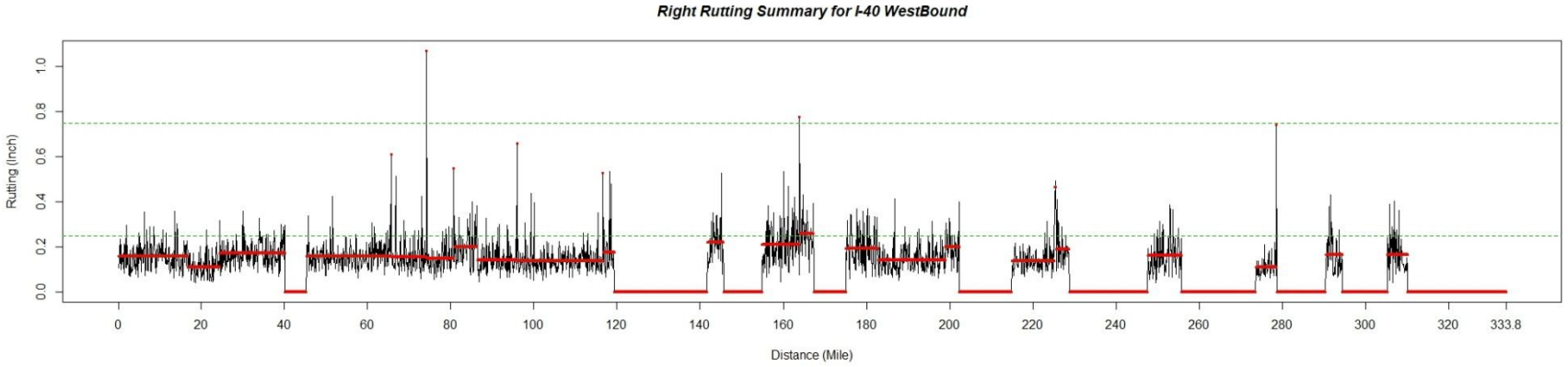

(b) Right Wheelpath

Figure 6.11 Rutting and PELT Segmentation for I-40 West Bound

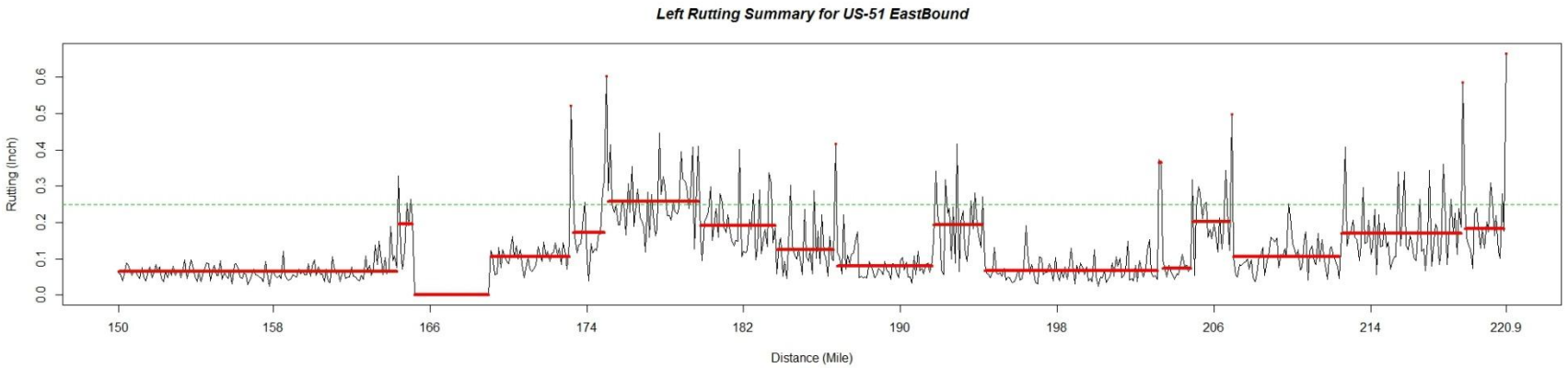

(a) Left Wheelpath

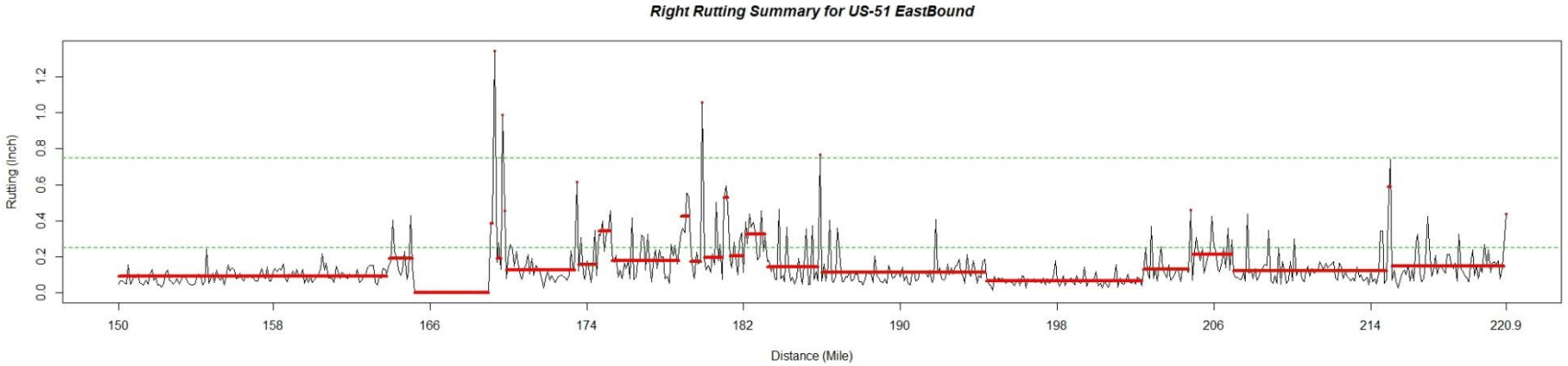

(b) Right Wheelpath

Figure 6.12 Rutting and PELT Segmentation for US-51 East Bound

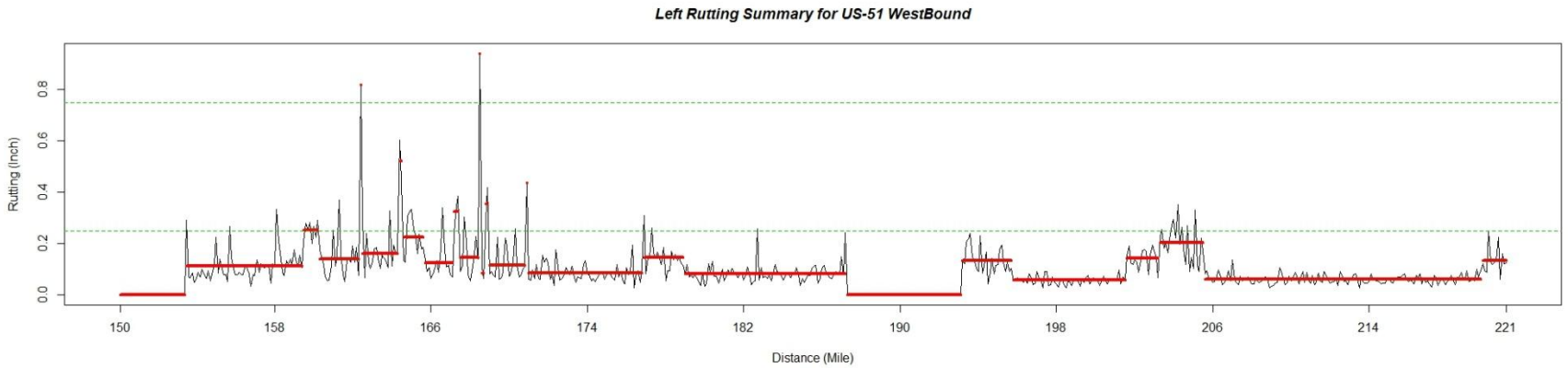

(a) Left Wheelpath

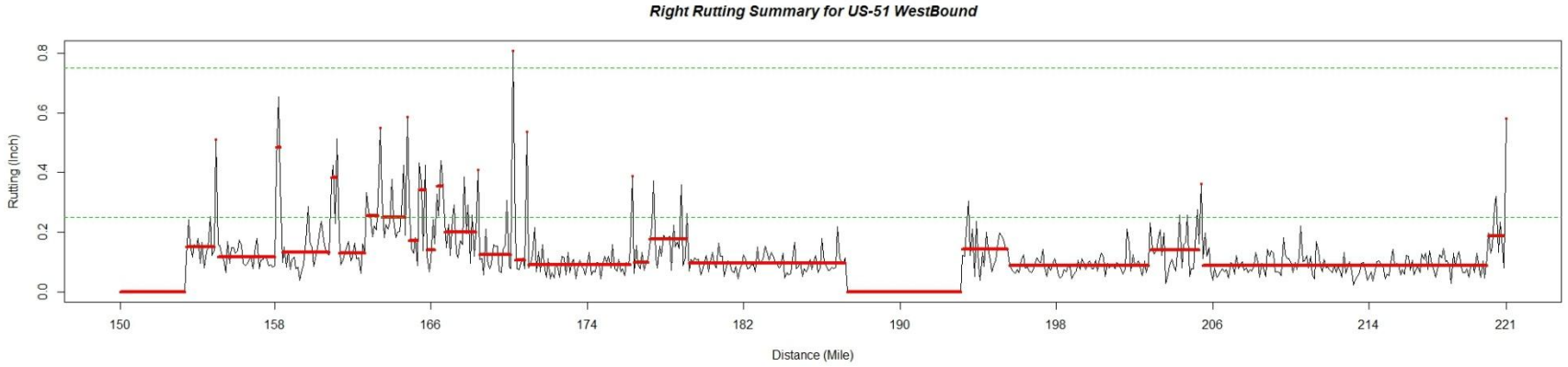

(b) Right Wheelpath

Figure 6.13 Rutting and PELT Segmentation for US-51 West Bound

6.5 Alligator Cracking Analysis

In order to produce manageable results, only fatigue cracking is investigated in this project, which is estimated from pattern cracking derived from PP 67-10 results in both wheelpaths and reported as the percentage of the wheelpath areas. Fatigue cracking in the left and right wheelpaths are calculated for each 0.1-mile pavement segment for the six roadways, as shown from Figure 6.14 to Figure 6.19. PELT changepoints are determined for each roadway. The figures provide decision makers with visuals where cracks have been developed on pavement surfaces.

Assuming fatigue cracking of 5% and 25% of wheelpath areas are the thresholds to classify pavement into "good", "moderate", and "poor" cracking conditions, most majority of the highways have fatigue cracking less than 5%, which are classified as “good” cracking condition. It is also observed that the cracking in the left and right wheelpaths and in two directions of the same roadway show similar trends.

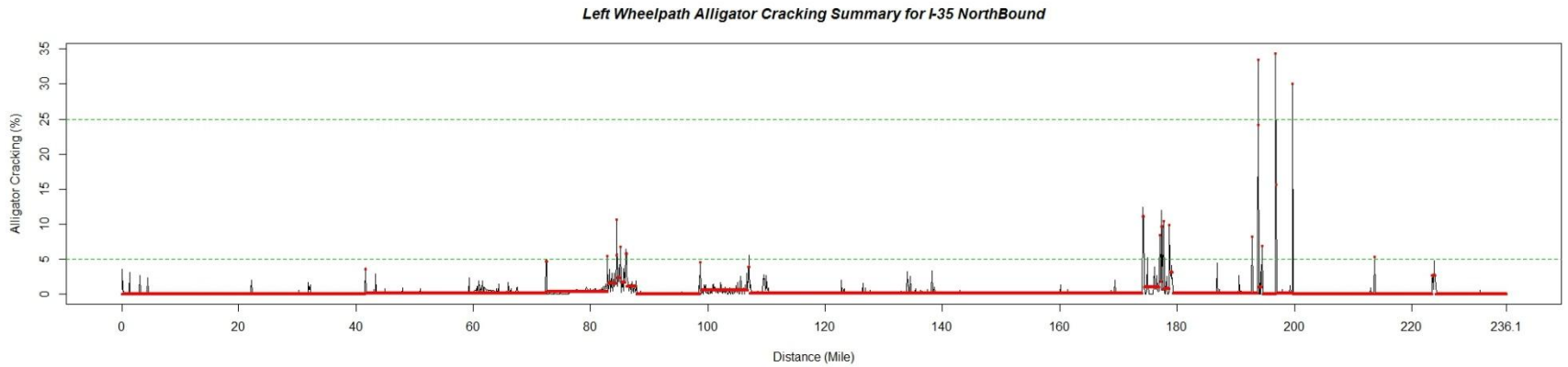

(a) Left Wheelpath

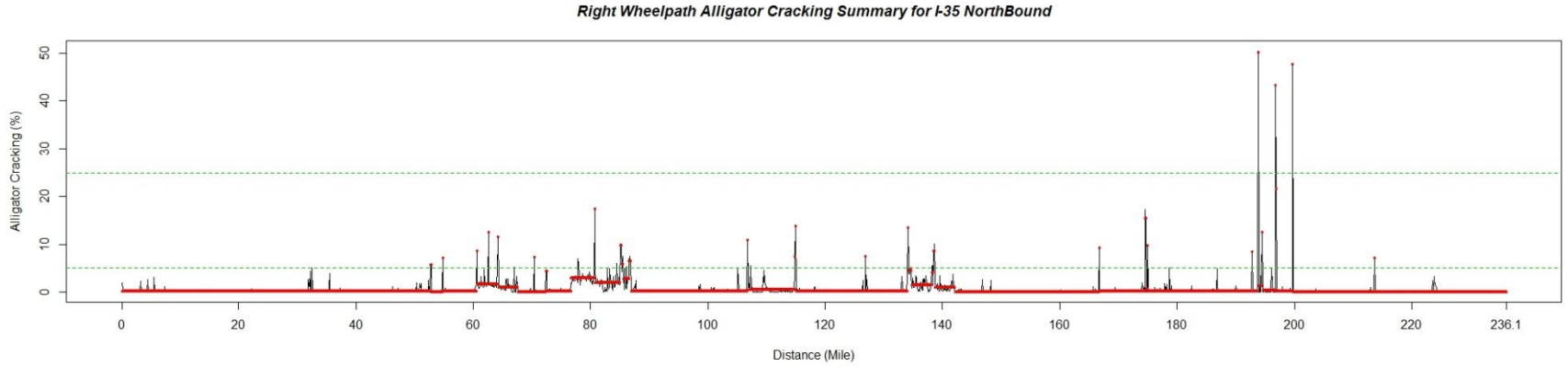

(b) Right Wheelpath

Figure 6.14 Alligator Cracking and PELT Segmentation for I-35 North Bound

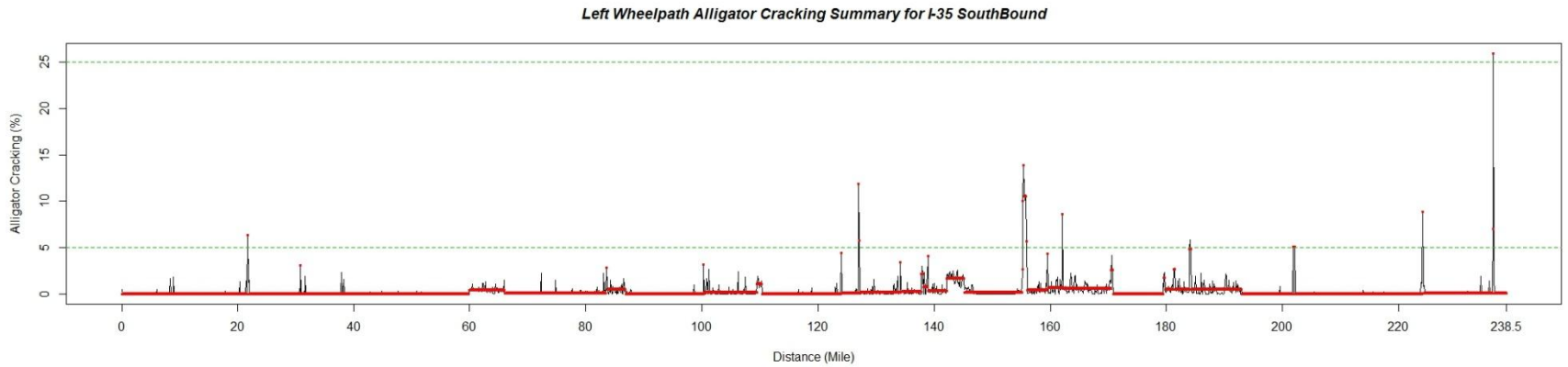

(a) Left Wheelpath

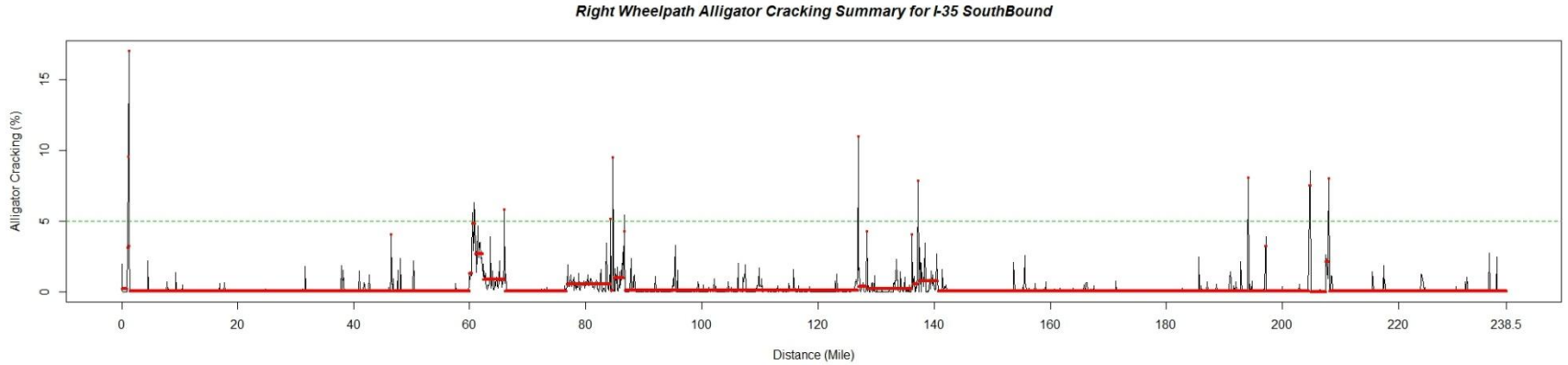

(b) Right Wheelpath

Figure 6.15 Alligator Cracking and PELT Segmentation for I-35 South Bound

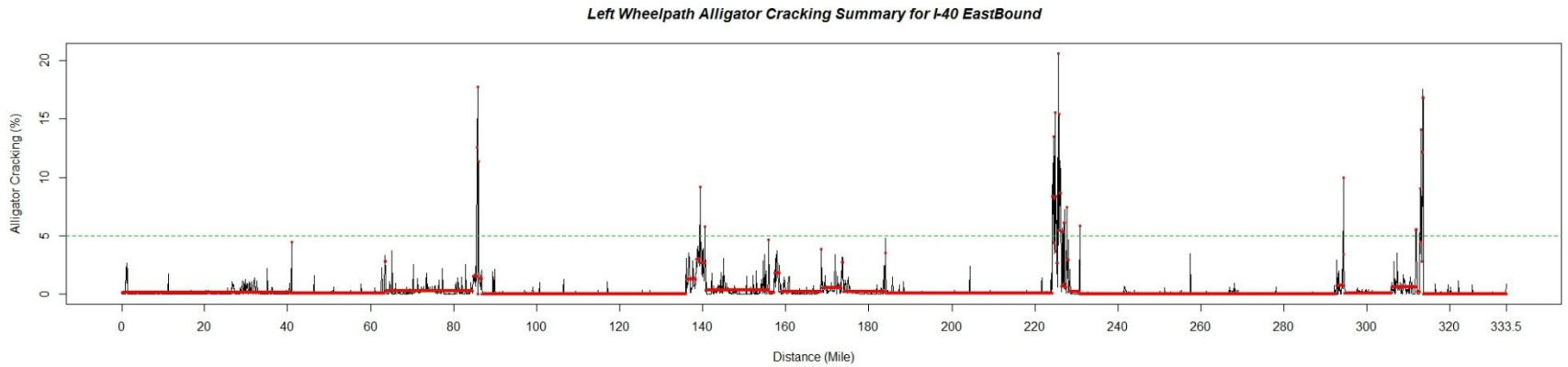

(a) Left Wheelpath

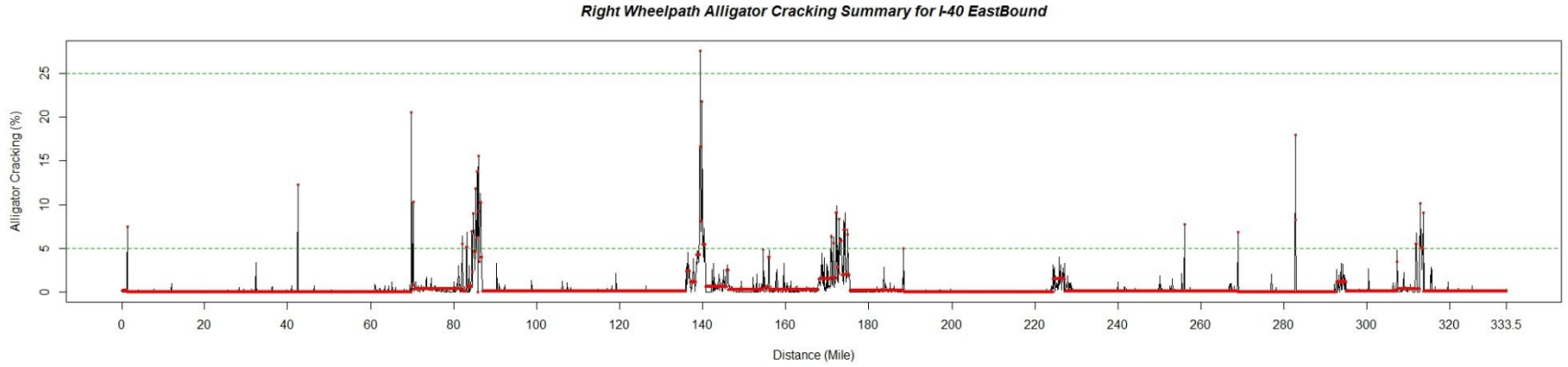

(b) Right Wheelpath

Figure 6.16 Alligator Cracking and PELT Segmentation for I-40 East Bound

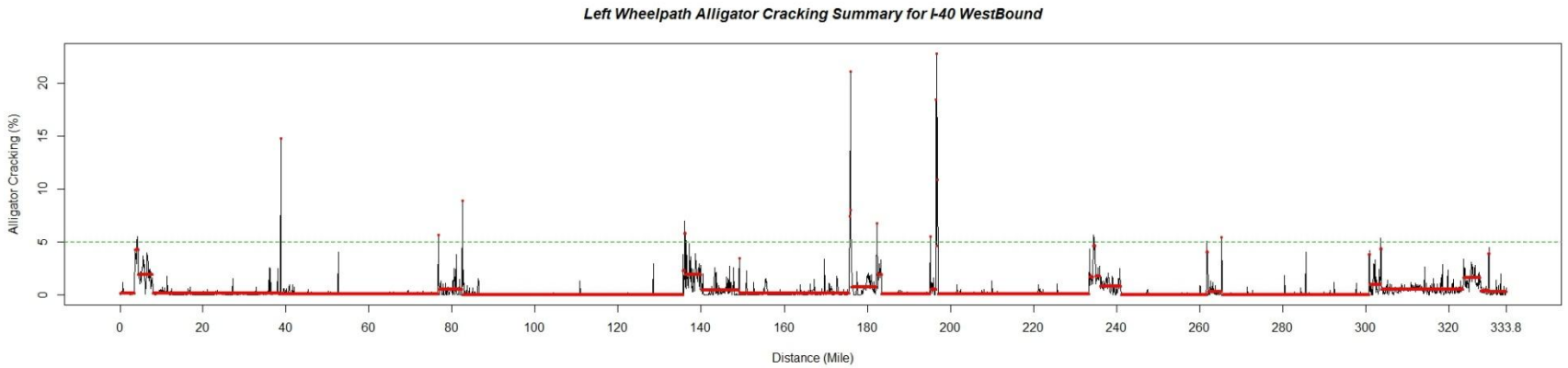

(a) Left Wheelpath

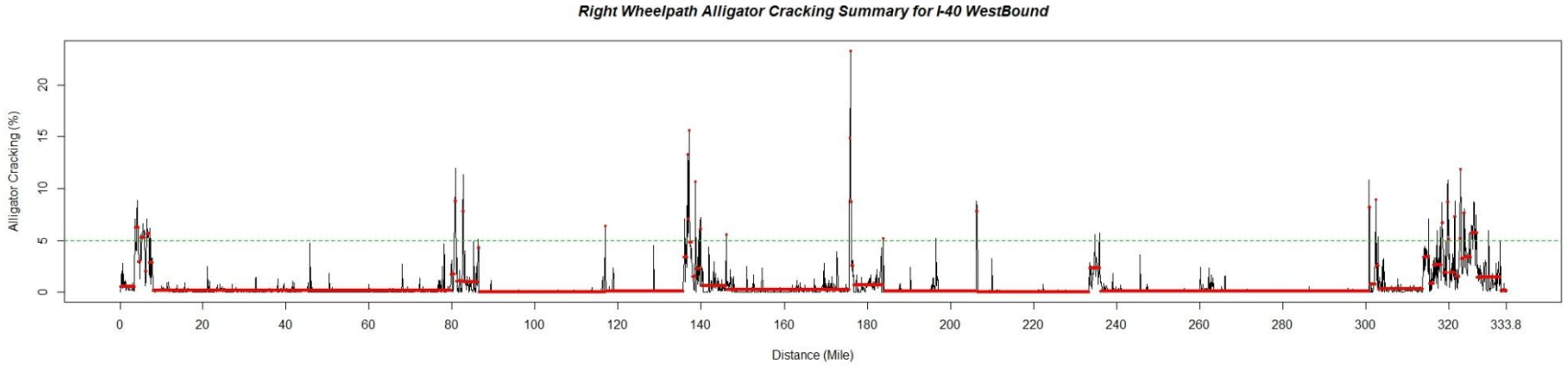

(b) Right Wheelpath

Figure 6.17 Alligator Cracking and PELT Segmentation for I-40 West Bound

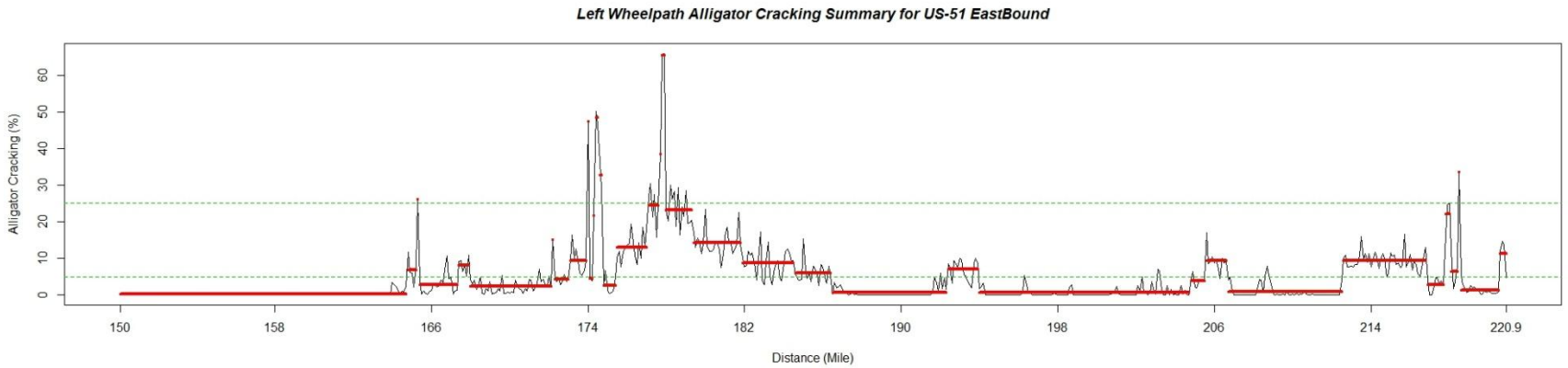

(a) Left Wheelpath

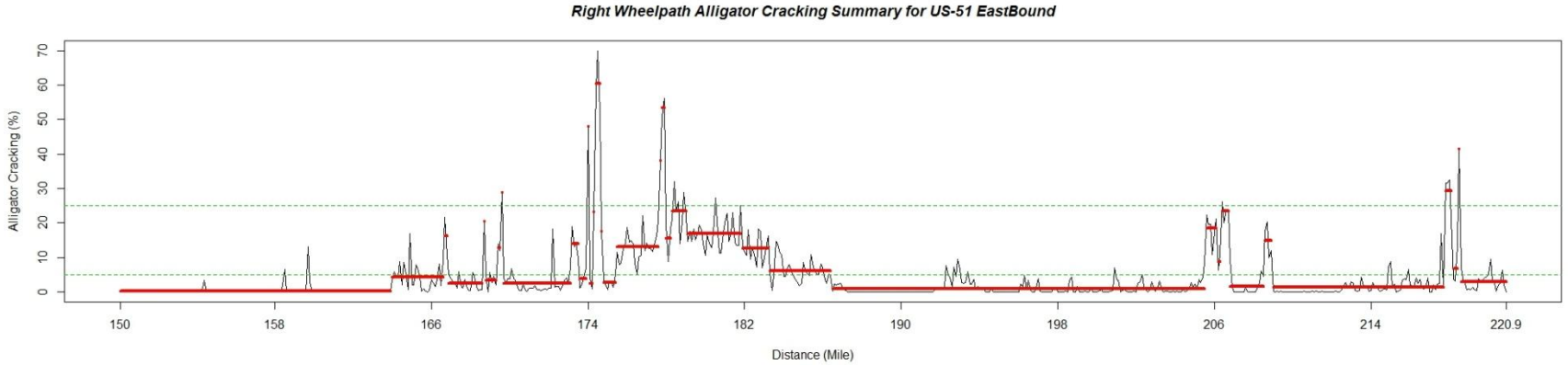

(b) Right Wheelpath

Figure 6.18 Alligator Cracking and PELT Segmentation for US-51 East Bound

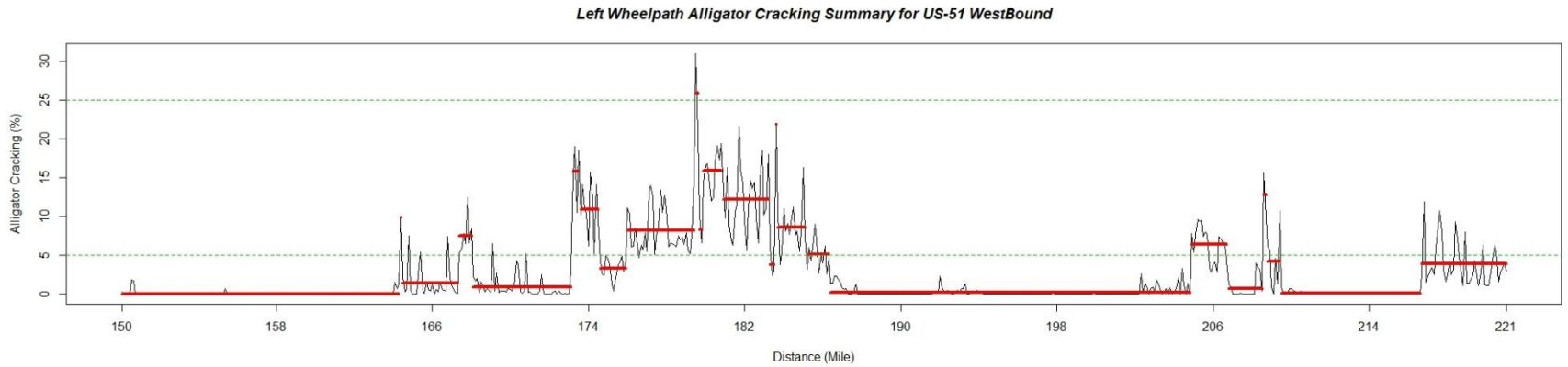

(a) Left Wheelpath

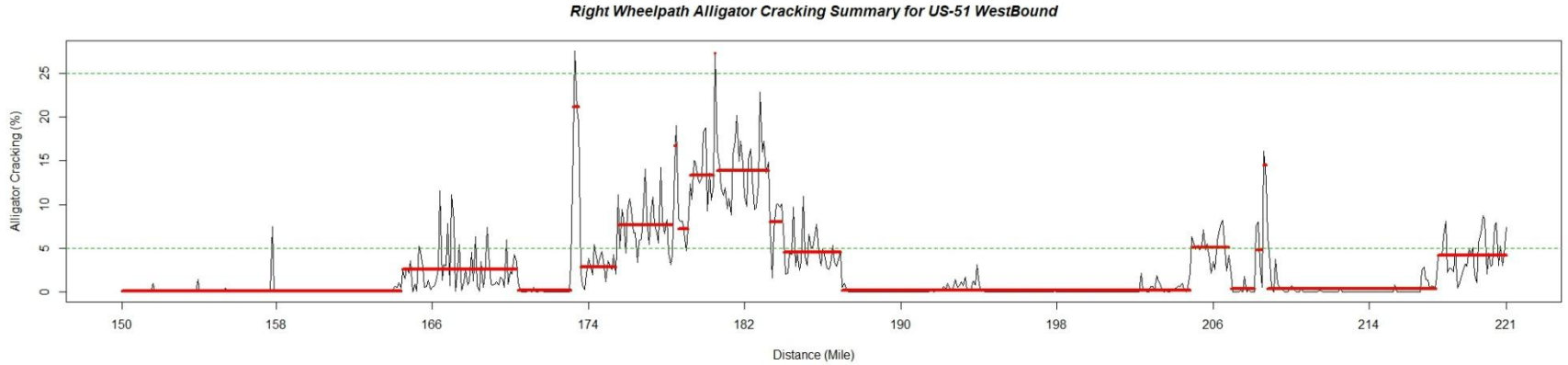

(b) Right Wheelpath

Figure 6.19 Alligator Cracking and PELT Segmentation for US-51 West Bound

6.6 Hydroplaning Analysis

Predicted hydroplaning speeds are calculated for each 0.1-mile pavement segment for the six roadways, as shown from Figure 6.20 to Figure 6.25. Moderate rain intensity is used for hydroplaning prediction. PELT changepoints are determined for each roadway.

Assuming predicted hydroplaning speed 5 mph higher and 15 mph lower than the posting speed limits are the thresholds to classify pavement into "good", "moderate", and "poor" safety conditions, most majority of the highways have predicted hydroplaning speeds between 55mph and 75mph, which are classified as "moderate" safety conditions. In case of moderate rain, driving at posted or higher speed will be subjected to hydroplaning for most majority of the pavement sections. Based on the prediction results, several segments have predicted hydroplaning speeds lower than 60mph.

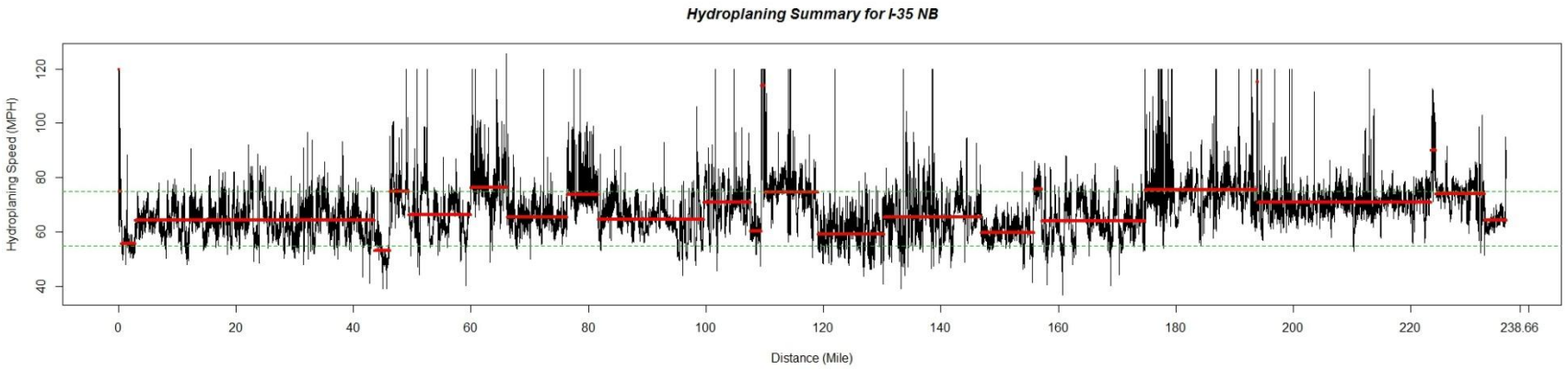

Figure 6.20 Hydroplaning Speeds and PELT Segmentation for I-35 North Bound

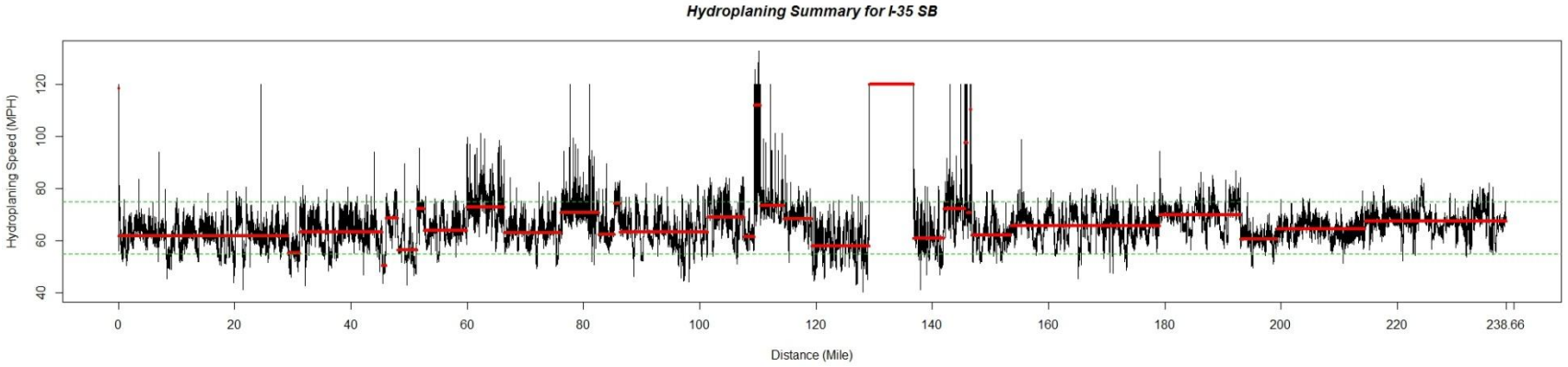

Figure 6.21 Hydroplaning Speeds and PELT Segmentation for I-35 South Bound

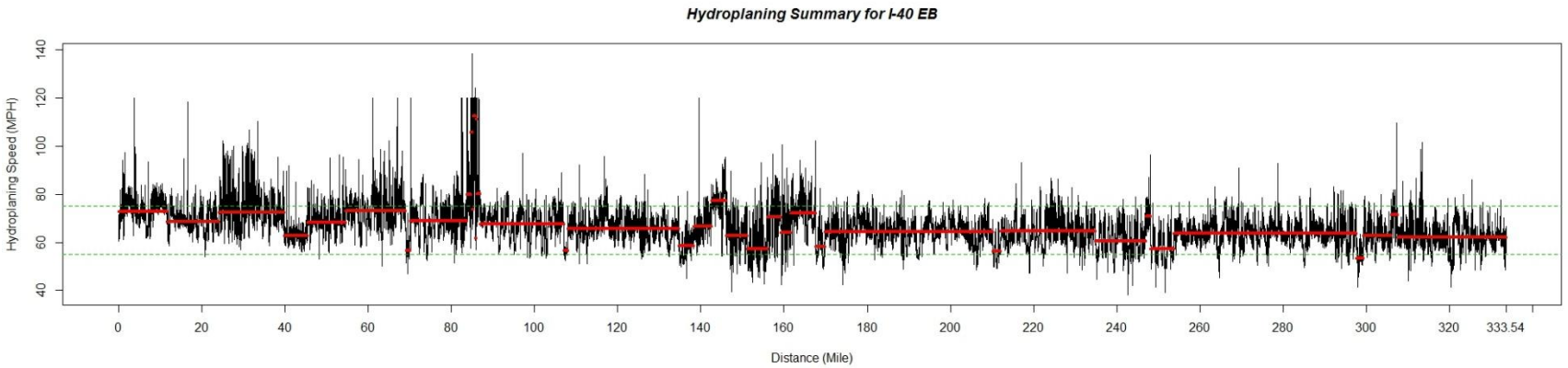

Figure 6.22 Hydroplaning Speeds and PELT Segmentation for I-40 East Bound

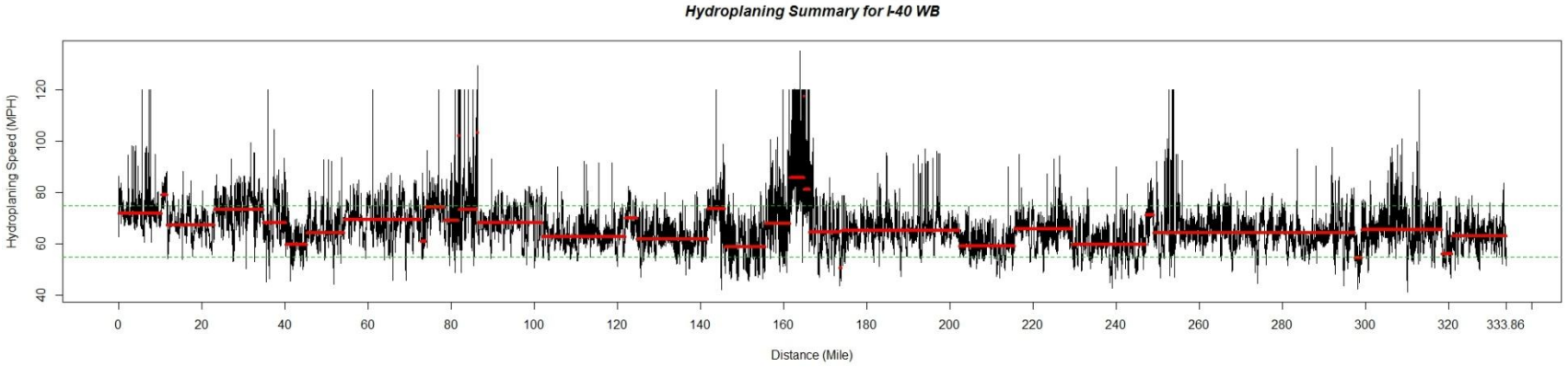

Figure 6.23 Hydroplaning Speeds and PELT Segmentation for I-40 West Bound

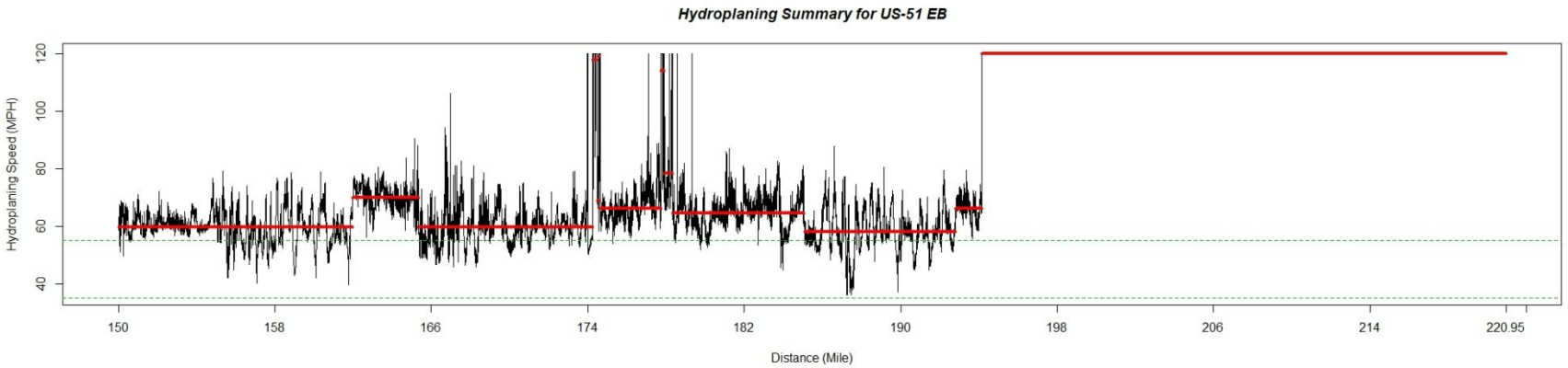

Figure 6.24 Hydroplaning Speeds and PELT Segmentation for US-51 East Bound

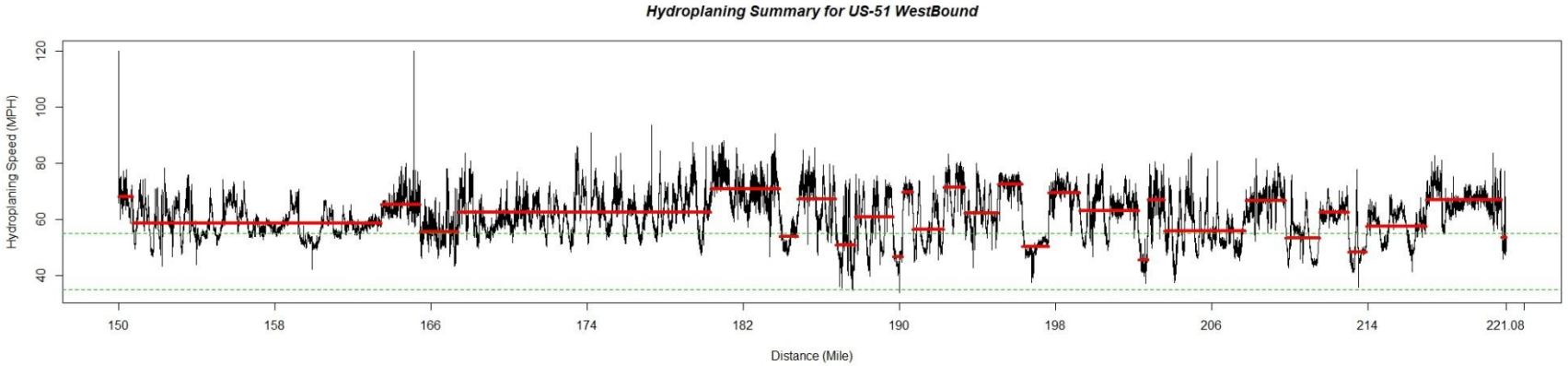

Figure 6.25 Hydroplaning Speeds and PELT Segmentation for US-51 West Bound

6.7 Discussions

Even though the two interstate highways (I-35 and I-40) in both directions are considered to be in "good" condition for most majority of pavement surfaces according to IRI, rutting, and estimated fatigue cracking, most pavement segments have "moderate" safety conditions based on predicted hydroplaning speeds. In other words, no roughness, rutting, and cracking issues are found on most pavements, while hydroplaning related safety hazards are presented for most majority of pavement locations if users drive at posted or higher speeds during moderate rain. The dynamic segmentation results can assist DOT decision makers to identify the locations where issues may be presented and evaluate pavement performance in a comprehensive manner from various perspectives.

For the interstates, it is observed that the pavement performance indicators in the left and right wheelpaths and in two directions of the same roadway show similar trends. However, such trends for state highway 51 are not as distinctive. In many occasions, differences and variations are clearly seen in different directions.

CHAPTER 7 OTHER APPLICATIONS OF PAVEVISION3D ULTRA

7.1 Bridge Deck Evaluation

7.1.1 Introduction

As requested by ODOT Bridge Office, the OSU research team performed surface condition survey for two bridge decks at highway speed using the 1mm 3D laser imaging technology. The two bridges identified in the initial phase include the North Canadian River Bridge on Interstate 40 in Oklahoma City and Boomer Lake Bridge in Stillwater Oklahoma.

The North Canadian River Bridge (Figure 7.1) has three lanes in each direction with a bridge length of approximately 800-ft (850-ft including approach slabs). The bridge portion including approach slab is shown in red. The two 300-ft long new asphalt pavement transition segments are shown in blue, between the bridge deck and the normal pavement surfaces (shown in black). The 1mm 3D data were collected at 60mph.

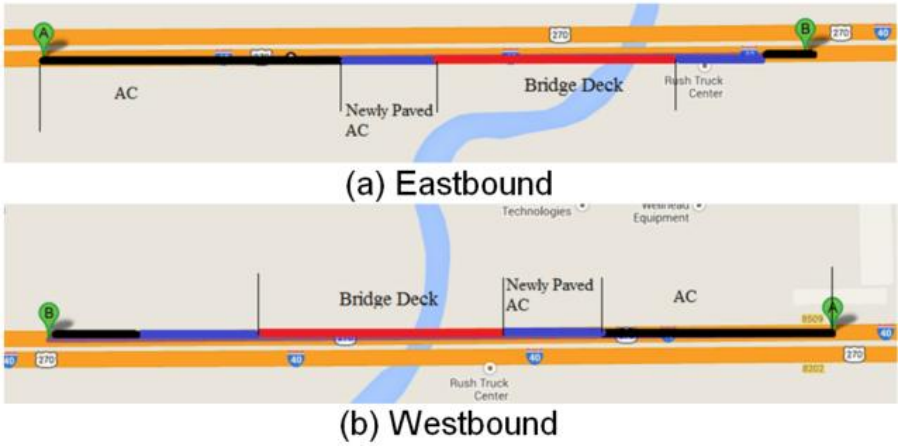

Figure 7.1 North Canadian Bridge Deck

The second bridge deck is located in Stillwater over the Boomer Creek on State Highway 177 (Figure 7.2). The survey was conducted in April 2014 covering all the four lanes in both directions. Both 1mm 3D data collected at highway posted speed (35mph) and 0.25mm resolution data collected at lower speed (15mph) were obtained. In total 8 passes of data collections were performed. Each pass covered 900ft of pavement surface in length, with about 140-ft of bridge deck, 344-ft and 315-ft of asphalt pavement segments before the deck in South and North Bound respectively, 425-ft and 454-ft of asphalt pavement surfaces after the deck for the South and North Bound.

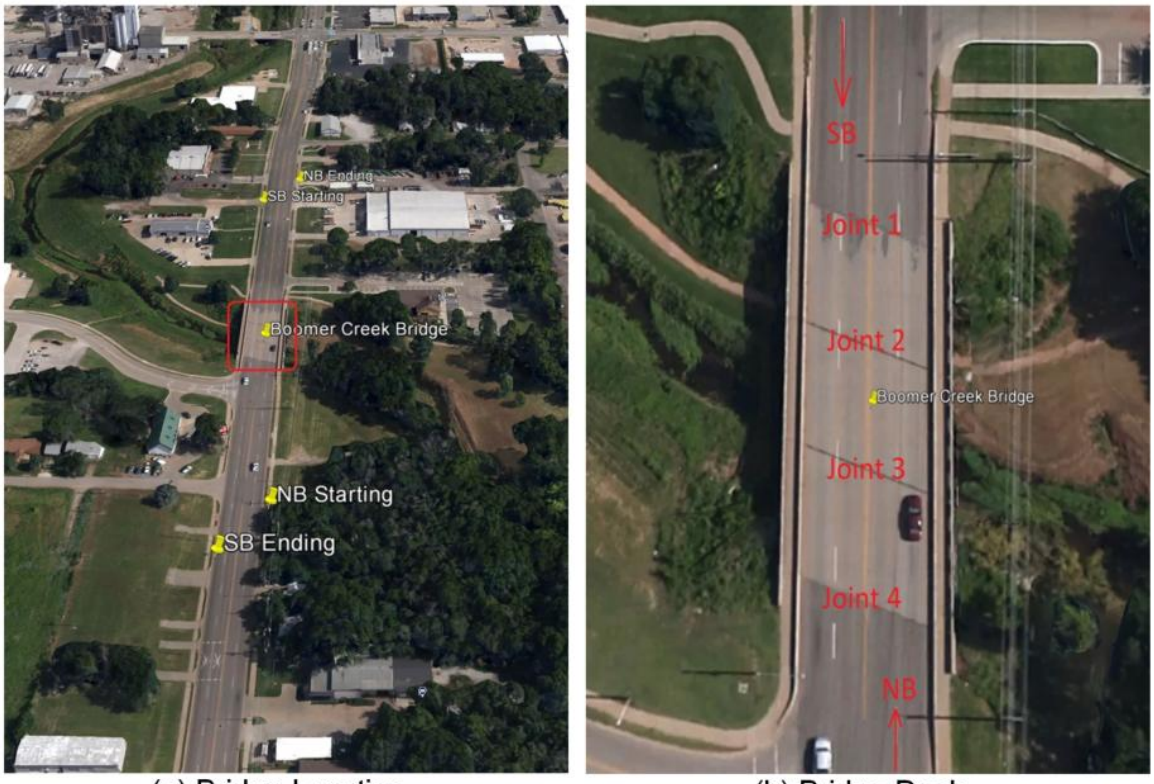

(a) Bridge Location (b) Bridge Deck

Figure 7.2 Stillwater Boomer Creek Bridge

7.1.2 Surface Cracking

7.1.2.1 North Canadian River Bridge

For the North Canadian River Bridge, few cracks are observed on the normal asphalt pavement surface. No crack is found on the bridge decks and the newly overlaid transition segments. An example of 1mm 3D longitudinal crack image is shown in Figure 7.3. This crack can be zoomed in and rotated for users to explore the height and the shape of the crack. The crack width and depth can be measured automatically or manually using the longitudinal and transverse profiling toolbars provided in MHIS.

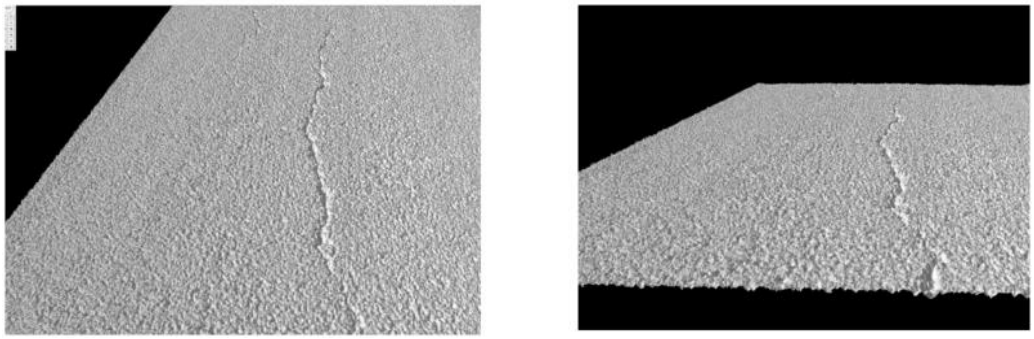

Figure 7.3 1mm 3D Longitudinal Crack on Bridge Deck

7.1.2.2 Boomer Creek Bridge

There are extensive cracks on the approaching and departing pavement surfaces. The 1mm 3D data are automatically processed using ADA-3D. An example pavement surface with detected crack map is shown in Figure 7.4. The same frame is demonstrated in Figure 7.5 in MHIS-3D.

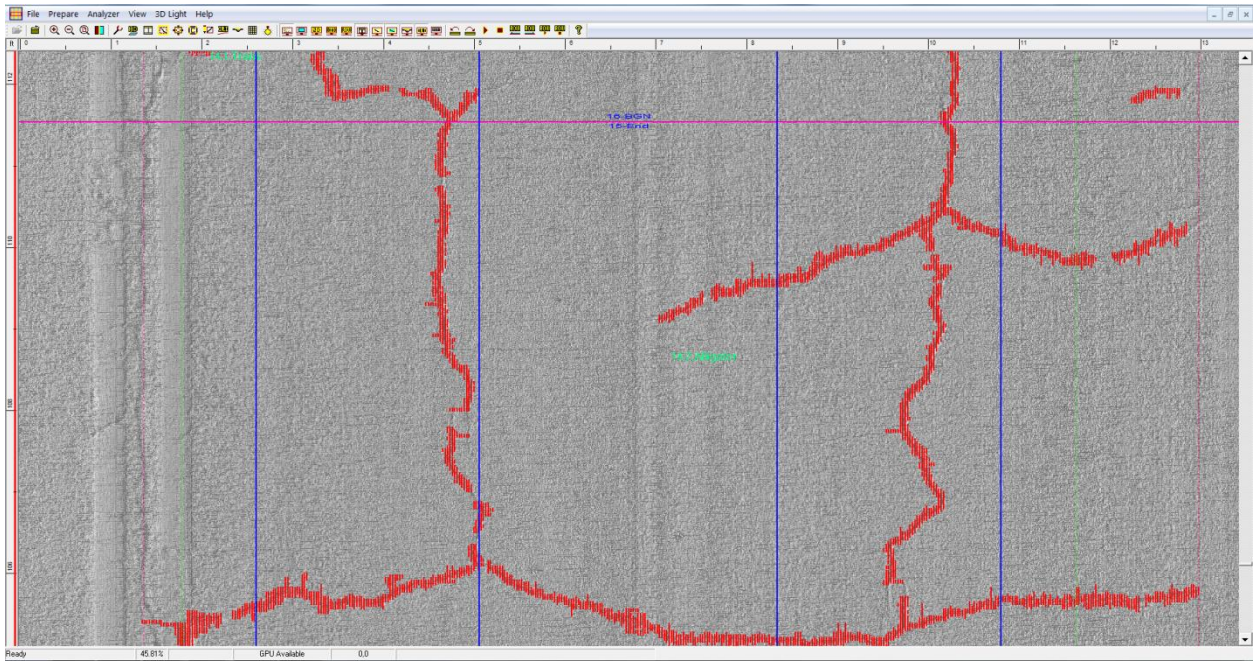

Figure 7.4 ADA-3D Crack Detection

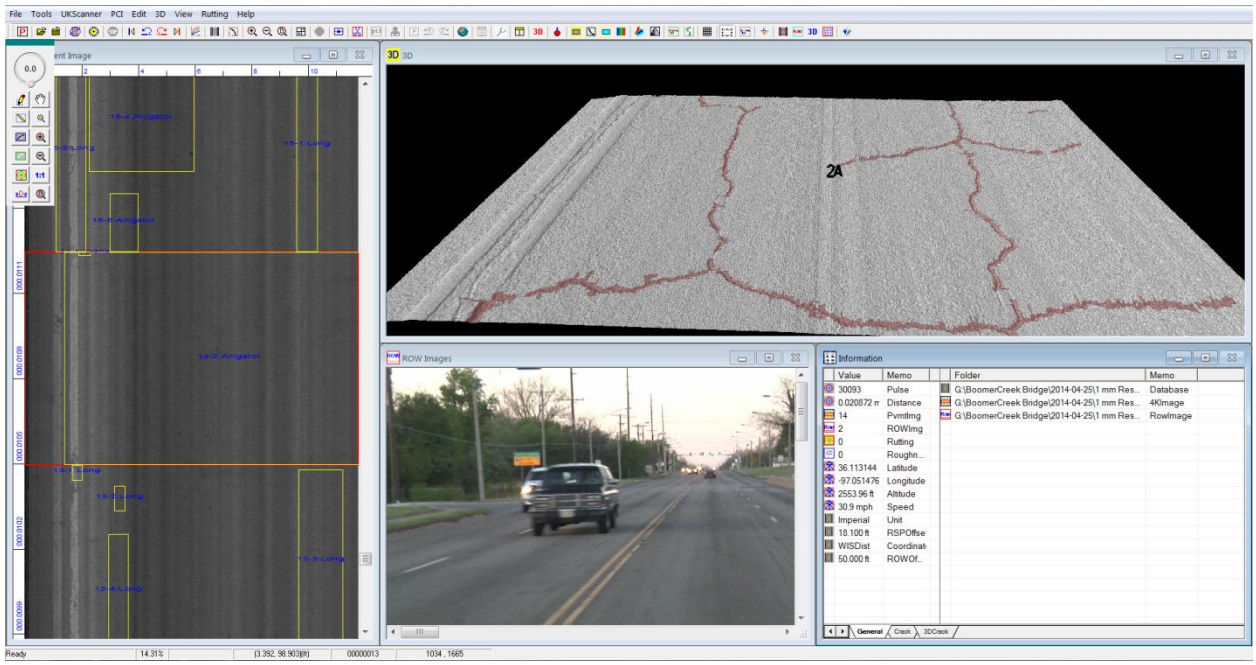

Figure 7.5 MHIS-3D Crack Visualization

After the cracks are detected using ADA-3D, they are reported in accordance with the AASHTO Protocol PP67-10. The crack length and width for each crack type

on the pavement surface are summarized from ADA-3D. The results are demonstrated in Figure 7.6 for total crack length and Figure 7.7 for average crack width by image frame for the three cracking types. Each image frame has a dimension of 6.7ft (2048mm) in length and 13.4 ft (4096mm) in width. There are very few cracks on the bridge deck, while various longitudinal, transverse, and pattern cracking on the approaching and departing pavement sections. Many longitudinal cracks almost extent all the way across the entire image frame, whose lengths are larger than 5ft. Many cracks are 1/2 inches to 1.0 inch wide on the approaching and departing pavement sections.

Figure 7.8 and Figure 7.9 provide summarized cracking data for the three segments: approaching pavement, bridge deck, and departing pavement. Figure 7.10 demonstrates the aggregated cracking length and width for the entire pavement section for the four lanes at both directions. The following observations are obtained:

- There are more longitudinal cracks in non-wheelpath than those in wheelpath for both approaching and departing pavements.
- More pattern cracks are observed on departing pavement sections than those on approaching sections.
- North Bound and South Bound inner lanes have more longitudinal and transverse cracking, while North Bound outer and inner lanes have more pattern cracking.
- Transverse cracking has the least total amount for all the four lanes.
- Longitudinal crakes in general have wider width than the other two cracking types.

- South Bound inner lane and North Bound outer lane have slightly wider cracks than other lanes.

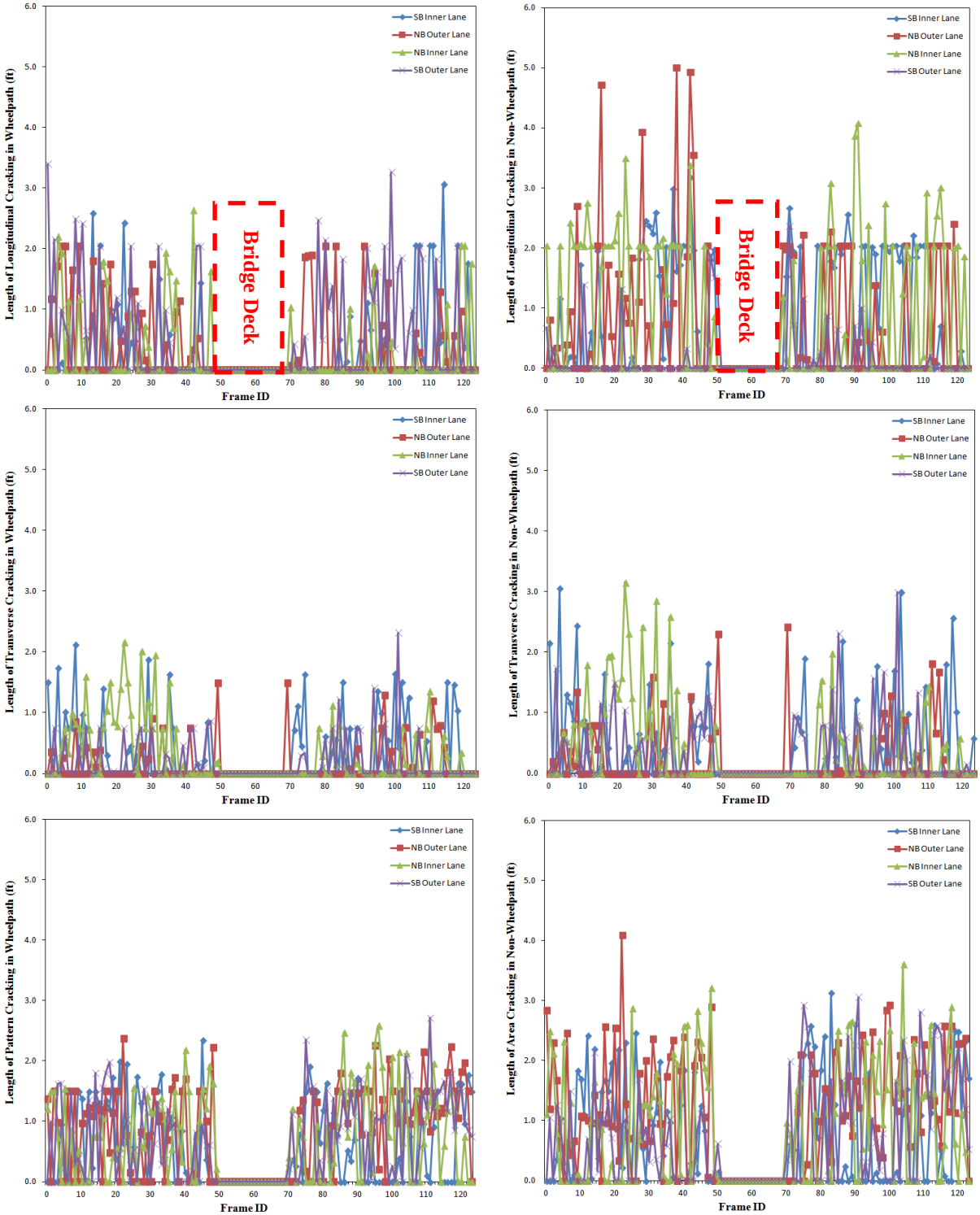

Figure 7.6 Total Crack Length by Image Frame

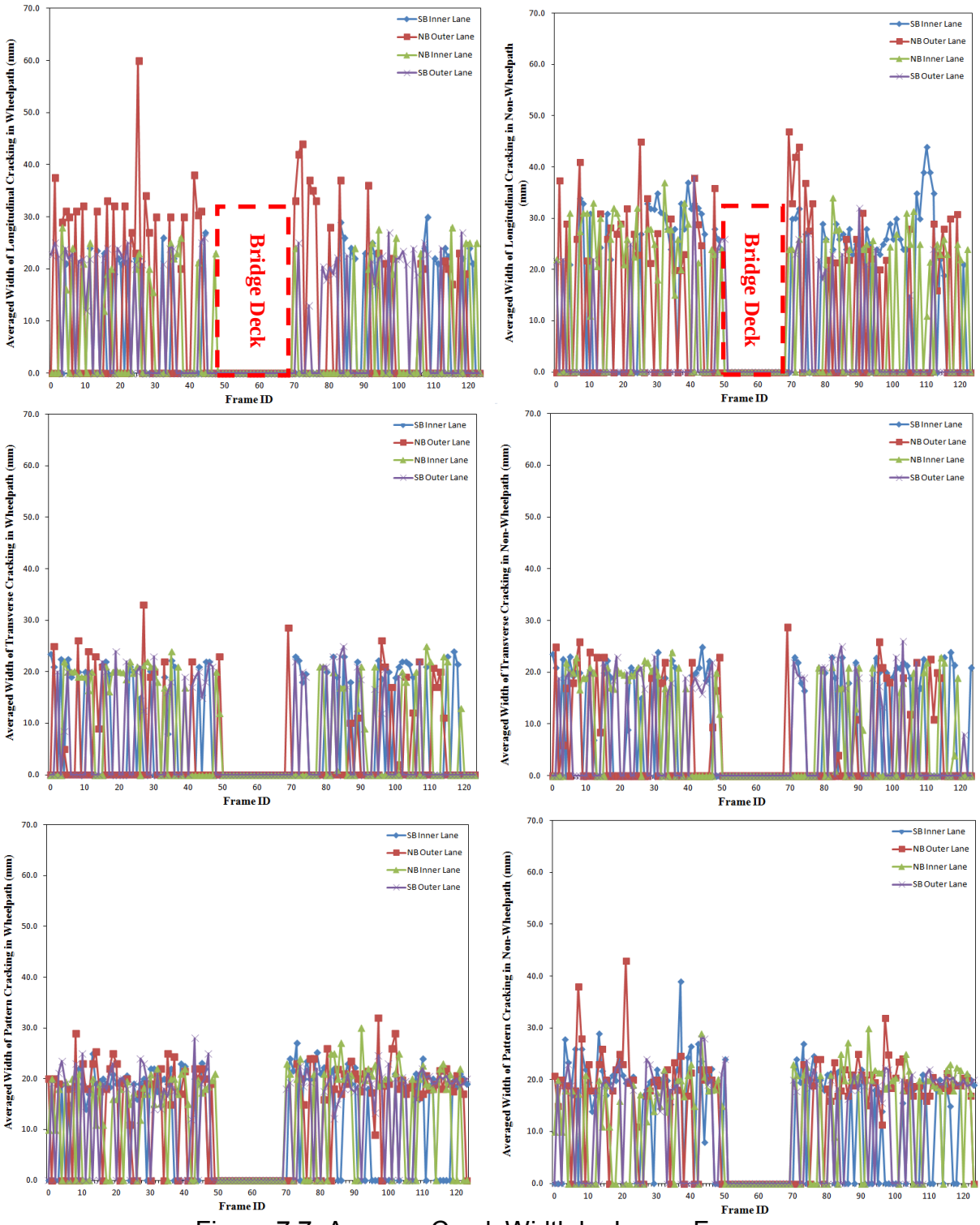

Figure 7.7 Average Crack Width by Image Frame

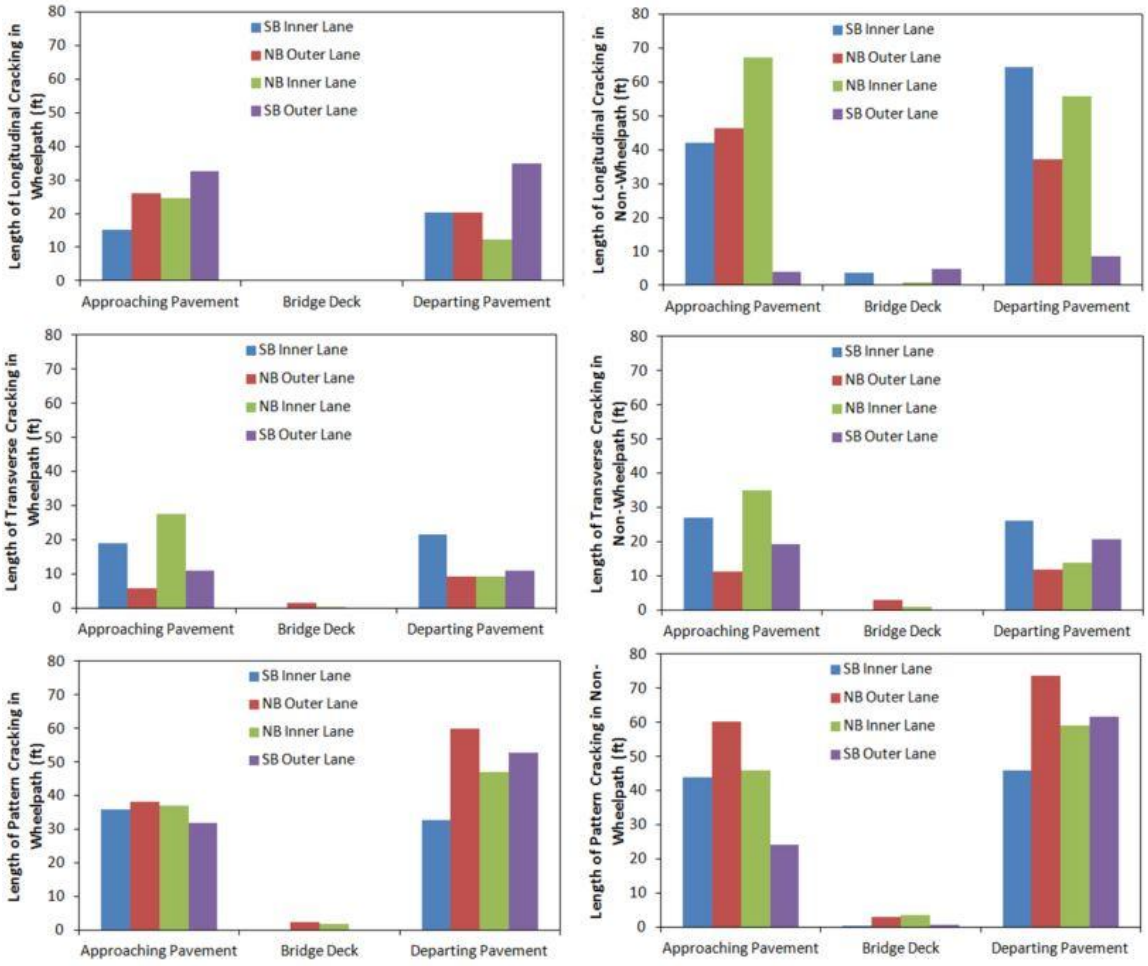

Figure 7.8 Total Crack Length by Pavement Section

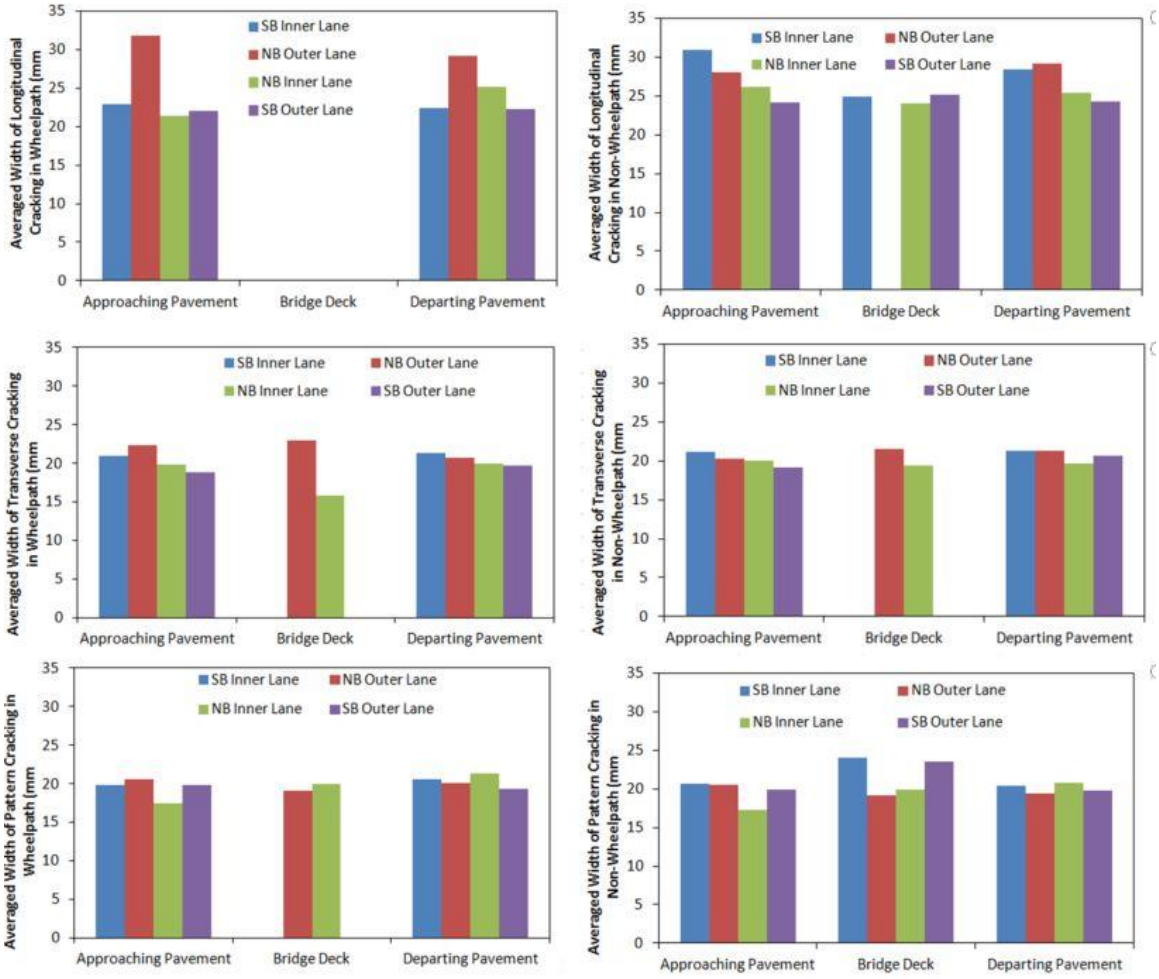

Figure 7.9 Average Crack Width by Pavement Section

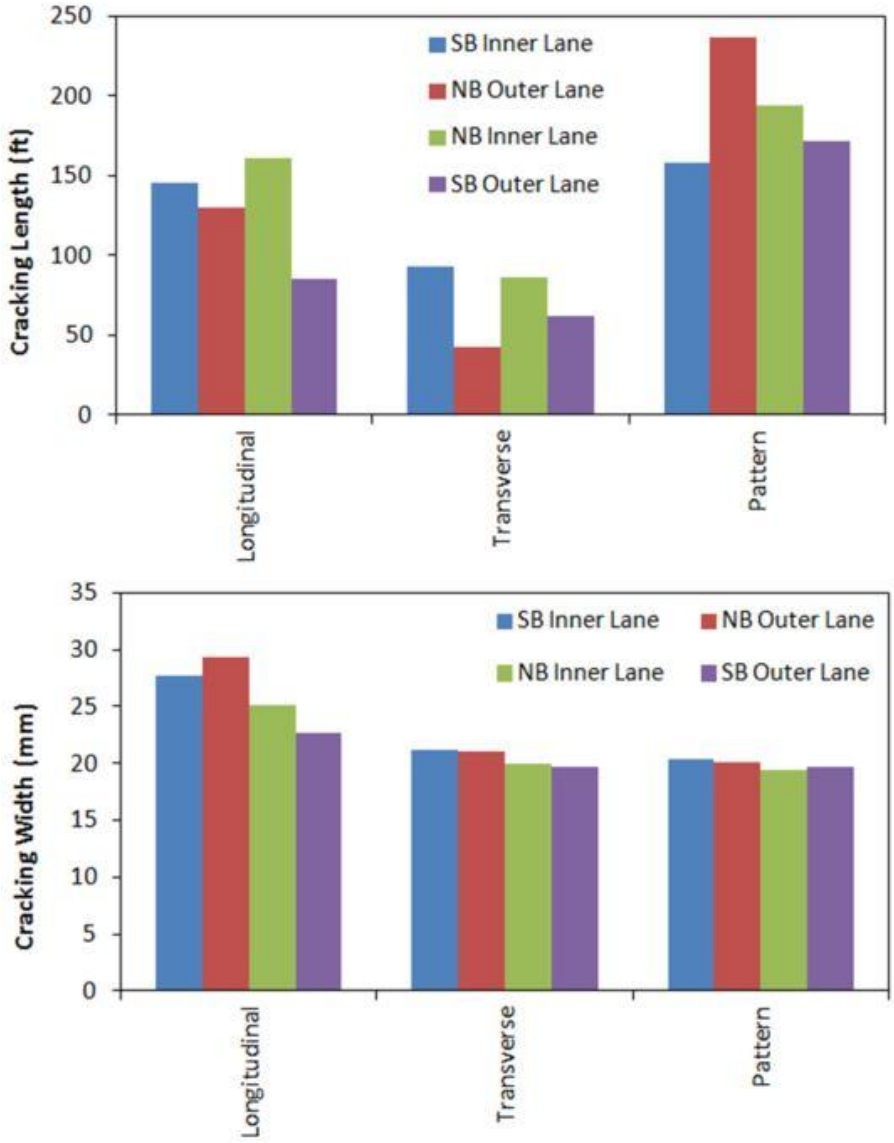

Figure 7.10 Summary Cracking Properties

7.1.3 Bridge Joint

7.1.3.1 North Canadian River Bridge

The 1mm data allow bridge engineers to evaluate joint conditions in details. An example joint on the West Bound of North Canadian River Bridge

deck is shown in Figure 7.11. The joint is demonstrated at four different scenarios for visualization. The vent holes are cleared shown on the data.

Bridge engineer can also investigate the joint from various directions and measure the shape and dimension of the joint with sealant. Figure 7.12 examines the same joint. The shapes and dimensions of the joints are taken from three locations. It can be seen that the shapes of the joint varies along the transverse direction, which can provide bridge engineers with visual and quantitative information to evaluate the condition of the joint and the sealant inside. In addition, it can be observed that there is distinctive height difference between the steel joint armor and the bridge deck.

7.1.3.2 Boomer Creek Bridge

There are four joints on the Boomer Creek bridge deck. All joints on four lanes are investigated. As a result, in total 16 joints are examined. For each joint, the 2D intensity image, 1mm 3D Range image at default lighting condition, rotated 1mm 3D Range image aiming to demonstrate specific joint problem(s), 1mm 3D intensity image, quarter millimeter 3D range image at default lighting direction, and rotated quarter millimeter 3D range images are provided, as shown from Figure 7.13 to Figure 7.28. Several distresses and damages are observed, as summarized in Table 7.1. Major problems include joint spalling, missing steel armor, bump at pavement bridge interface, popouts on bridge decks. In total approximately 26.52 square feet of spalling and 47.9 feet of missing steel armor are estimated. Drain holes and pavement cores are found on the bridge deck. It is found that coring work has been

conducted on the bridge. It is also observed that the first Joint at SB and the deck panel are partially covered by a thin layer of spilled asphalt mixture.

Table 7.1 Investigation of Bridge Deck Joints

Direction	Lane	Joint #	Spalling (square ft)	Missing Steel Armor (ft)	Interface Bump	Popouts	Other Features
SB	Outer	1	1.66		√	√	Spilled asphalt mixture on deck
		2	0.97			√	
		3	1.49			√	Coring
		4	2.93	7	√	√	
	Inner	1	2.81		√		
		2	2.13			√	
		3	1.34			√	
		4	3.02	14	√	√	
NB	Outer	1	1.12	14	√		
		2	0.95			√	
		3	0.91			√	Drain hole
		4	1.32	3.3	√	√	
	Inner	1	1.70	3.6	√	√	
		2	1.51			√	
		3	1.12			√	
		4	1.54	6	√	√	

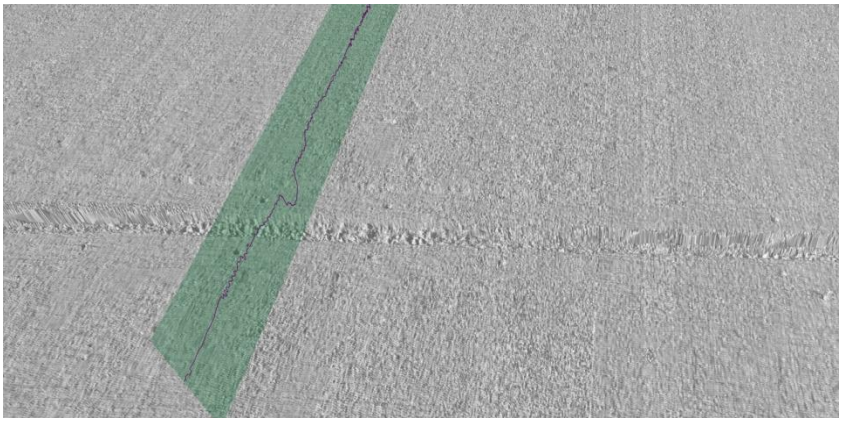

(a) Default View

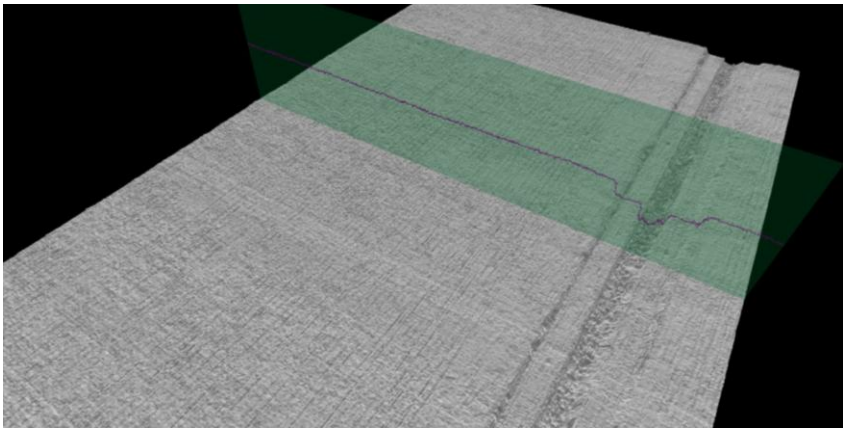

(b) Rotated View

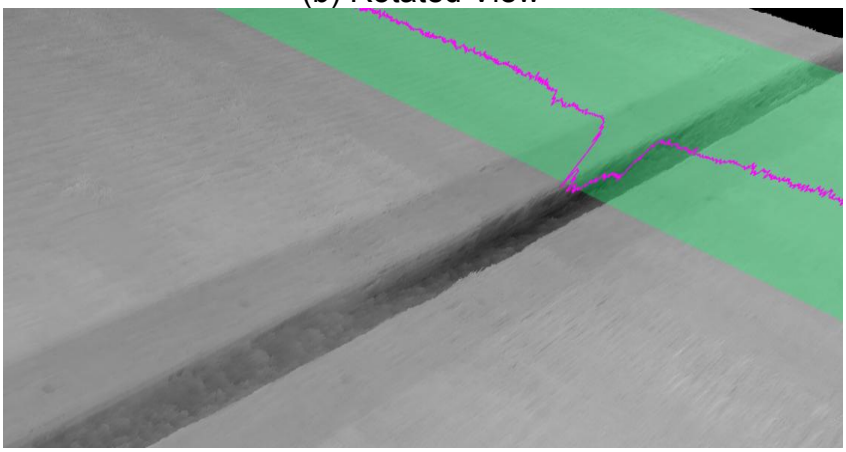

(c) Different Lighting Model

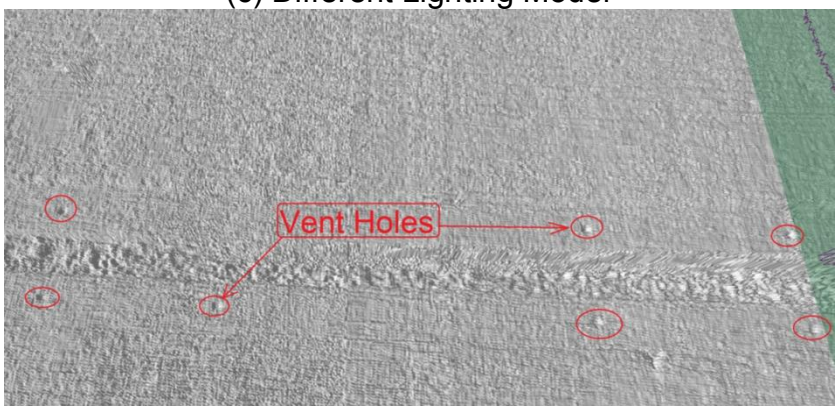

(d) Zoomed-in View

Figure 7.11 Visualization of An Expansion Joint (North Canadian River Bridge)

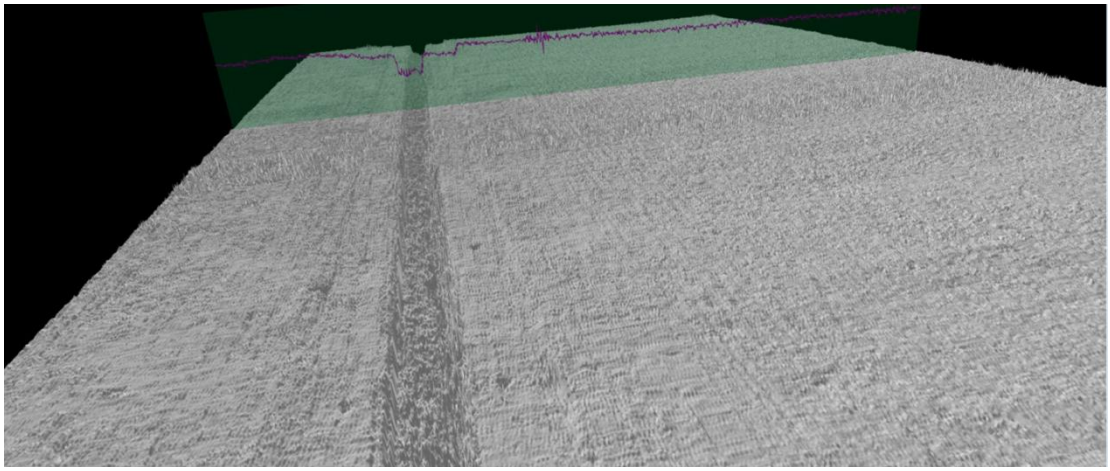

(a) Location 1

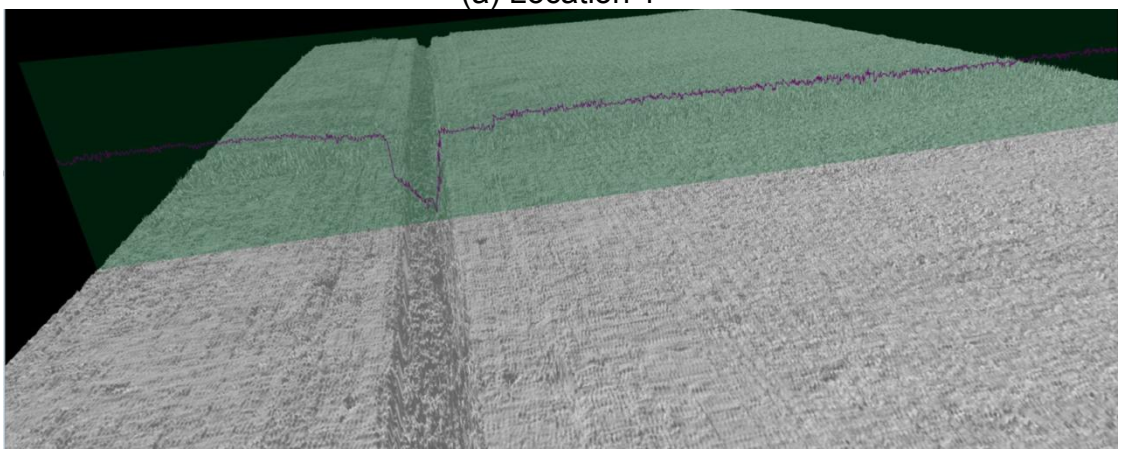

(b) Location 2

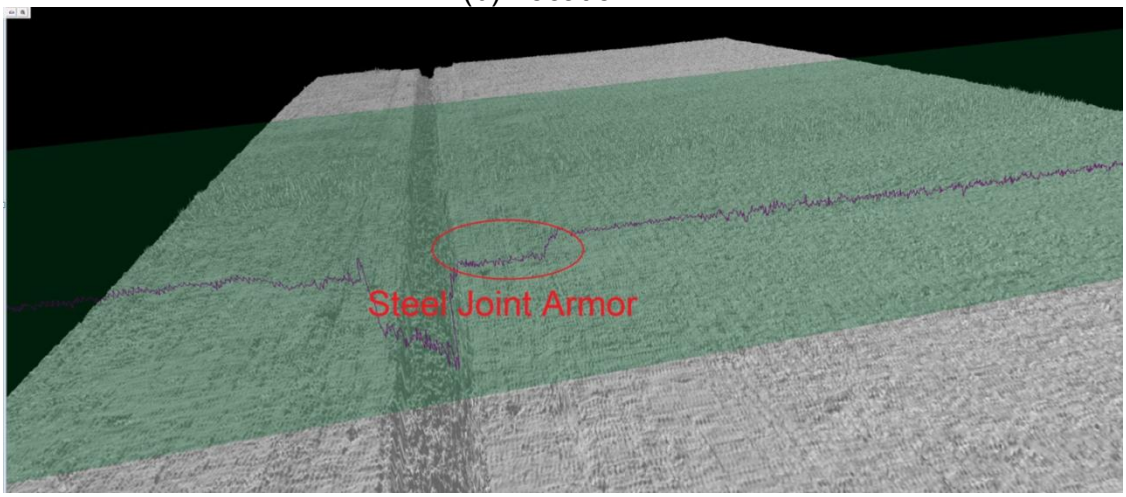

(c) Location 3

Figure 7.12 Shapes and Dimensions of A Joint at Various Locations (North Canadian River Bridge)

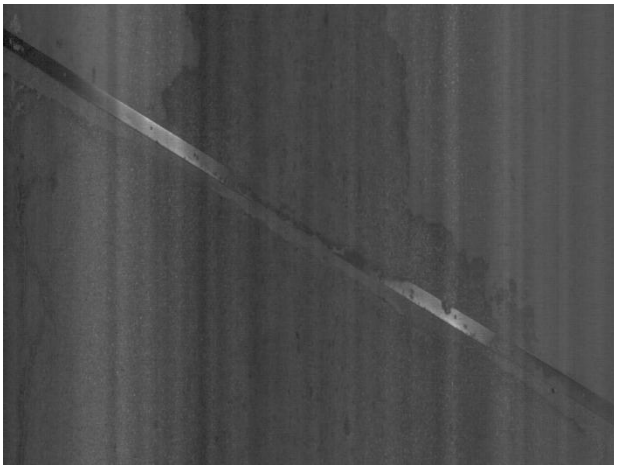

(a) 2D Intensity

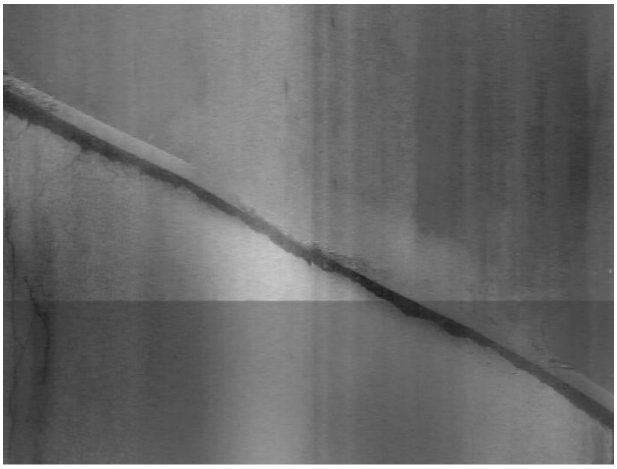

(b) 1mm 3D Range

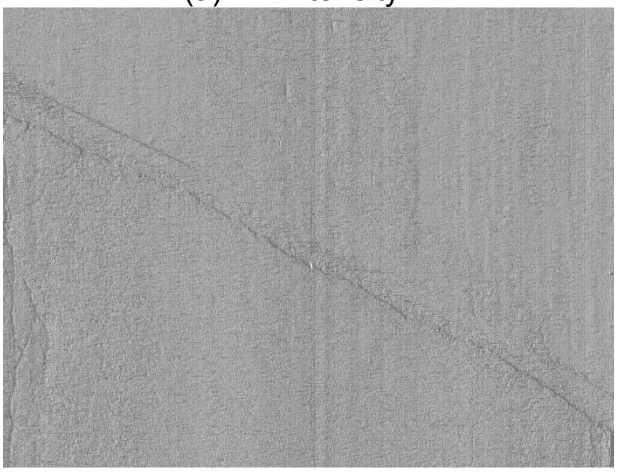

(c) 1mm 3D Intensity

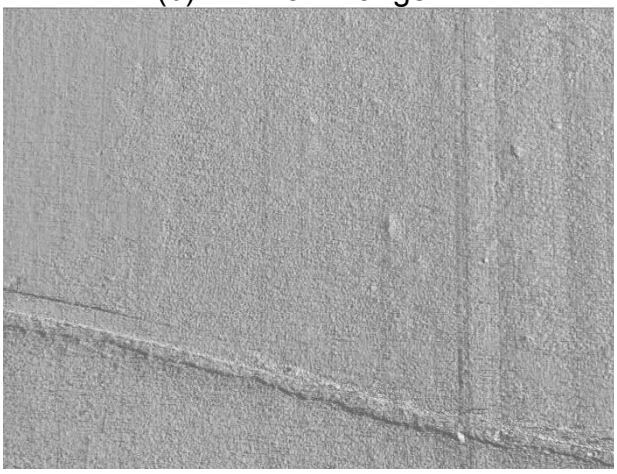

(d) Rotated 1mm 3D Range

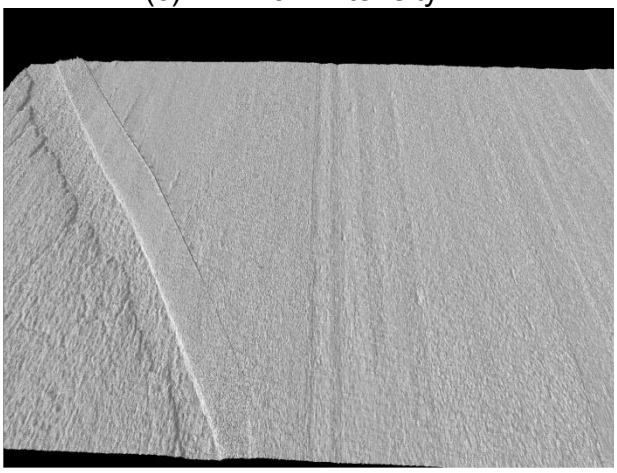

(e) 1/4 mm 3D Range (Before Correction)

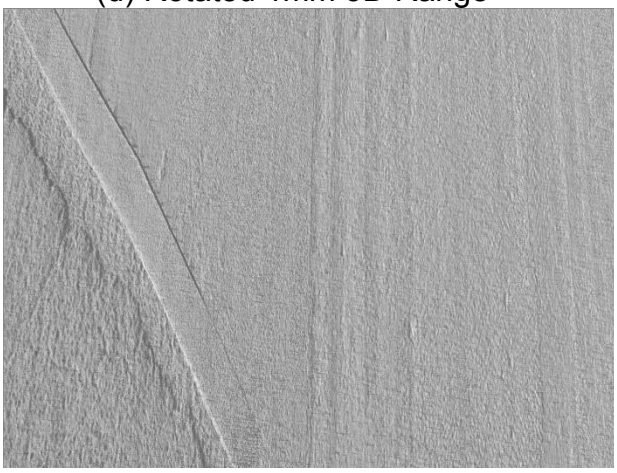

(f) Rotated 1/4 mm 3D Range (Before Correction)

Figure 7.13 South Bound Outer Lane Joint #1 (Boomer Creek Bridge)

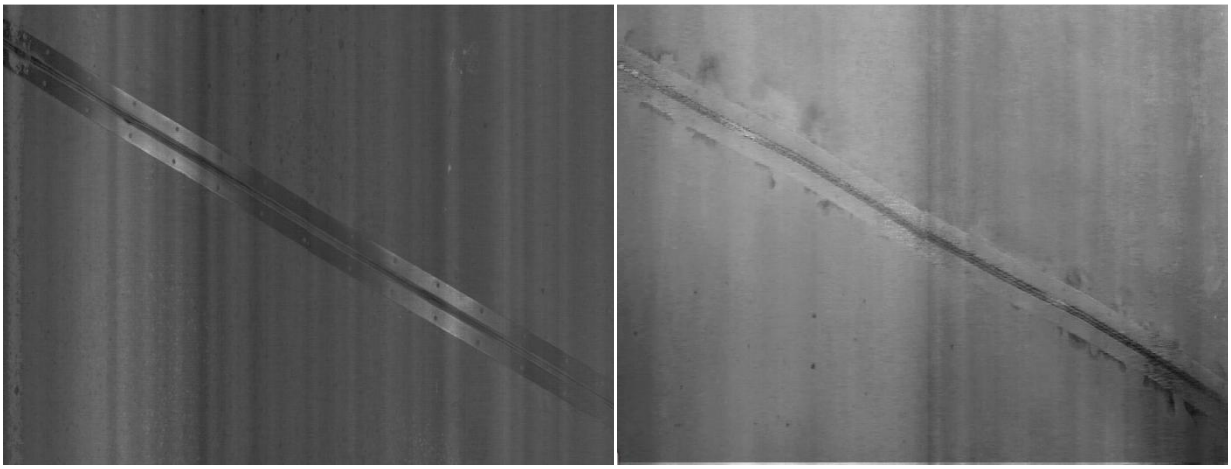

(a) 2D Intensity (b) 1mm 3D Range

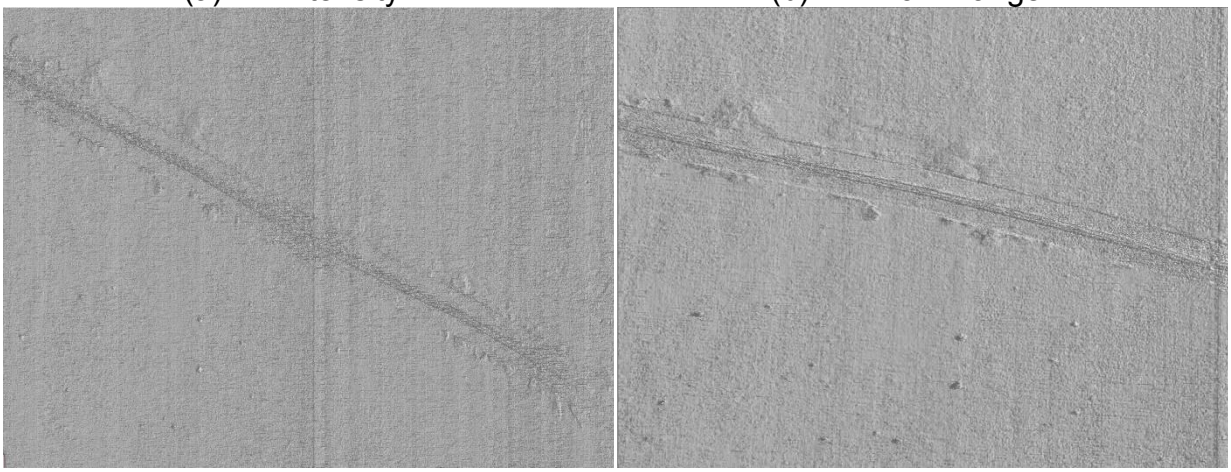

(c) 1mm 3D Intensity (d) Rotated 1mm 3D Range

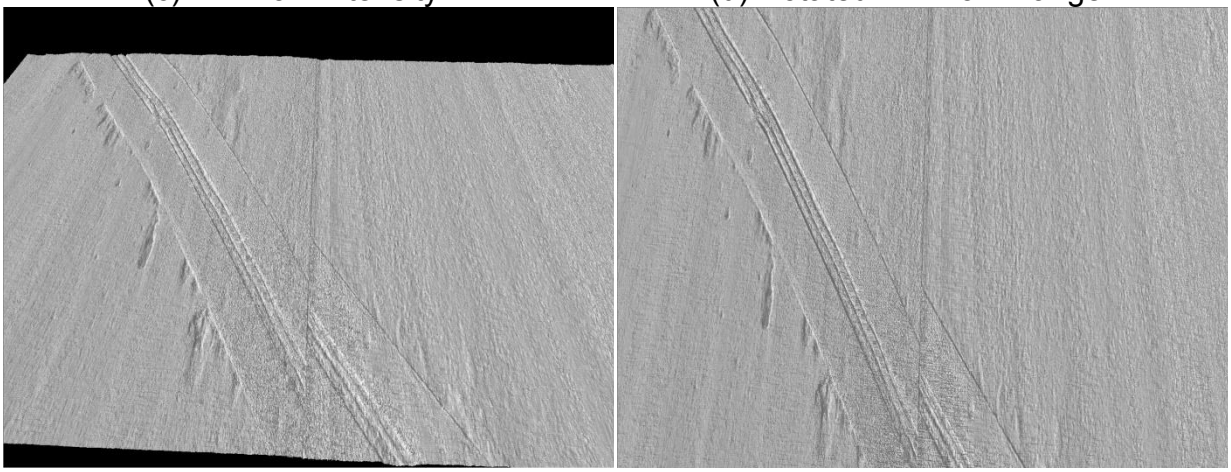

(e) 1/4 mm 3D Range (Before Correction) (f) Rotated 1/4 mm 3D Range (Before Correction)

Figure 7.14 South Bound Outer Lane Joint #2 (Boomer Creek Bridge)

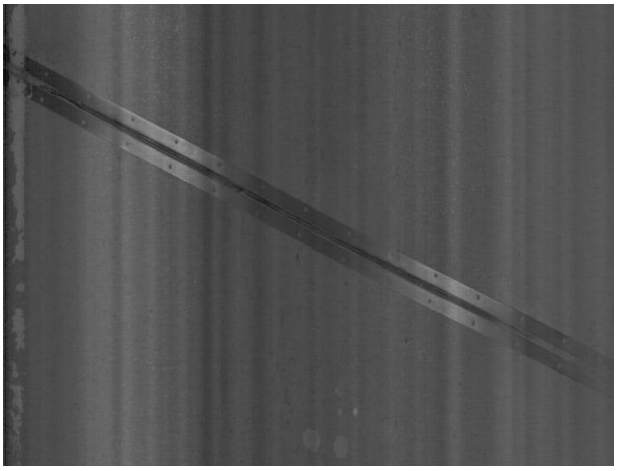

(a) 2D Intensity

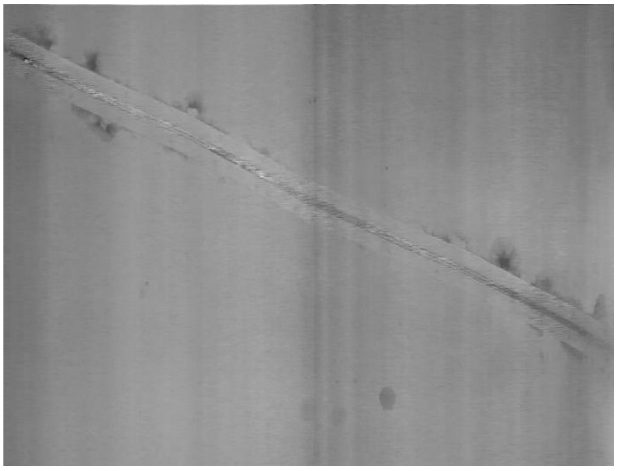

(b) 1mm 3D Range

(c) 1mm 3D Intensity

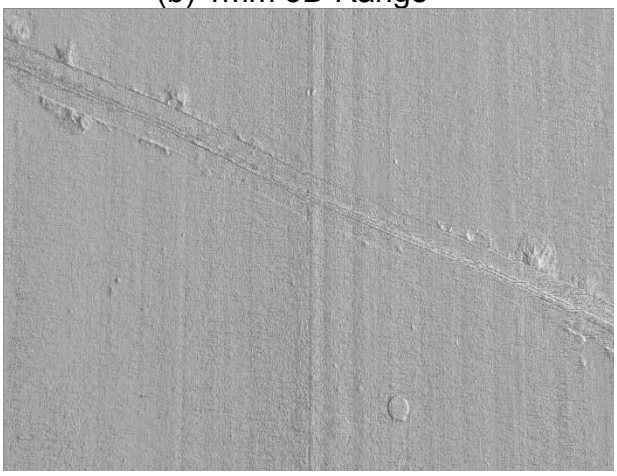

(d) Rotated 1mm 3D Range

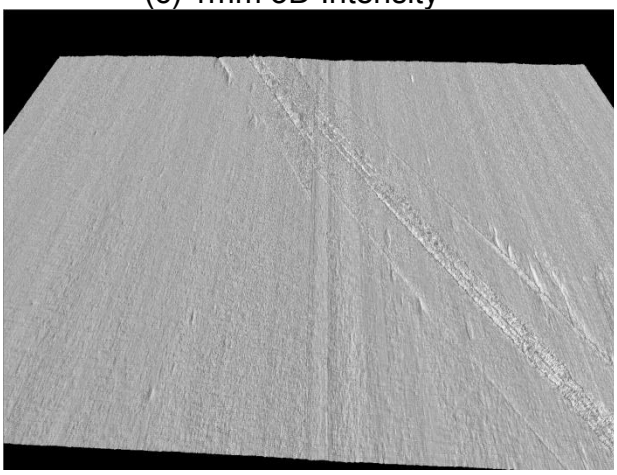

(e) 1/4 mm 3D Range (Before Correction)

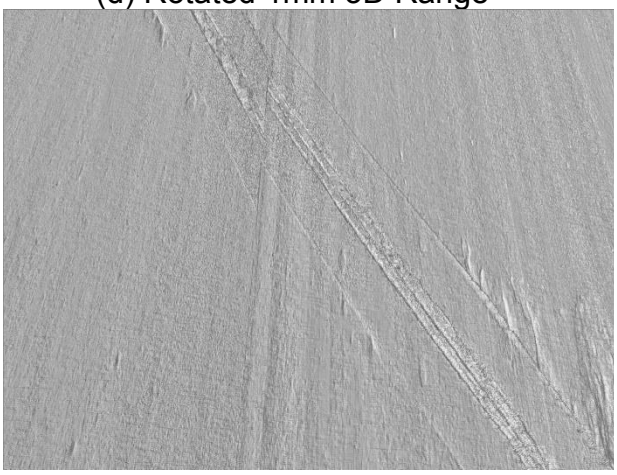

(f) Rotated 1/4 mm 3D Range (Before Correction)

Figure 7.15 South Bound Outer Lane Joint #3 (Boomer Creek Bridge)

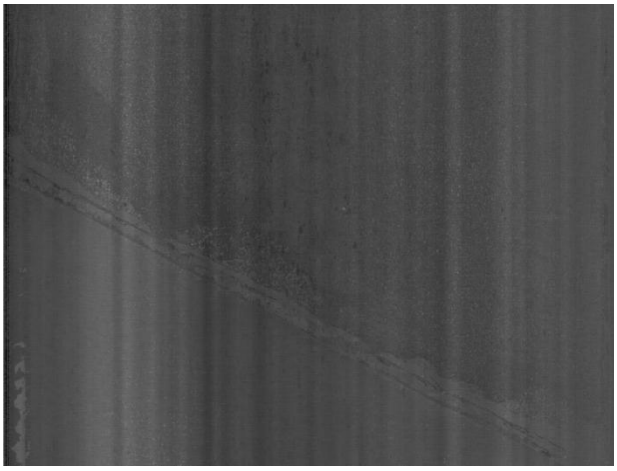

(a) 2D Intensity

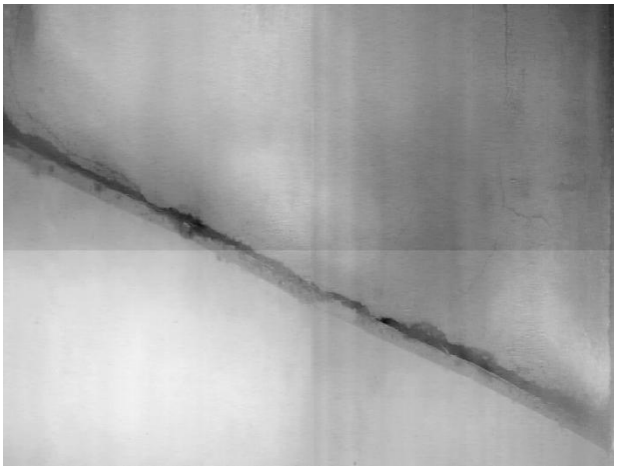

(b) 1mm 3D Range

(c) 1mm 3D Intensity

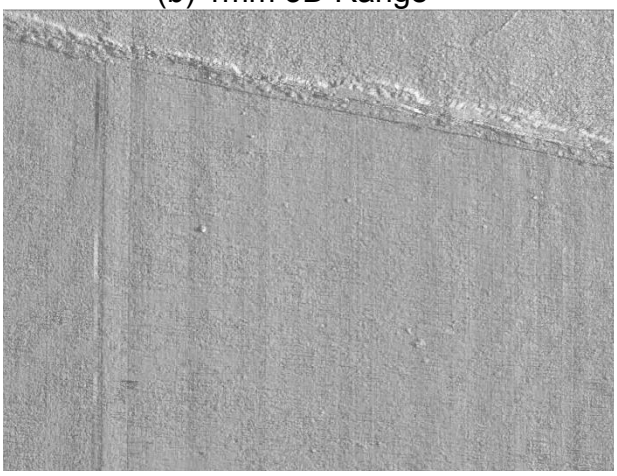

(d) Rotated 1mm 3D Range

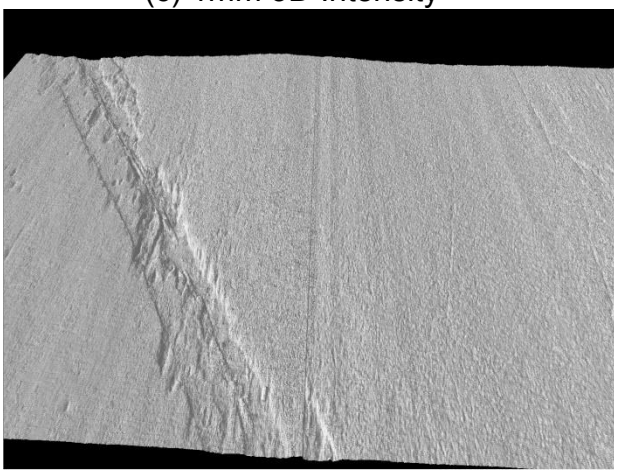

(e) 1/4 mm 3D Range (Before Correction)

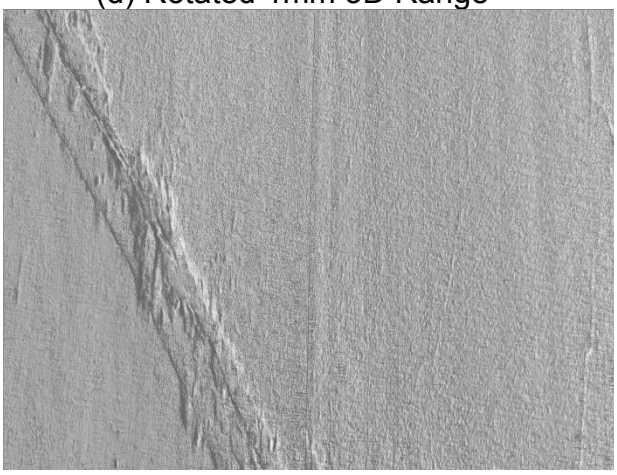

(f) Rotated 1/4 mm 3D Range (Before Correction)

Figure 7.16 South Bound Outer Lane Joint #4 (Boomer Creek Bridge)

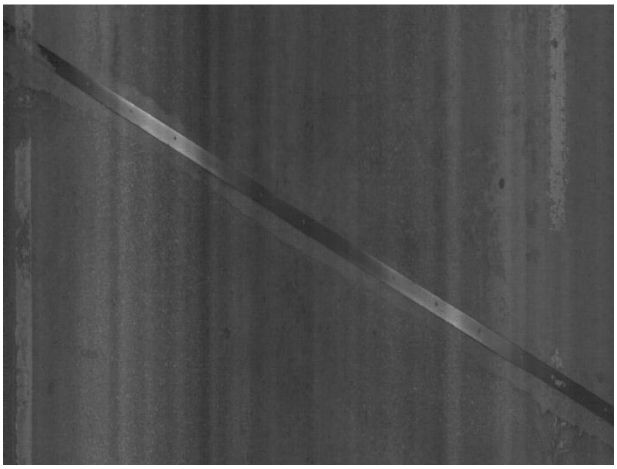

(a) 2D Intensity

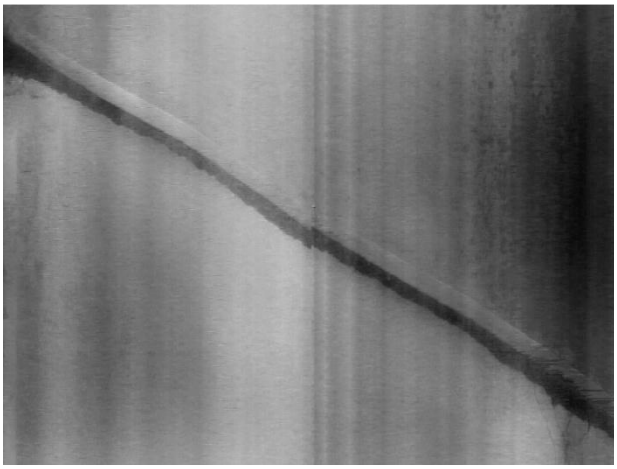

(b) 1mm 3D Range

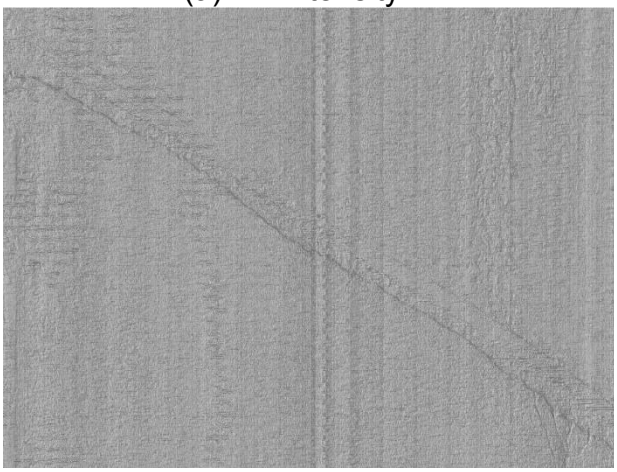

(c) 1mm 3D Intensity

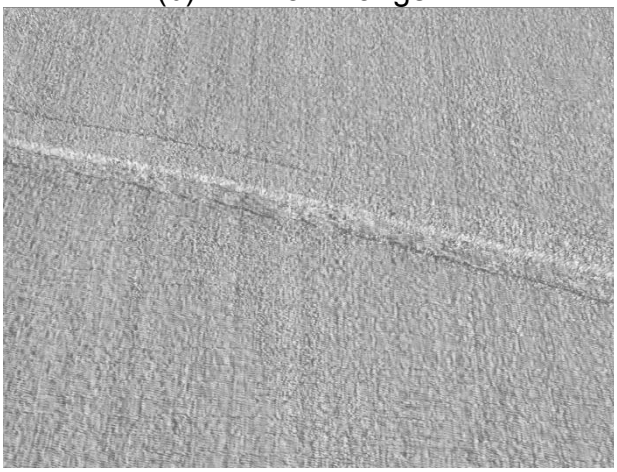

(d) Rotated 1mm 3D Range

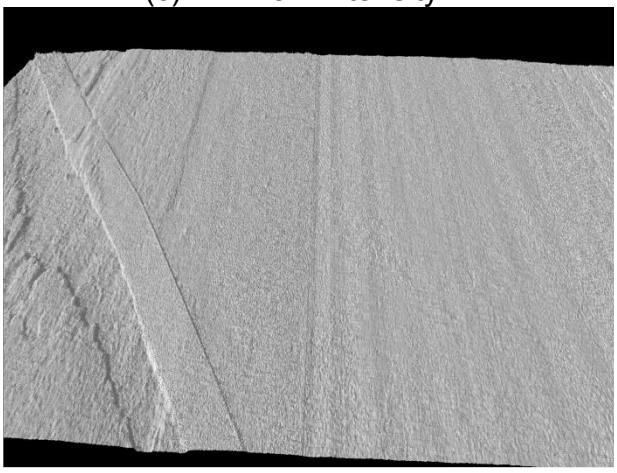

(e) 1/4 mm 3D Range (Before Correction)

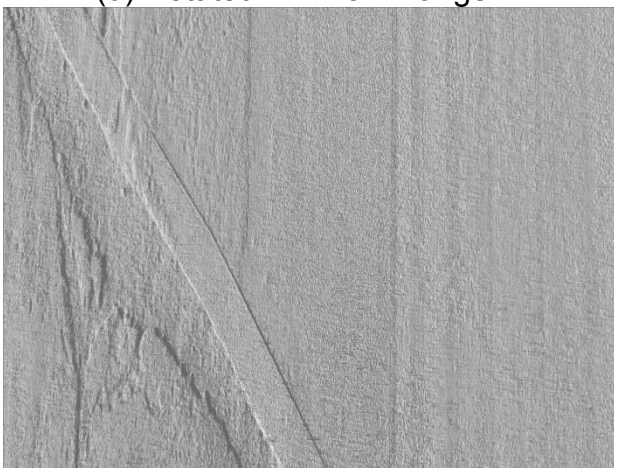

(f) Rotated 1/4 mm 3D Range (Before Correction)

Figure 7.17 South Bound Inner Lane Joint #1 (Boomer Creek Bridge)

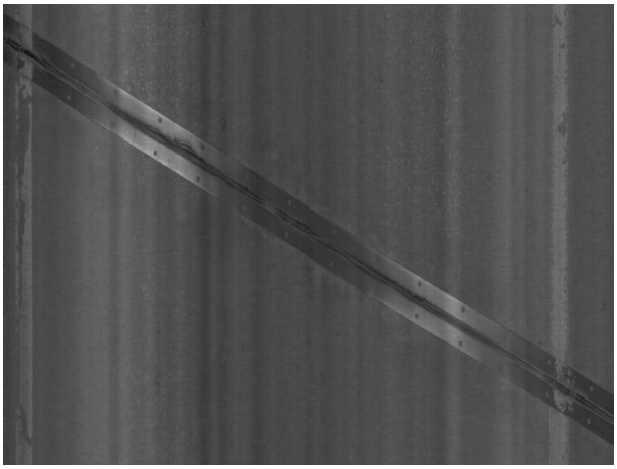

(a) 2D Intensity

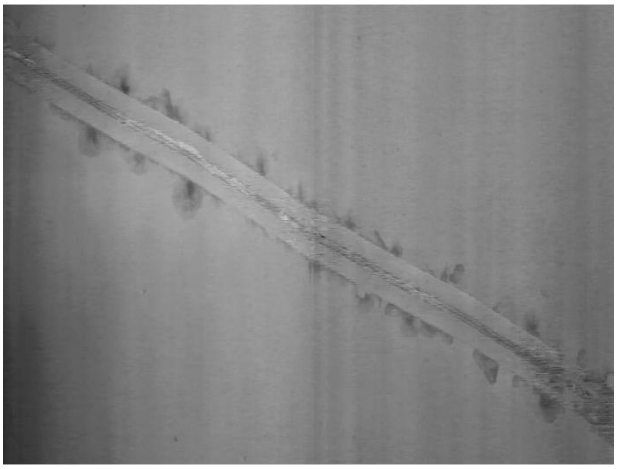

(b) 1mm 3D Range

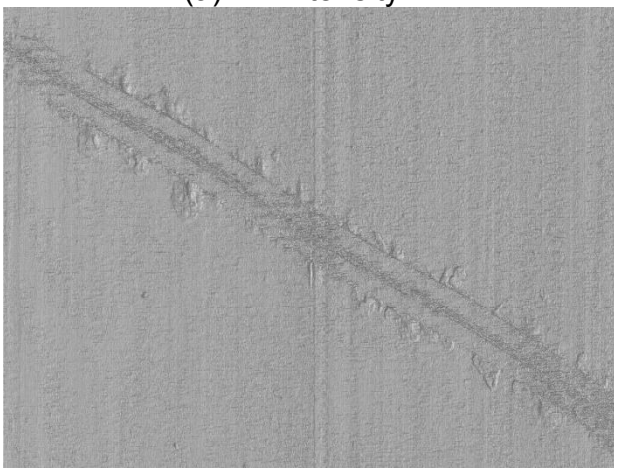

(c) 1mm 3D Intensity

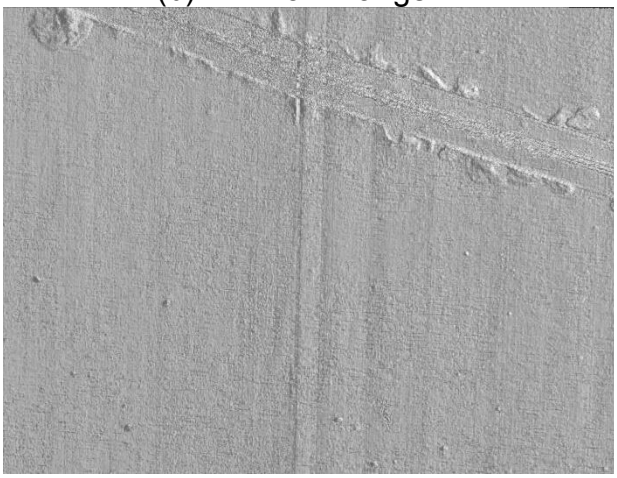

(d) Rotated 1mm 3D Range

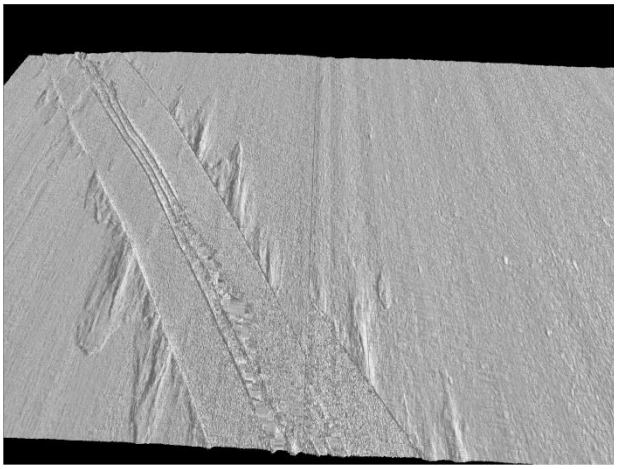

(e) 1/4 mm 3D Range (Before Correction)

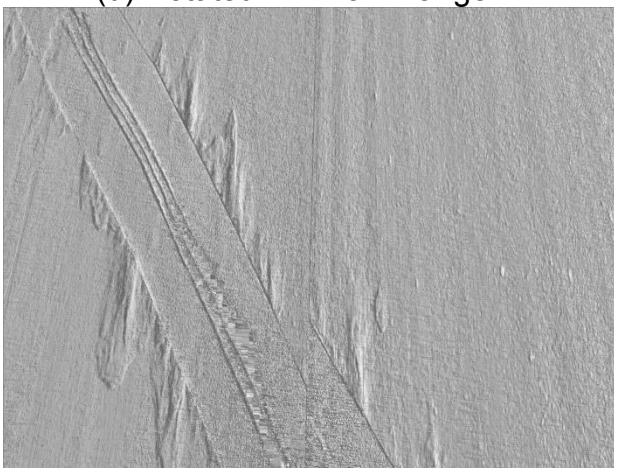

(f) Rotated 1/4 mm 3D Range (Before Correction)

Figure 7.18 South Bound Inner Lane Joint #2 (Boomer Creek Bridge)

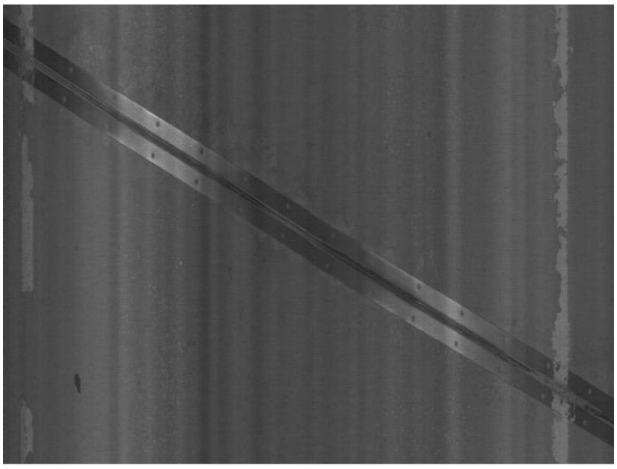

(a) 2D Intensity

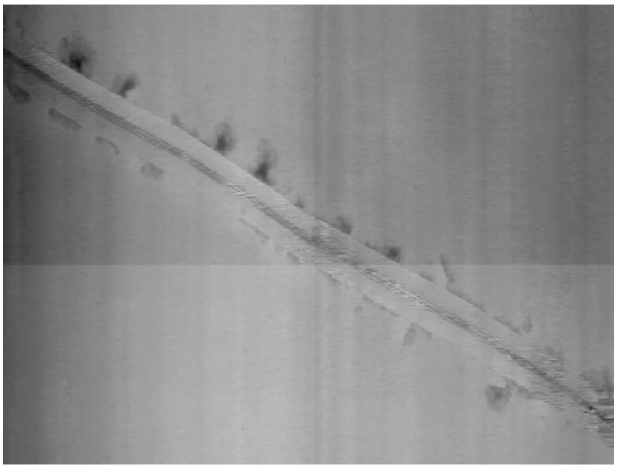

(b) 1mm 3D Range

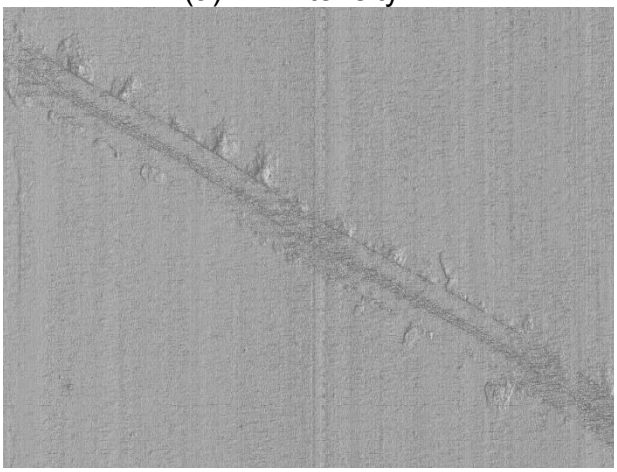

(c) 1mm 3D Intensity

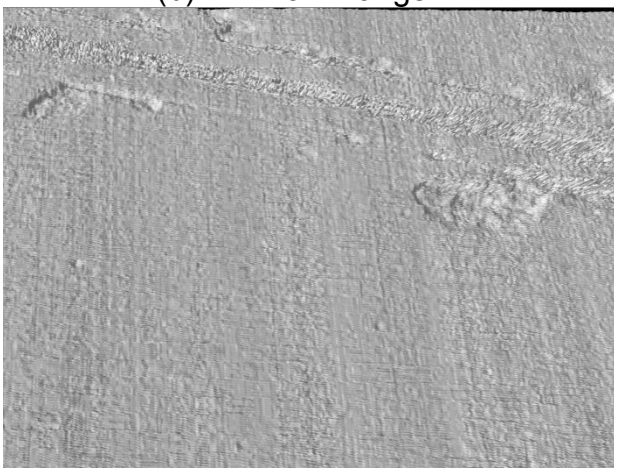

(d) Rotated 1mm 3D Range

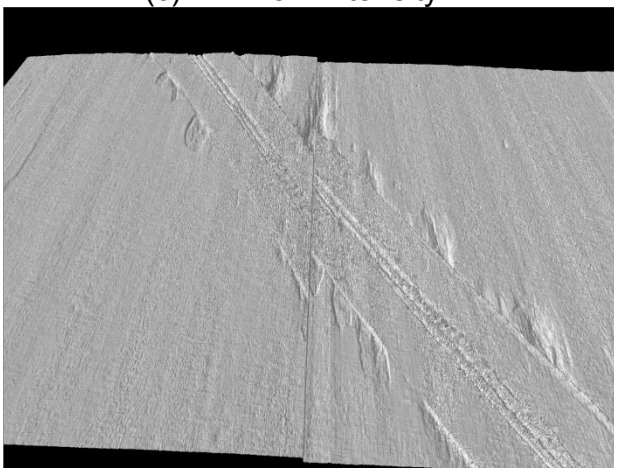

(e) 1/4 mm 3D Range (Before Correction)

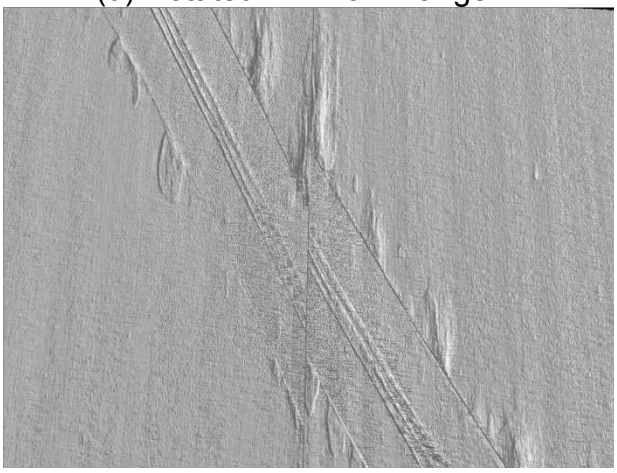

(f) Rotated 1/4 mm 3D Range (Before Correction)

Figure 7.19 South Bound Inner Lane Joint #3 (Boomer Creek Bridge)

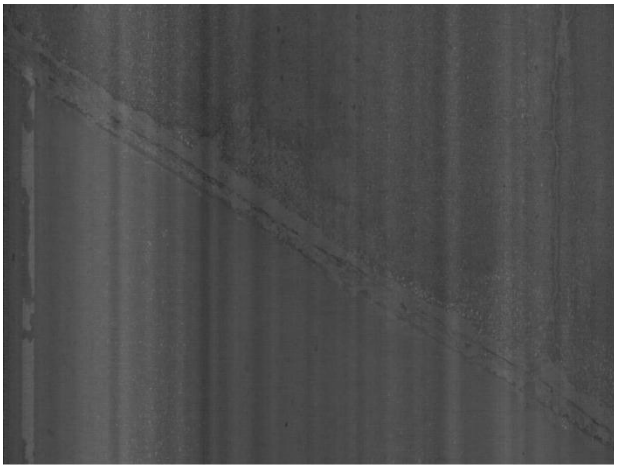

(a) 2D Intensity

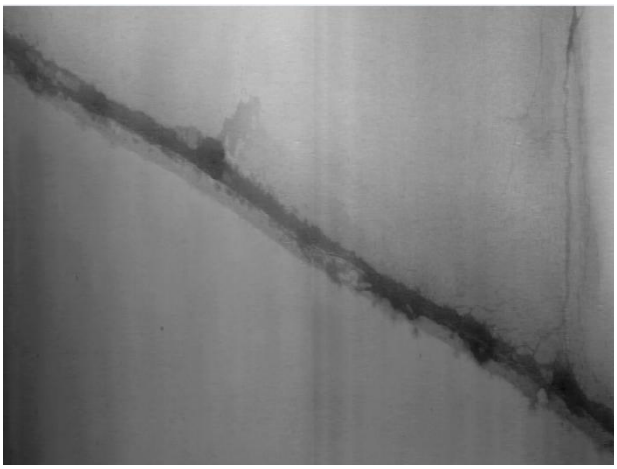

(b) 1mm 3D Range

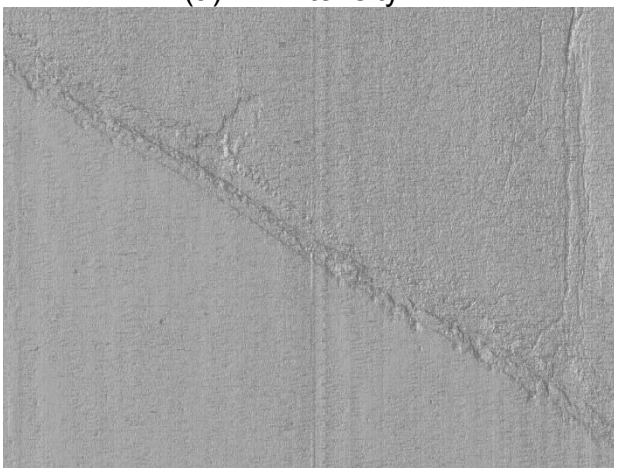

(c) 1mm 3D Intensity

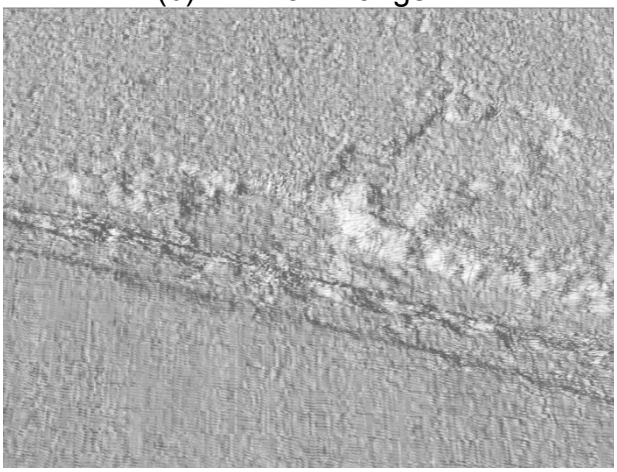

(d) Rotated 1mm 3D Range

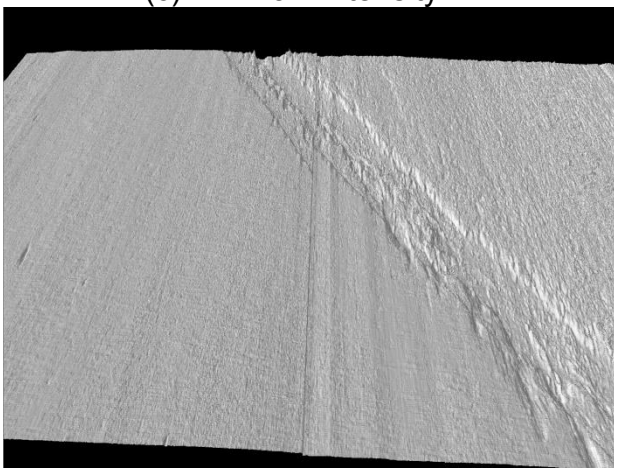

(e) 1/4 mm 3D Range (Before Correction)

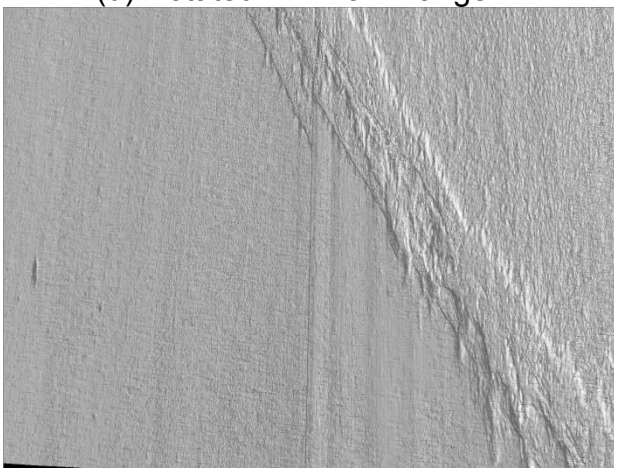

(f) Rotated 1/4 mm 3D Range (Before Correction)

Figure 7.20 South Bound Inner Lane Joint #4 (Boomer Creek Bridge)

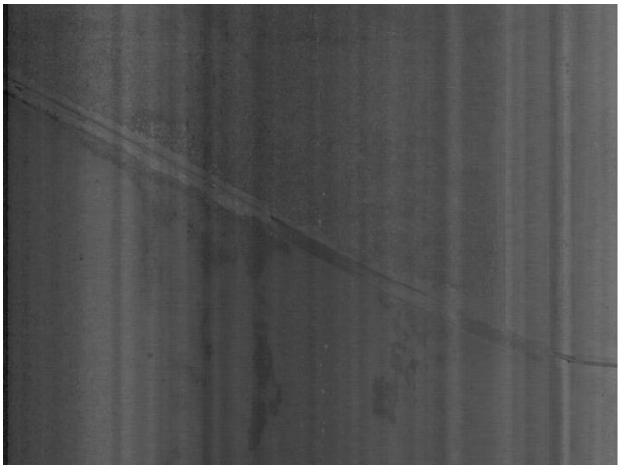

(a) 2D Intensity

(b) 1mm 3D Range

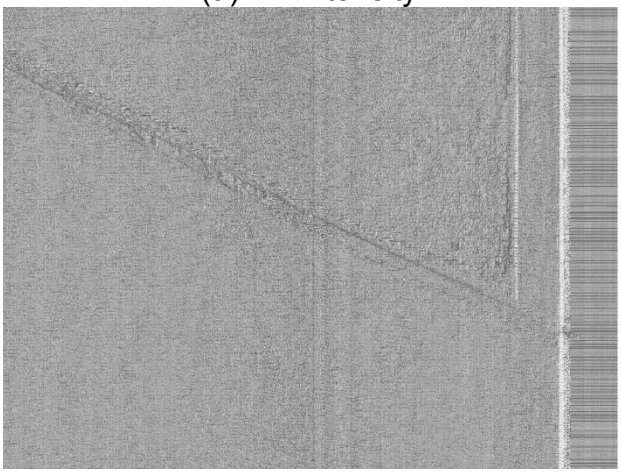

(c) 1mm 3D Intensity

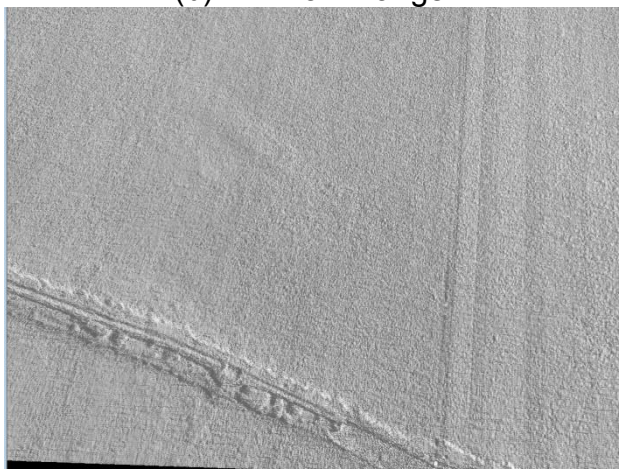

(d) Rotated 1mm 3D Range

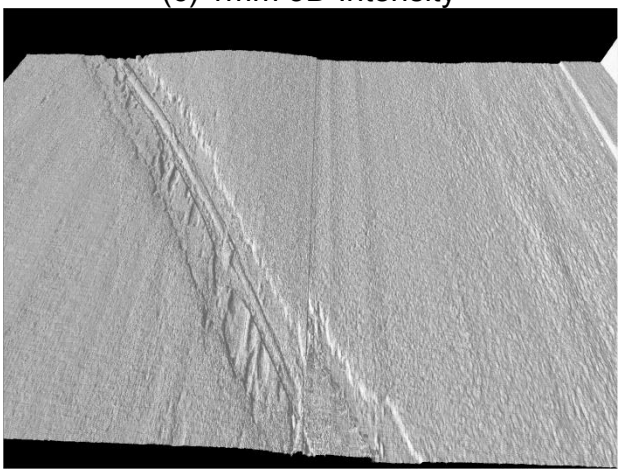

(e) 1/4 mm 3D Range (Before Correction)

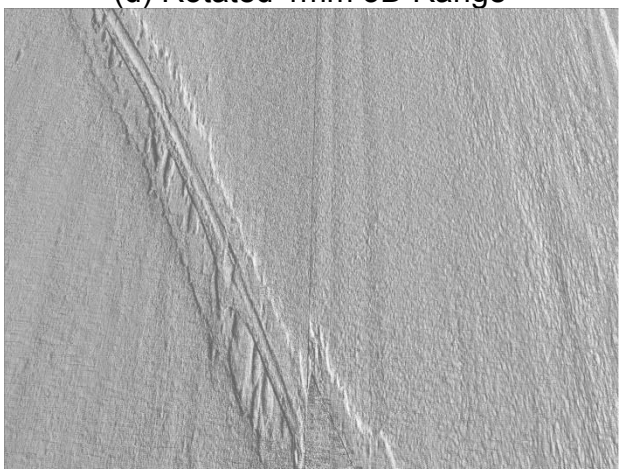

(f) Rotated 1/4 mm 3D Range (Before Correction)

Figure 7.21 North Bound Outer Lane Joint #1 (Boomer Creek Bridge)

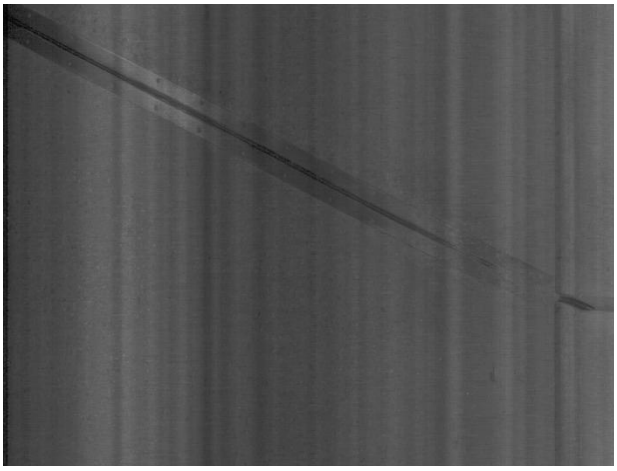

(a) 2D Intensity

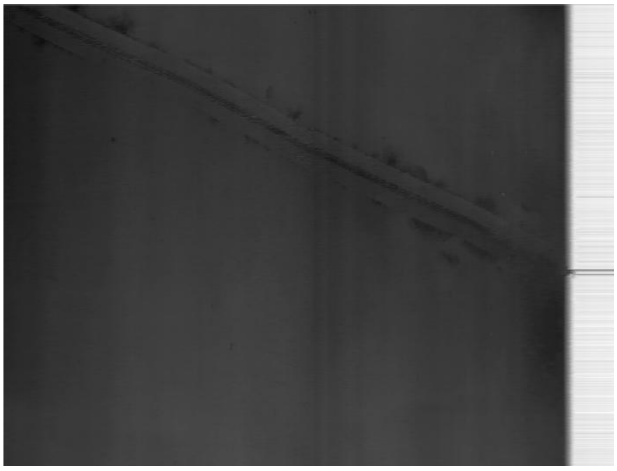

(b) 1mm 3D Range

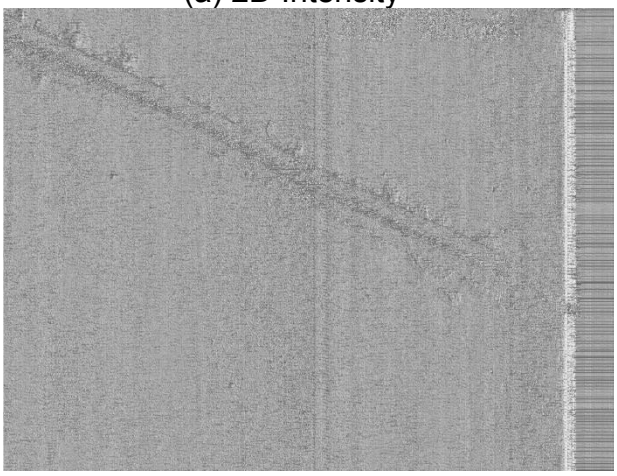

(c) 1mm 3D Intensity

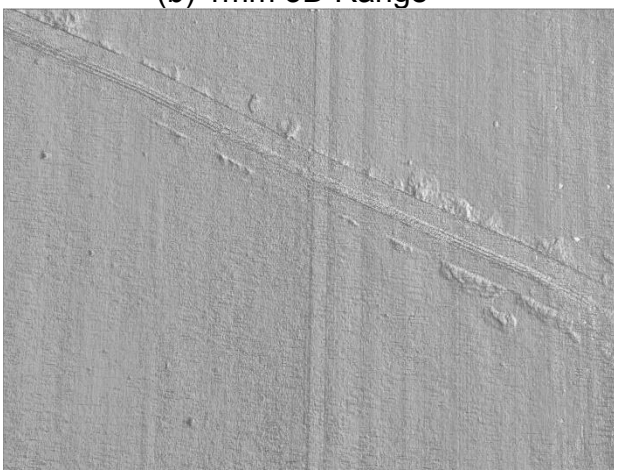

(d) Rotated 1mm 3D Range

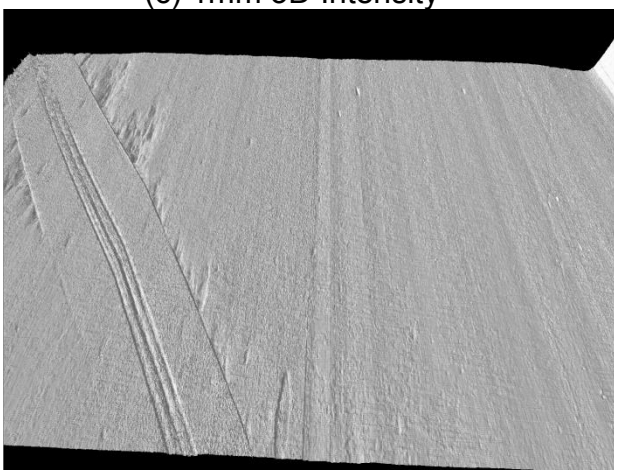

(e) 1/4 mm 3D Range (Before Correction)

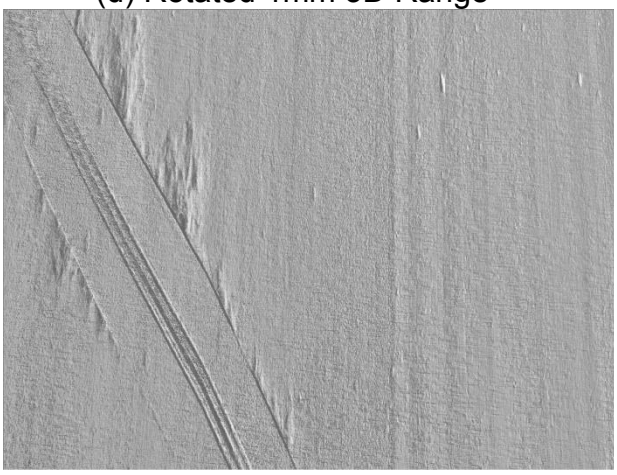

(f) Rotated 1/4 mm 3D Range (Before Correction)

Figure 7.22 North Bound Outer Lane Joint #2 (Boomer Creek Bridge)

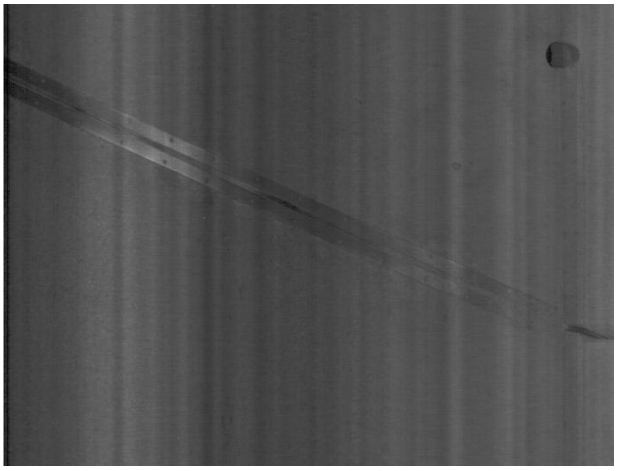

(a) 2D Intensity

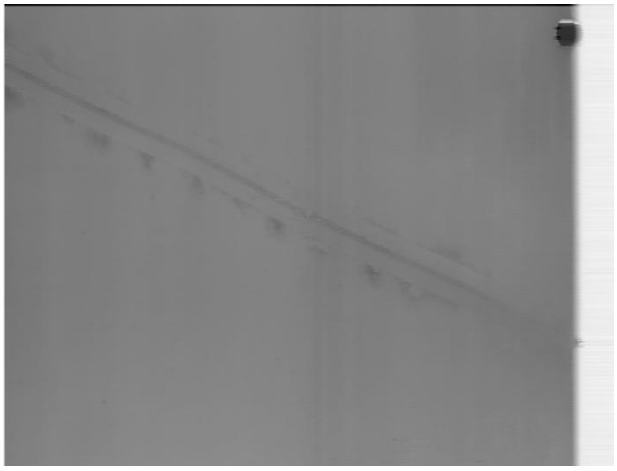

(b) 1mm 3D Range

(c) 1mm 3D Intensity

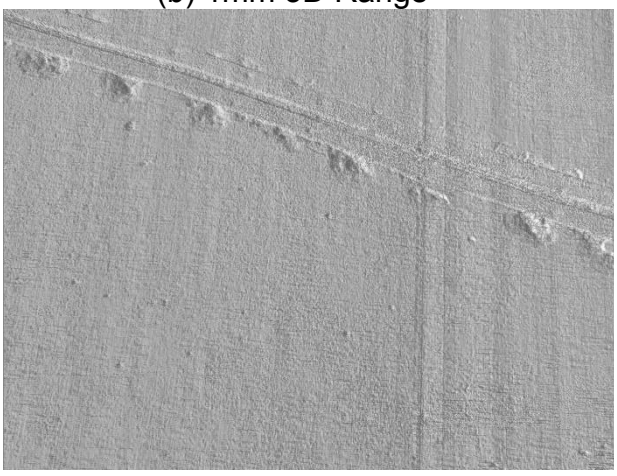

(d) Rotated 1mm 3D Range

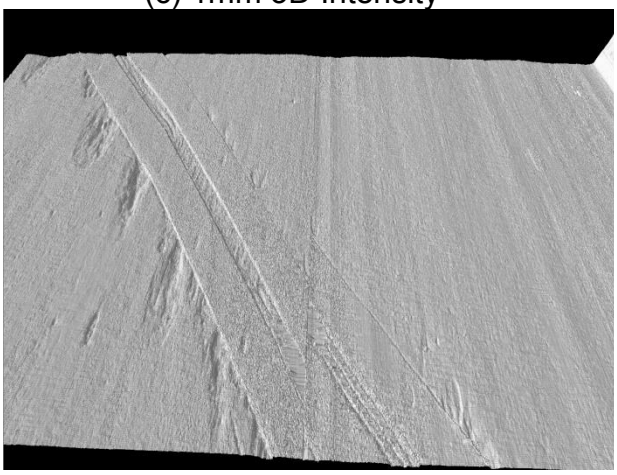

(e) 1/4 mm 3D Range (Before Correction)

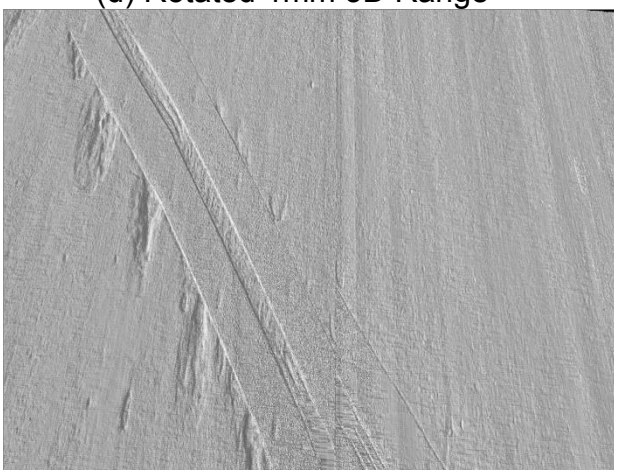

(f) Rotated 1/4 mm 3D Range (Before Correction)

Figure 7.23 North Bound Outer Lane Joint #3 (Boomer Creek Bridge)

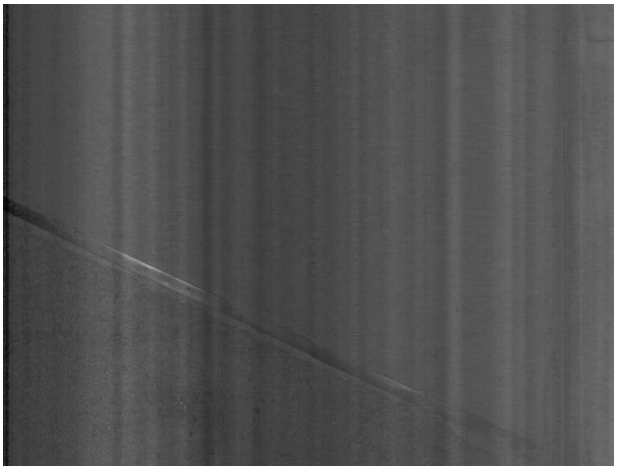

(a) 2D Intensity

(b) 1mm 3D Range

(c) 1mm 3D Intensity

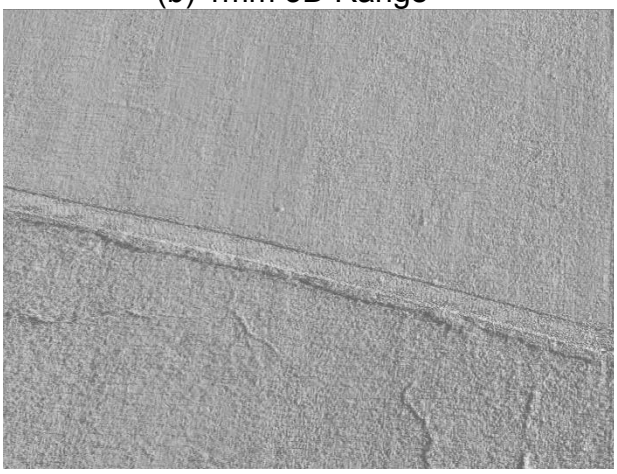

(d) Rotated 1mm 3D Range

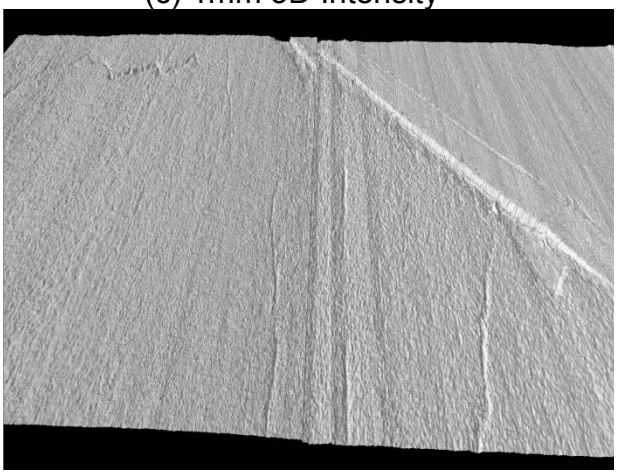

(e) 1/4 mm 3D Range (Before Correction)

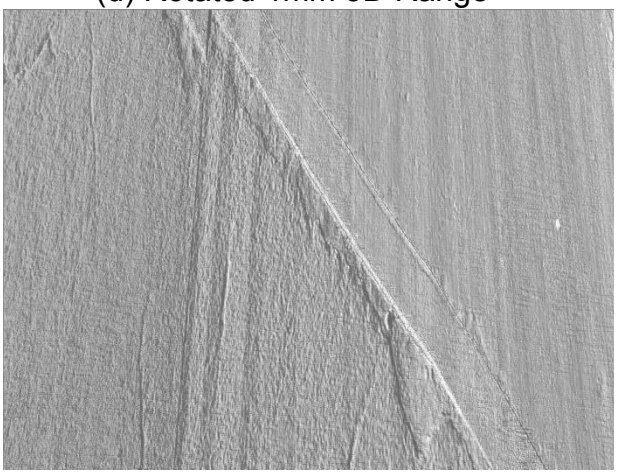

(f) Rotated 1/4 mm 3D Range (Before Correction)

Figure 7.24 North Bound Outer Lane Joint #4 (Boomer Creek Bridge)

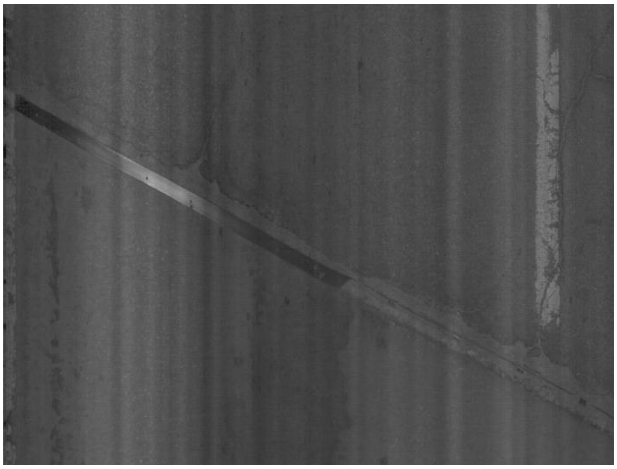

(a) 2D Intensity

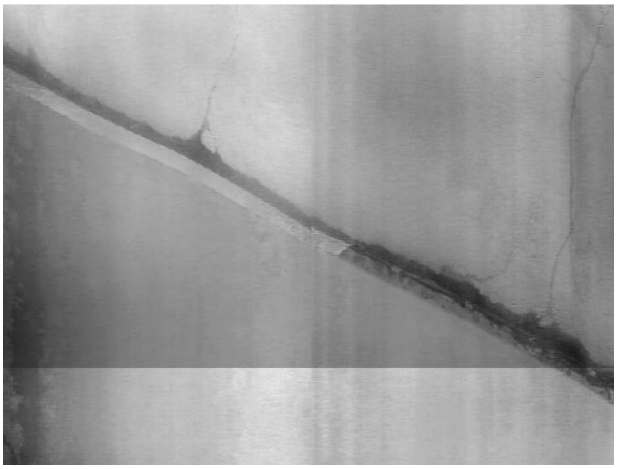

(b) 1mm 3D Range

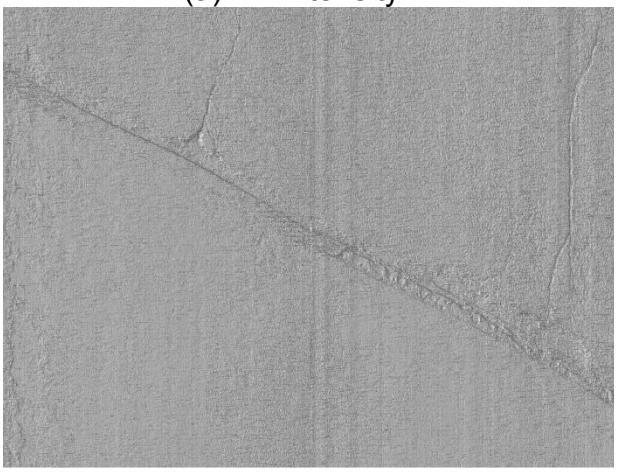

(c) 1mm 3D Intensity

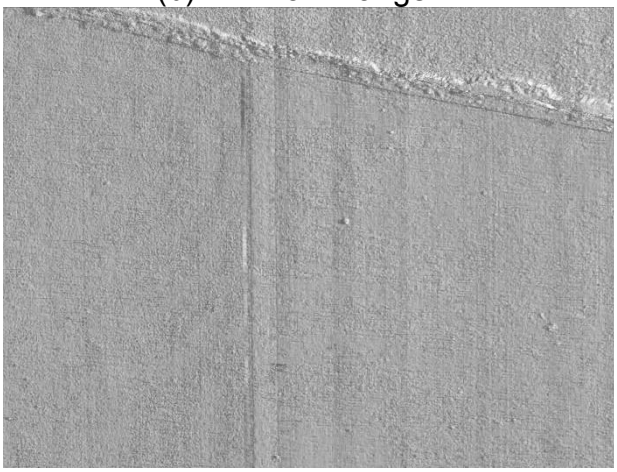

(d) Rotated 1mm 3D Range

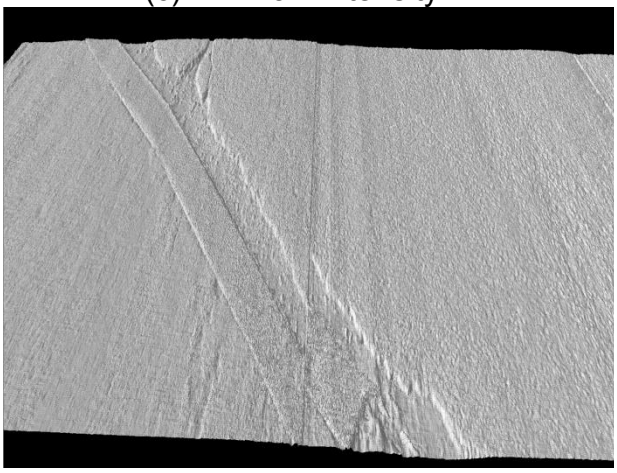

(e) 1/4 mm 3D Range (Before Correction)

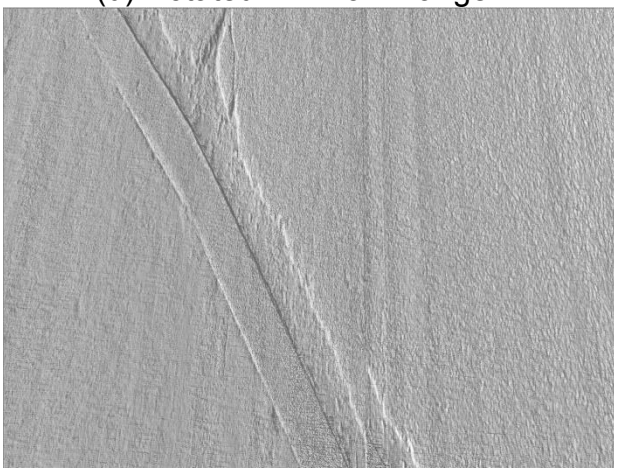

(f) Rotated 1/4 mm 3D Range (Before Correction)

Figure 7.25 North Bound Inner Lane Joint #1 (Boomer Creek Bridge)

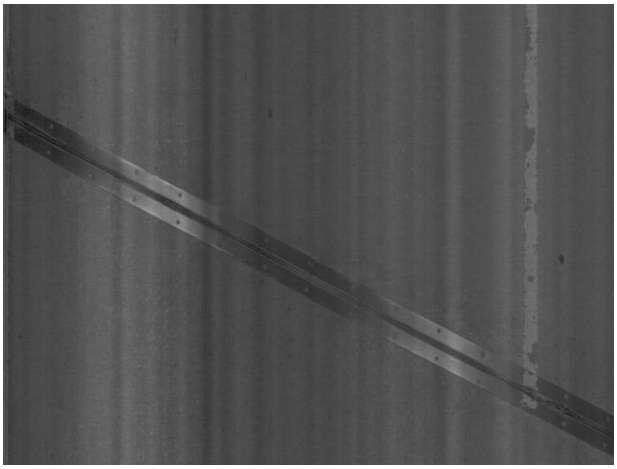

(a) 2D Intensity

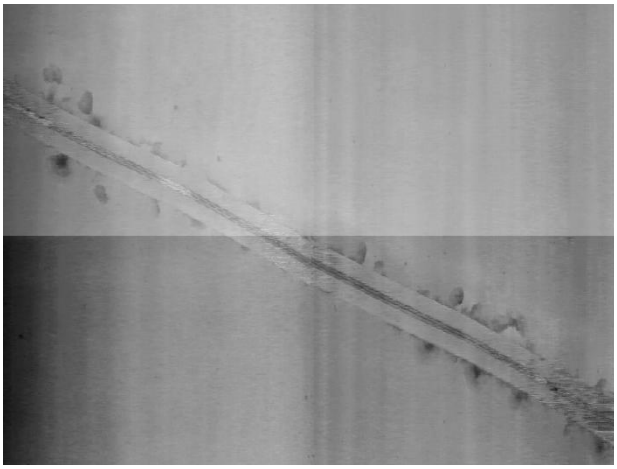

(b) 1mm 3D Range

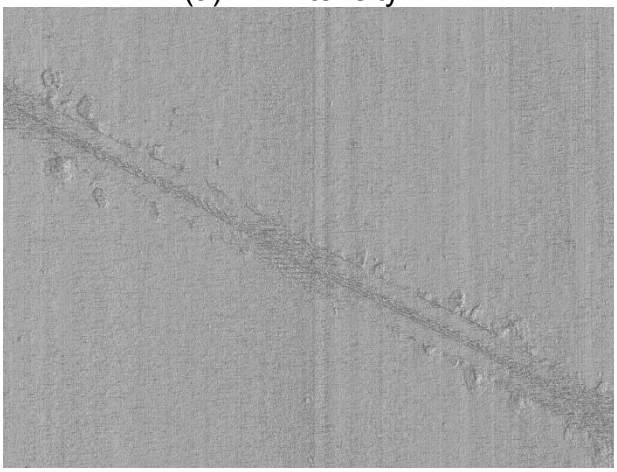

(c) 1mm 3D Intensity

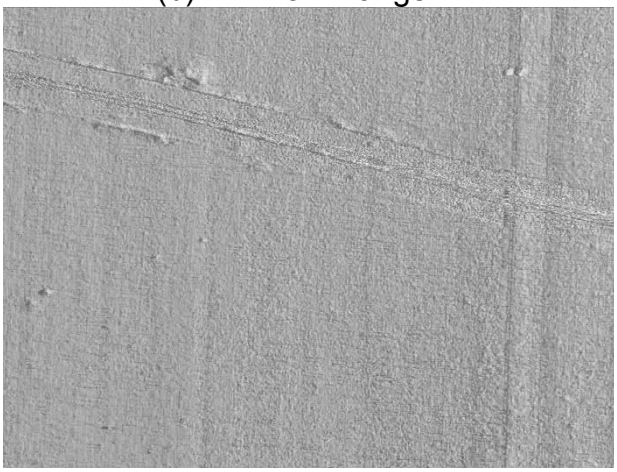

(d) Rotated 1mm 3D Range

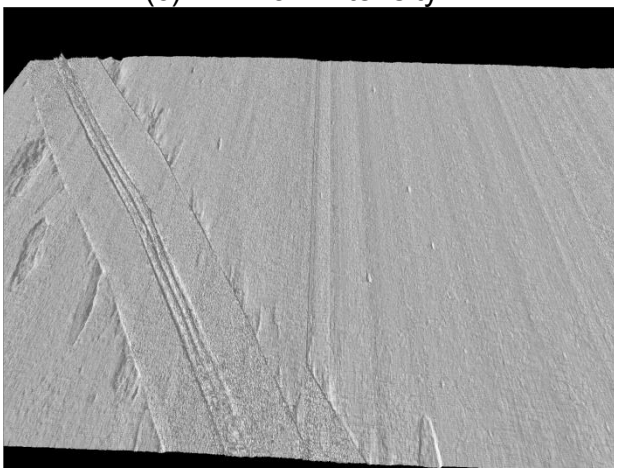

(e) 1/4 mm 3D Range (Before Correction)

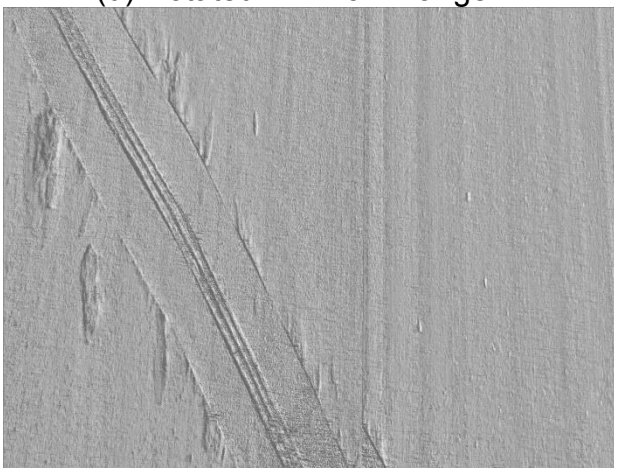

(f) Rotated 1/4 mm 3D Range (Before Correction)

Figure 7.26 North Bound Inner Lane Joint #2 (Boomer Creek Bridge)

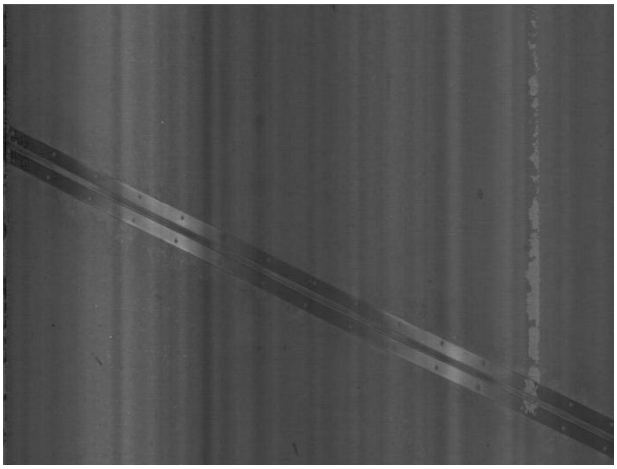

(a) 2D Intensity

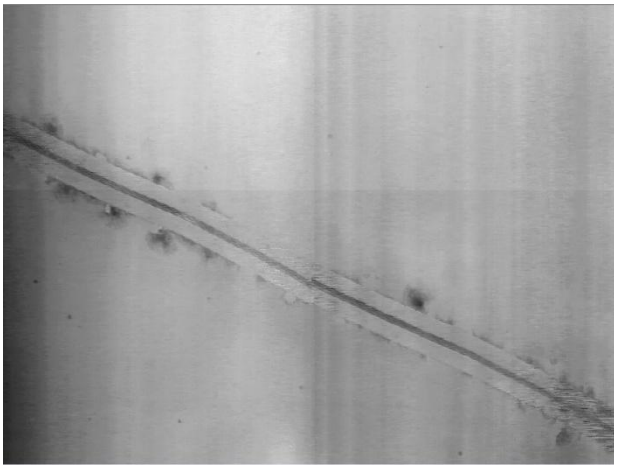

(b) 1mm 3D Range

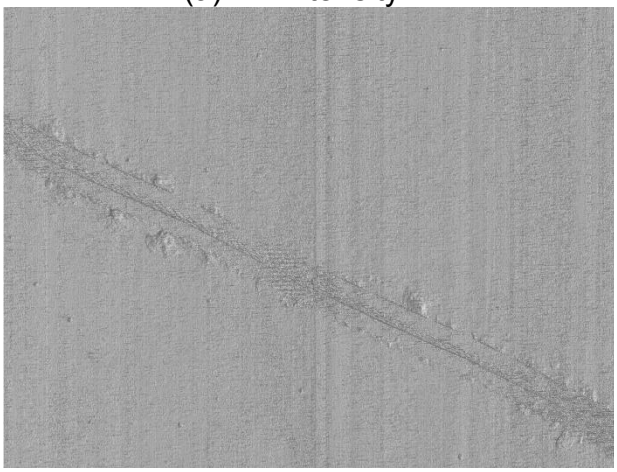

(c) 1mm 3D Intensity

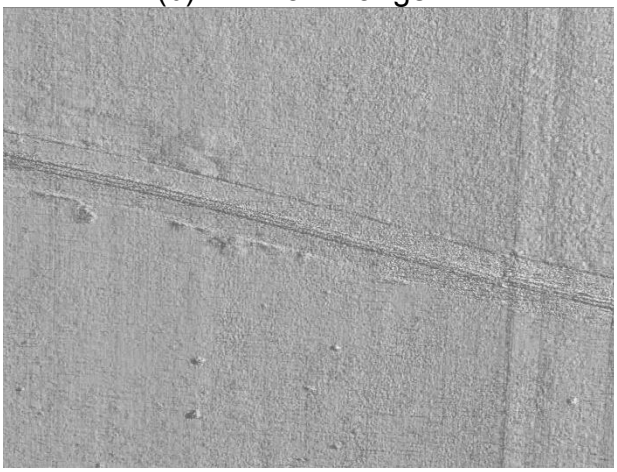

(d) Rotated 1mm 3D Range

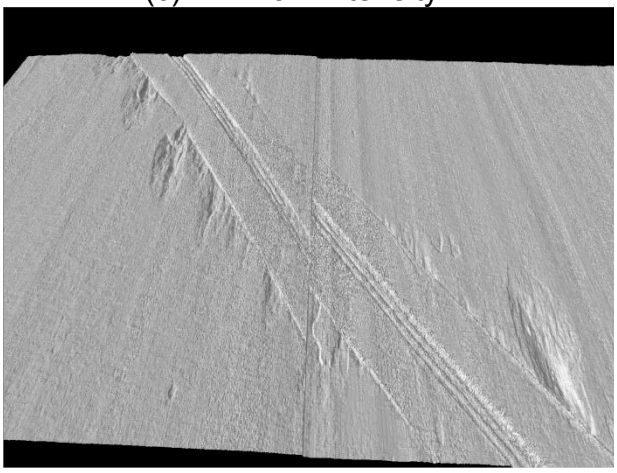

(e) 1/4 mm 3D Range (Before Correction)

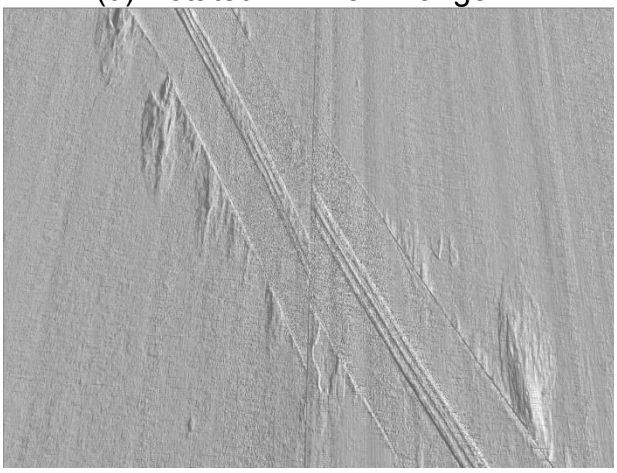

(f) Rotated 1/4 mm 3D Range (Before Correction)

Figure 7.27 North Bound Inner Lane Joint #3 (Boomer Creek Bridge)

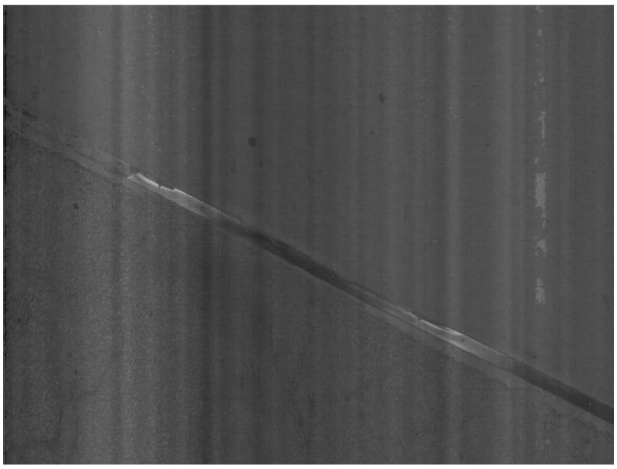

(a) 2D Intensity

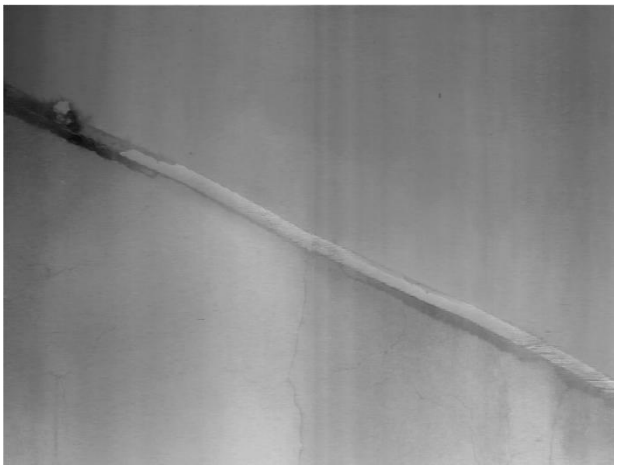

(b) 1mm 3D Range

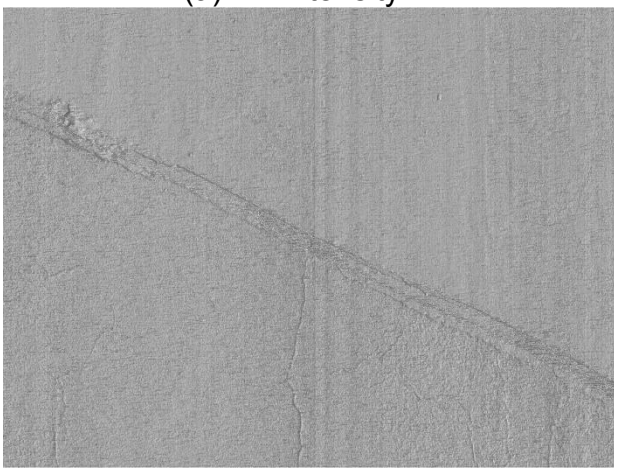

(c) 1mm 3D Intensity

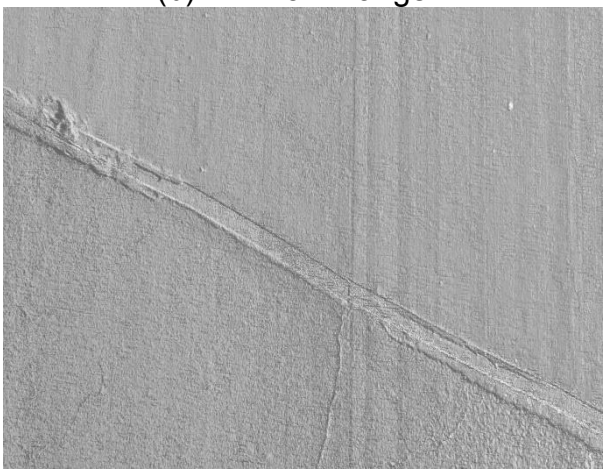

(d) Rotated 1mm 3D Range

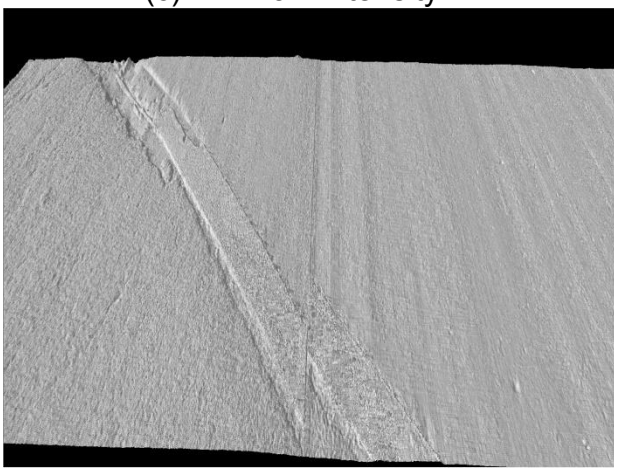

(e) 1/4 mm 3D Range (Before Correction)

(f) Rotated 1/4 mm 3D Range (Before Correction)

Figure 7.28 North Bound Inner Lane Joint #4 (Boomer Creek Bridge)

7.1.4 Other Features

7.1.4.1 North Canadian River Bridge

The 1mm 3D can also provide users with high resolution demonstration of many other objects. For example, lane marking paint and the transition from asphalt pavement to bridge deck cans be clearly viewed with distinctive differences from the collected data, as shown in Figure 7.29.

In addition, the DHDV collects high quality 2D image data and ROW data, as shown in Figure 7.30. These data can also provide users with useful information for the evaluation of bridge deck condition and the adjacent pavement sections.

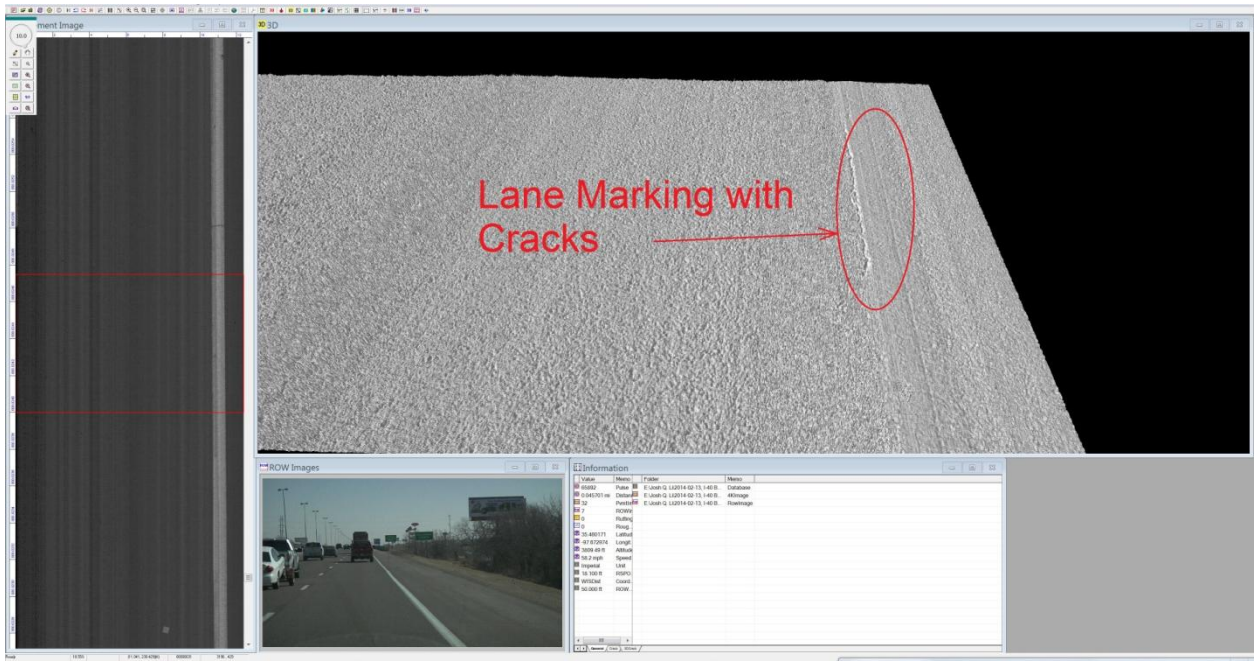

(a) Lane Marking with Cracks

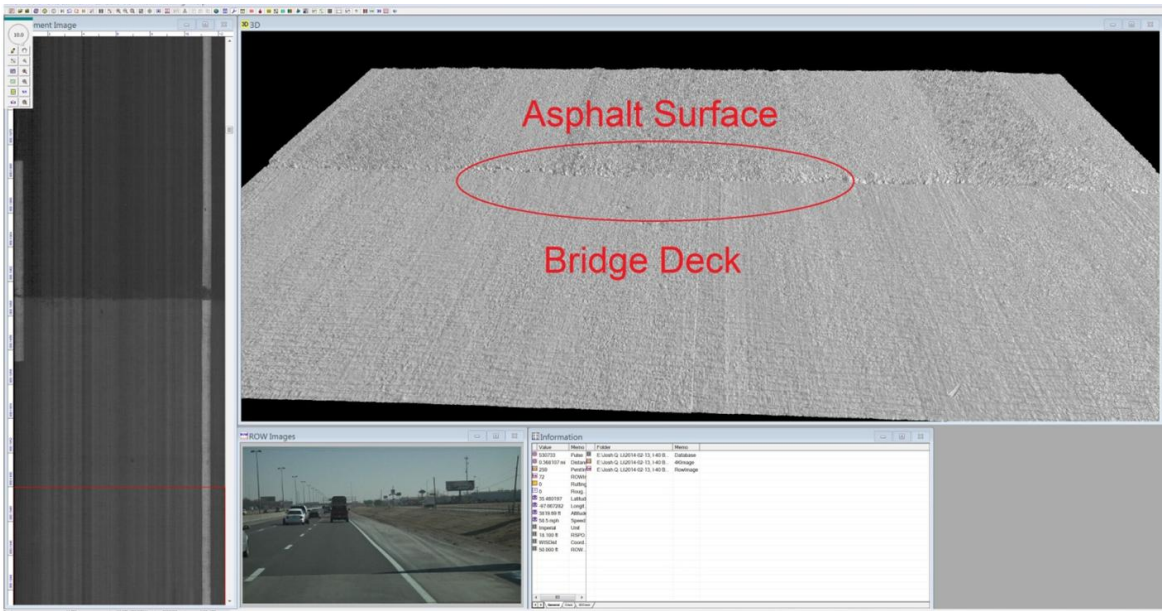

(b) Transition Area

Figure 7.29 1mm 3D Data with Distinctive Surface Characteristics

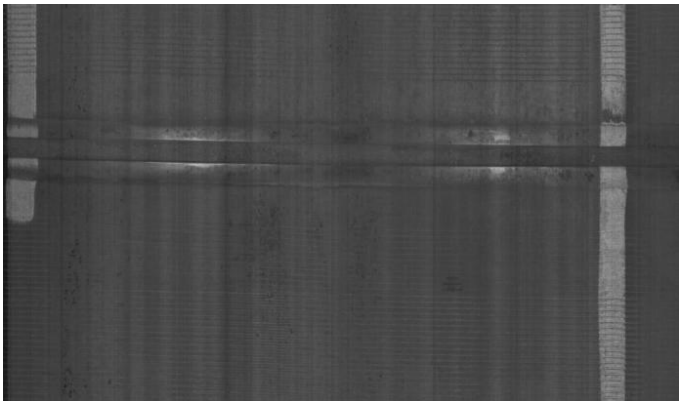

(a) 2D Image

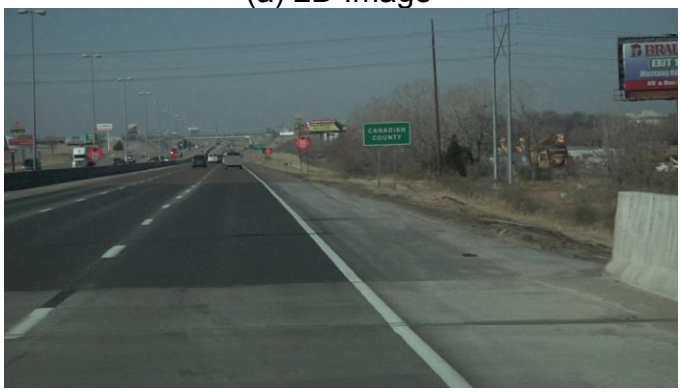

(b) ROW Image

Figure 7.30 2D and ROW Data

7.1.4.2 Boomer Creek Bridge

The 1mm 3D can also provide users with high resolution demonstration of many other objects. Drain hole, manhole, gutter hole, coring, spill of asphalt mixture on bridge deck, gutter spalling, and bumps at pavement bridge interface are demonstrated from Figure 7.31 to Figure 7.36.

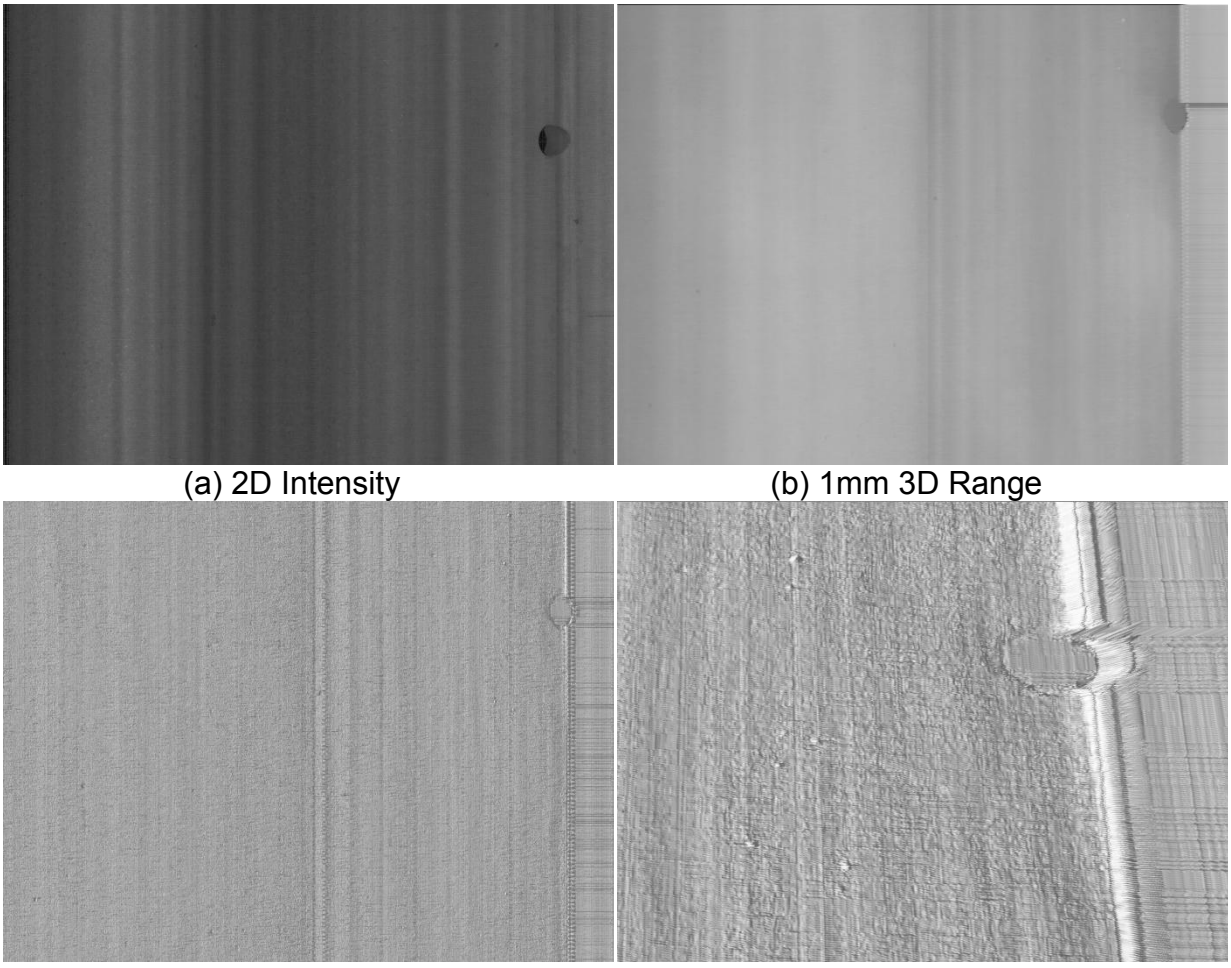

(a) 2D Intensity (b) 1mm 3D Range

(c) 1mm 3D Intensity (d) Rotated 1mm 3D Range

Figure 7.31 Drain Hole

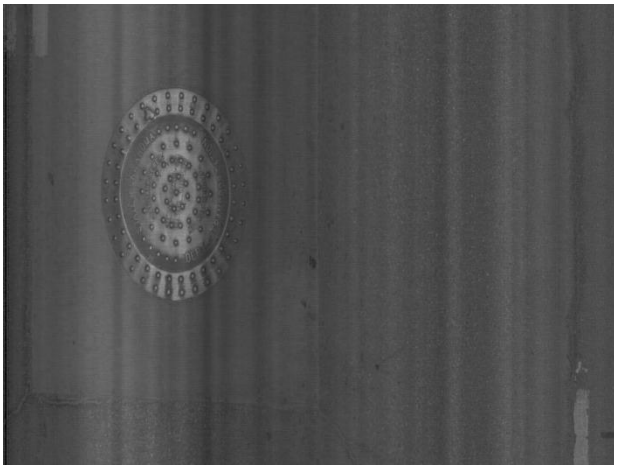

(a) 2D Intensity

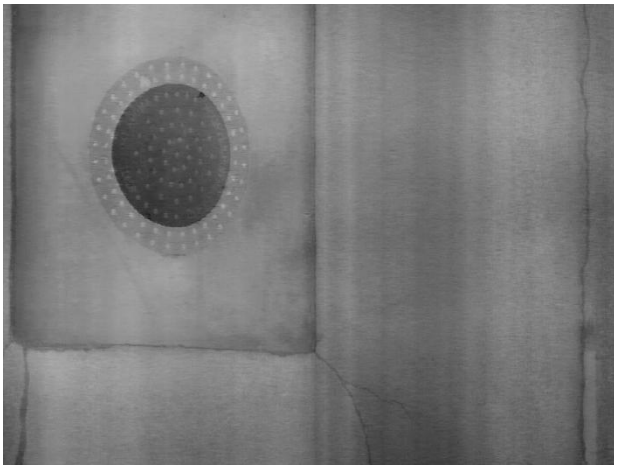

(b) 1mm 3D Range

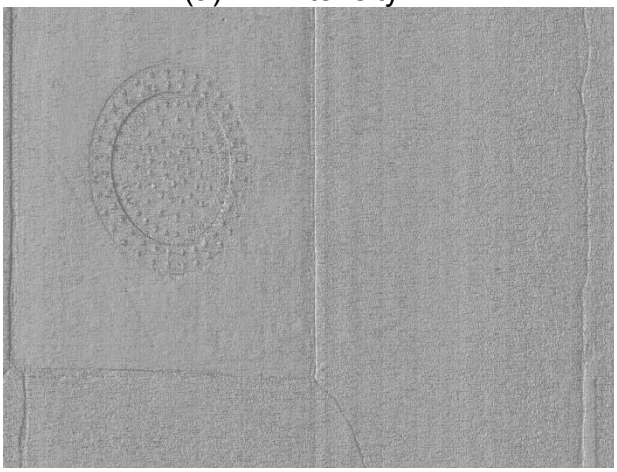

(c) 1mm 3D Intensity

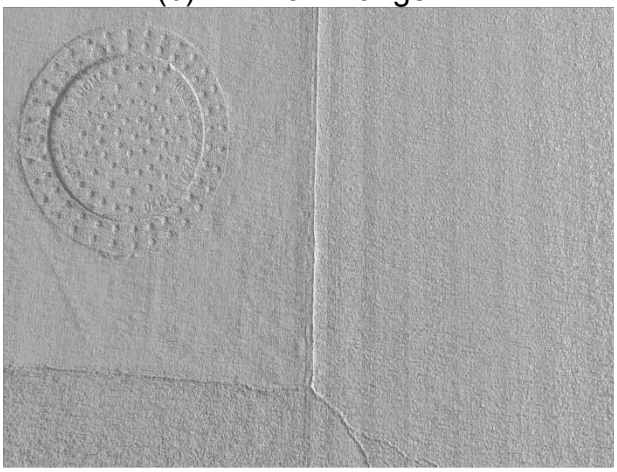

(d) Rotated 1mm 3D Range

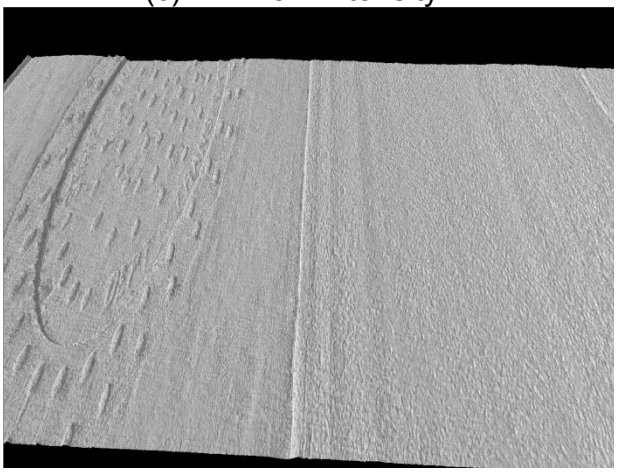

(e) 1/4 mm 3D Range (Before Correction)

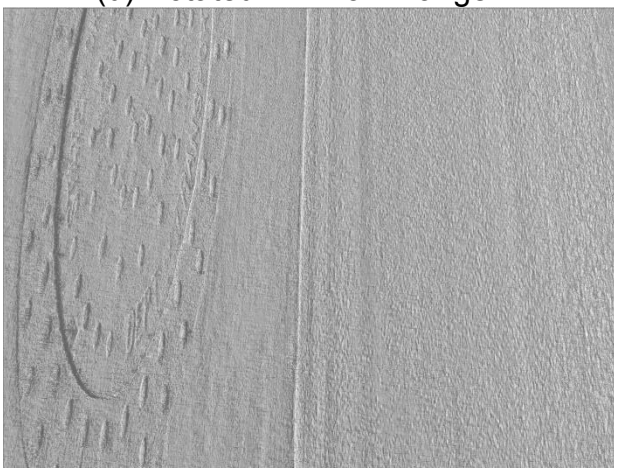

(f) Rotated 1/4 mm 3D Range (Before Correction)

Figure 7.32 Manhole

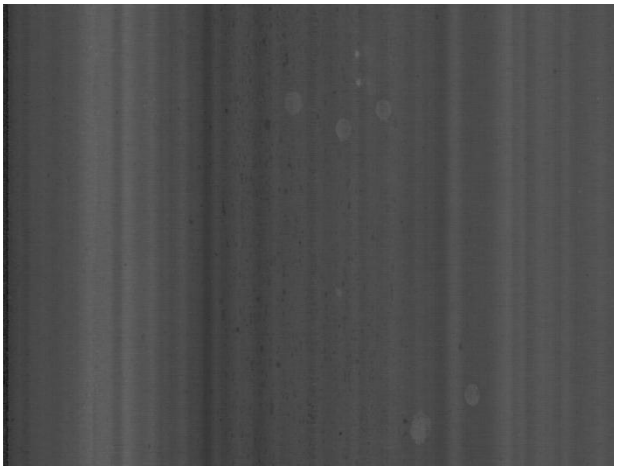

(a) 2D Intensity

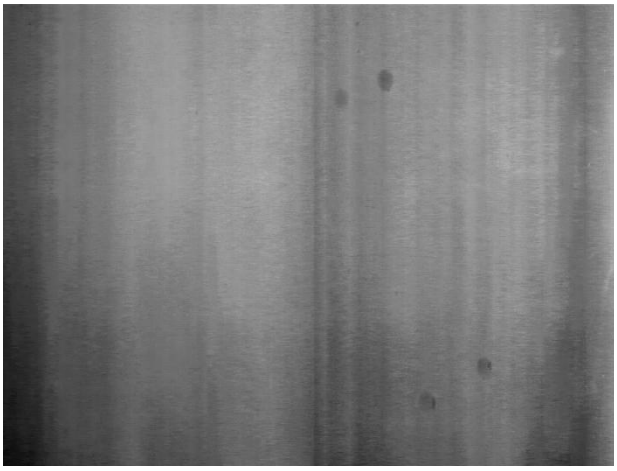

(b) 1mm 3D Range

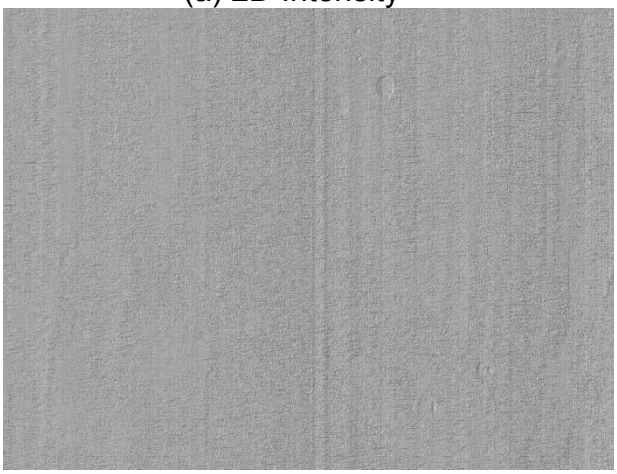

(c) 1mm 3D Intensity

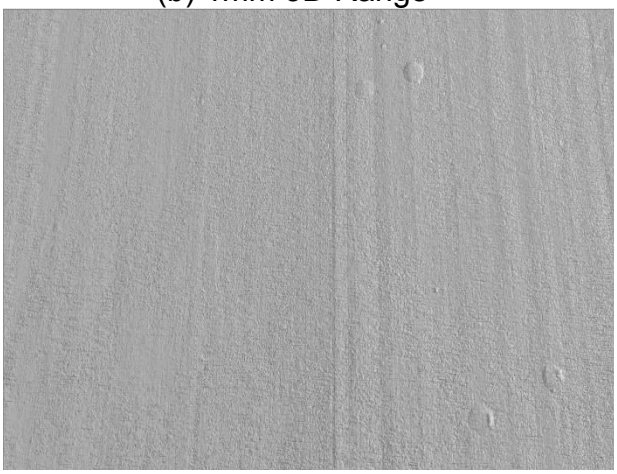

(d) Rotated 1mm 3D Range

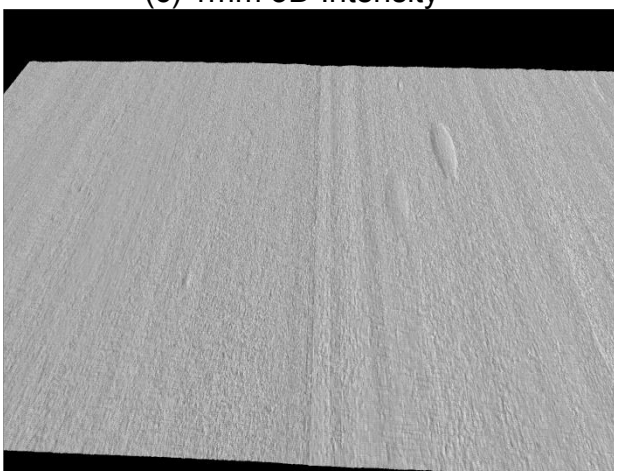

(e) 1/4 mm 3D Range (Before Correction)

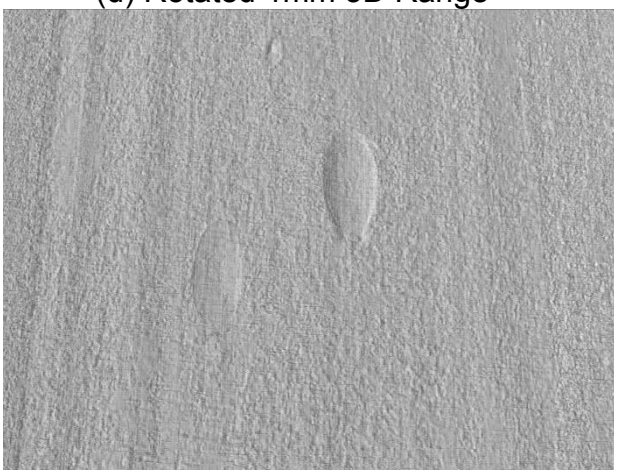

(f) Rotated 1/4 mm 3D Range (Before Correction)

Figure 7.33 Pavement Coring

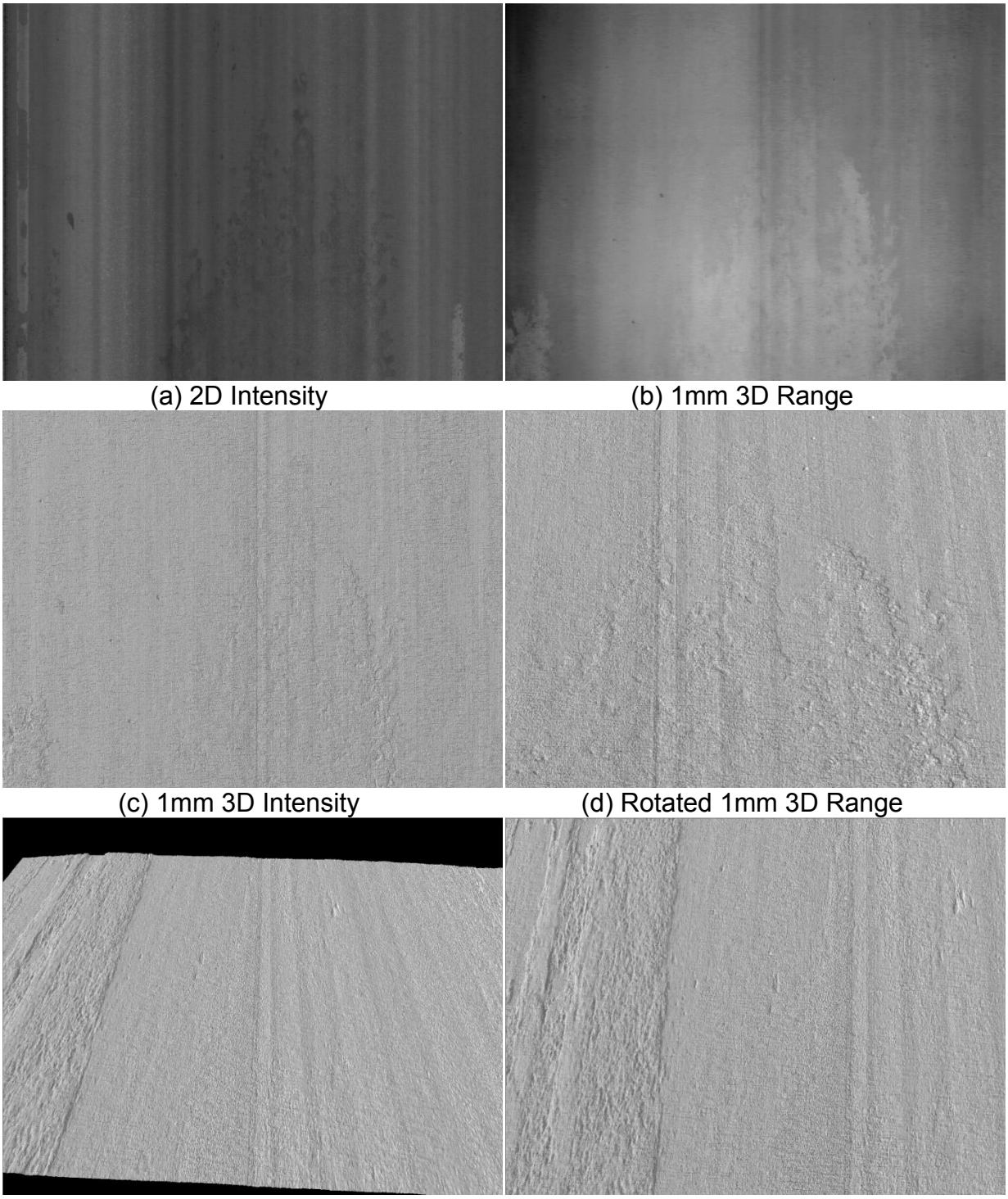

(a) 2D Intensity (b) 1mm 3D Range

(c) 1mm 3D Intensity (d) Rotated 1mm 3D Range

(e) 1/4 mm 3D Range (Before Correction) (f) Rotated 1/4 mm 3D Range (Before Correction)

Figure 7.34 Spill of Asphalt Mixture

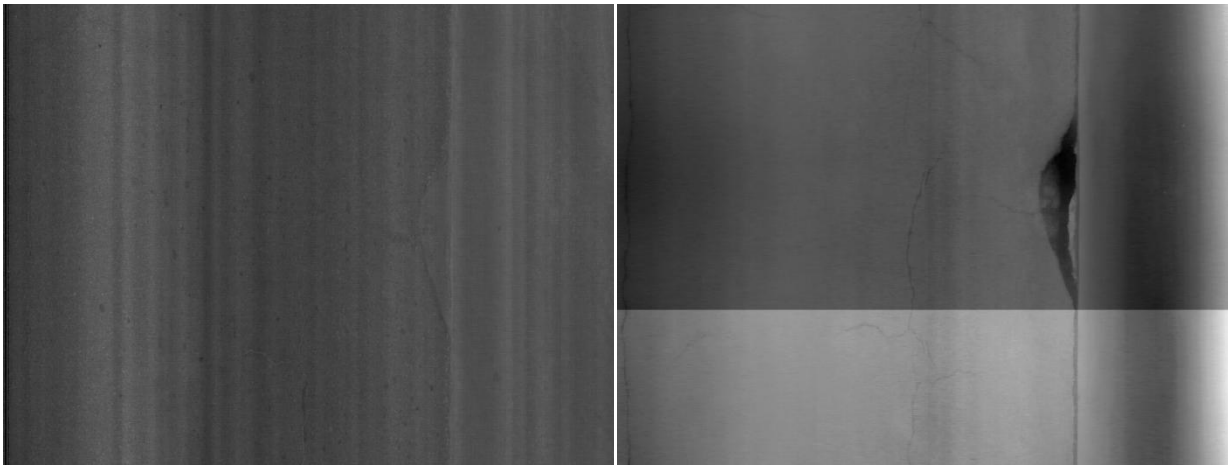

(a) 2D Intensity (b) 1mm 3D Range

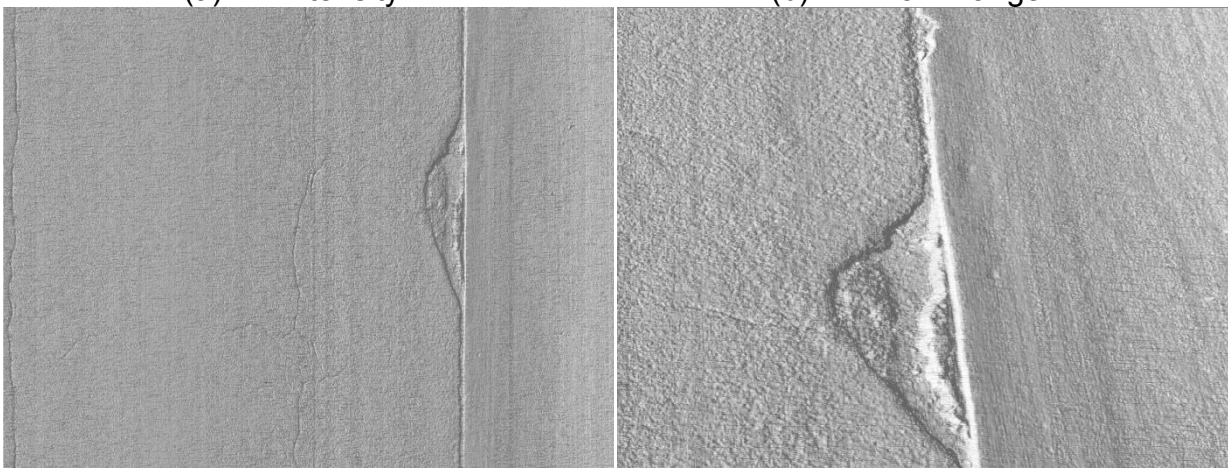

(c) 1mm 3D Intensity (d) Rotated 1mm 3D Range

Figure 7.35 Gutter Spalling

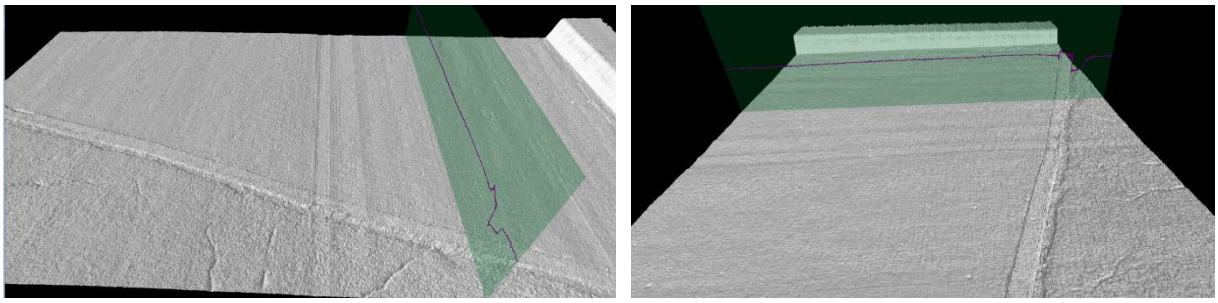

Figure 7.36 Pavement Bridge Interface Bump

It should be pointed out that the PaveVisino3D system was specifically modified to handle 0.25mm resolution in the longitudinal direction for the bridge survey for the first time. It is apparent from the visual demonstrations that the left

and right sensors were not aligned properly for 0.25mm data collection. In addition, due to the increased resolution in the longitudinal direction and no change in resolution for the transverse resolution, the 3D displays of bridge decks at 0.25mm resolution appears to be stretched in the longitudinal direction. Both issues will be resolved in later iterations of the sensors calibration and software modifications. However, it is also apparent from the visuals that 0.25mm resolution visuals present substantially higher definition that that of 1mm resolution visuals.

7.1.5 Pavement Roughness

7.1.5.1 North Canadian River Bridge

International Roughness Index (IRI) is widely used worldwide to evaluate pavement smoothness. Generally the testing pavement section has a smooth pavement surface condition with IRI values less than 90 in/mile in both directions, as shown in Table 7.2. The IRI values are reported every 50ft for the survey shown in Figure 7.37. The bridge deck is masked in a box window. The abrupt change of IRI is due to the expansion joints, or pavement transition segments.

Table 7.2 IRI of North Canadian River Bridge

Direction	IRI(in/mile)	
	Left Wheel Path	Right Wheel Path
East Bound	70.87	74.65
West Bound	71.94	74.90

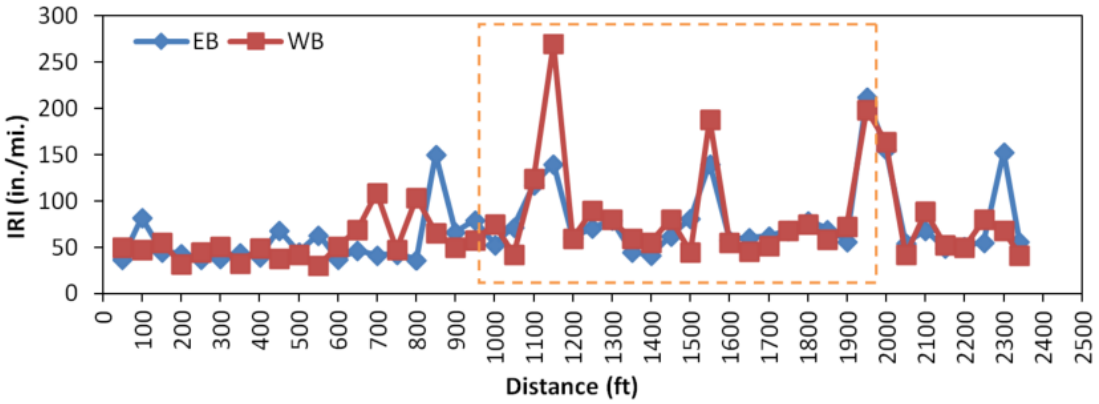

Figure 7.37 IRI of North Canadian River Bridge

7.1.5.2 Boomer Creek Bridge

The IRI values are reported every 50ft, as shown in Figure 7.38. The approximate bridge deck location is masked in a box window. The abrupt change of IRI is due to the expansion joints, or bump at pavement bridge interface. The average IRI values for each lane are summarized for the three pavement segments in Table 7.3. The IRI values on bridge decks are much higher than those on approaching and departing pavements. It is found that inner lanes have better pavement smoothness than the outer lanes.

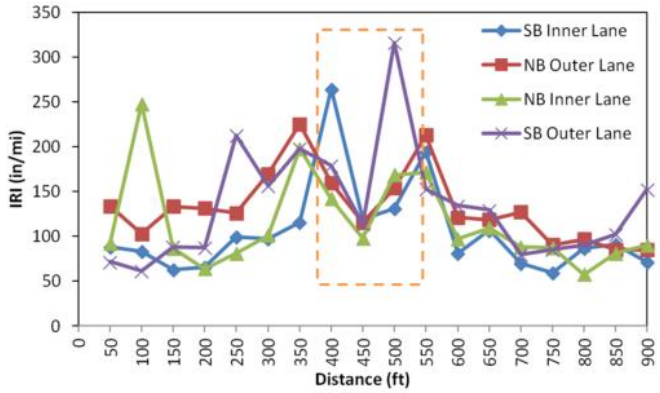

Figure 7.38 IRI of Boomer Creek Bridge

Table 7.3 IRI of Boomer Creek Bridge

Direction	Lane	Pavement Segments	IRI (in/mi)	Average IRI (in/mi)
SB	Outer	Approaching	113	134
		Bridge Deck	202	
		Departing	116	
	Inner	Approaching	83	105
		Bridge Deck	158	
		Departing	95	
NB	Outer	Approaching	133	133
		Bridge Deck	164	
		Departing	117	
	Inner	Approaching	112	115
		Bridge Deck	152	
		Departing	98	

7.1.6 Hydroplaning for Safety Evaluation

7.1.6.1 North Canadian River Bridge

For this analysis, rainfall intensity is assumed to 3 in/hr and Manning's n value is initially set to the 0.013 since this section is constructed with transverse tines. The cross slope and longitudinal grade are acquired from the IMU instrument mounted on the 3D Ultra vehicle, and the texture properties are calculated using the Estimated Mean Texture Depth (EMTD) based on the 3D texture data. The predicted hydroplaning speeds are shown in Figure 7.39 for both directions. The predicted hydroplaning speed is close to or higher than the 70 MPH speed limit. In other words, if drivers abide by the speed limit, hydroplaning risks during wet weather condition would not be considered on this pavement section.

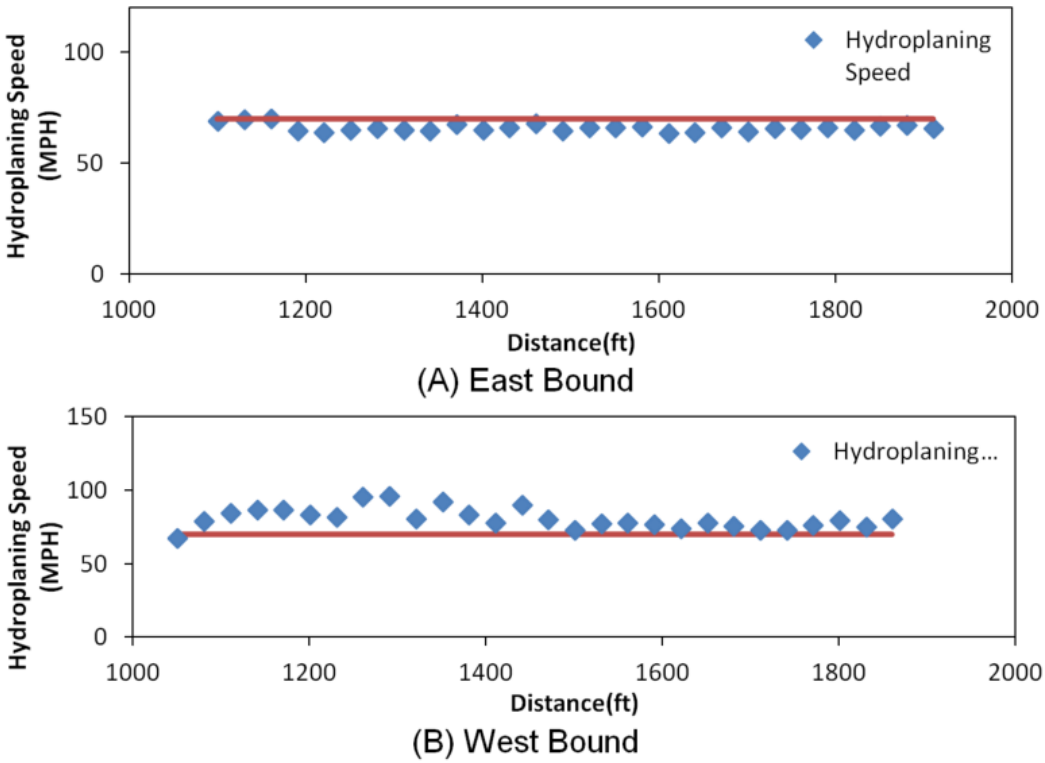

Figure 7.39 Hydroplaning Speeds for North Canadian River Bridge

7.1.6.2 Boomer Creek Bridge

The average predicted hydroplaning speeds for each lane are summarized for the three pavement segments in Table 7.4 and Figure 7.40. The predicted hydroplaning speeds are higher than the posted speed limit (35 MPH). In other words, if drivers abide by the speed limit, hydroplaning risks during wet weather condition would not occur on this pavement section. The predicted hydroplaning speeds on bridge decks are slightly lower than those on approaching and departing pavements.

Table 7.4 Hydroplaning Speeds for Boomer Creek Bridge

Direction	Lane	Segments	WFD (mm)	Hydroplaning Speed (mph)
SB	Outer	Approaching	0.99	60.51
		Bridge Deck	1.25	58.86
		Departing	1.14	60.01
	Inner	Approaching	1.28	63.04
		Bridge Deck	1.40	60.21
		Departing	1.60	63.99
NB	Outer	Approaching	0.95	62.02
		Bridge Deck	1.13	60.23
		Departing	1.02	63.32
	Inner	Approaching	1.35	70.52
		Bridge Deck	1.21	62.44
		Departing	1.31	70.15

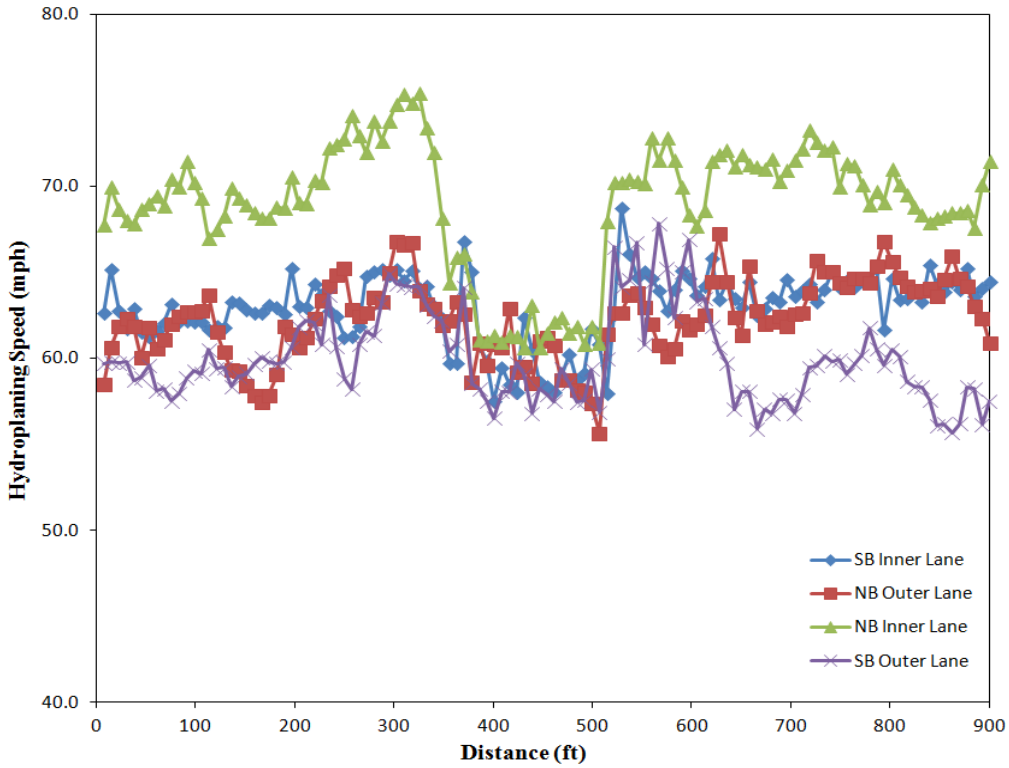

Figure 7.40 Predicted Hydroplaning Speeds for Boomer Creek Bridge

7.2 Pavement ME Design (DARWin-ME)

In Pavement ME Design (DARWin-ME), the following performance indicators for asphalt concrete pavement are predicted and monitored data are required for the local calibration process:

- **IRI**: IRI is derived from the simulation of a 'quarter-car" traveling along the longitudinal profile of the road and is calculated from the mean of the longitudinal profiles in each wheel path. In the Pavement ME Design, IRI is predicted empirically as a function of pavement distresses, site factors that represent the foundation's shrinklswell and frost heave capabilities, and an estimate of the IRI at the time of construction (the initial IRI). The pavement distress types that enter the IRI prediction are a function of the pavement or rehabilitation type under consideration. The unit of smoothness is inches per mile.
- **Alligator Cracking (Bottom-Up Cracking)**: Alligator cracks initially show up as multiple short, longitudinal or transverse cracks in the wheel path that become interconnected laterally with continued truck loadings. Alligator cracking is calculated as a percent of total lane area. The Pavement ME Design does not predict the severity of alligator cracking, but includes low, medium, and high in the definition.
- **Longitudinal Cracking (Top-Down Cracking)**: A form of fatigue or load related cracking that occurs within the wheel path and is defined as cracks parallel to the pavement centerline. The unit of longitudinal cracking

calculated by the Pavement ME Design is feet per mile. The Pavement ME Design does not predict severity of the longitudinal cracks, but includes low, medium, and high in the definition.

- **Reflective Cracking**: Fatigue cracks in HMA overlays of flexible pavements and of semi-rigid and composite pavements, plus transverse cracks that occur over transverse cracks and joints and cracks in jointed PCC pavements. The unit of reflective cracking is feet per mile. The MEPDG does not predict the severity of reflective cracks but includes low, medium, and high in the definition.
- **Rutting or Rut Depth**: A longitudinal surface depression in the wheel path resulting from plastic or permanent deformation in each pavement layer. The rut depth is representative of the maximum vertical difference in elevation between the transverse profile of the HMA surface and a wire-line across the lane width. The unit of rutting is inches (millimeters). The Pavement ME Design also computes the rut depths within the HMA, unbound aggregate layers, and foundation.
- **Transverse Cracking**: Non-wheel load related cracking that is predominately perpendicular to the pavement centerline and caused by low temperatures or thermal cycling. The unit of transverse cracking is feet per mile or spacing of transverse cracks in feet. The MEPDG does not predict the severity of transverse cracks but includes low, medium, and high in the definition.

It can be seen that PaveVision3D can provide most majority of the data that are required in the Pavement ME Design. IRI and rut depth in the wheel-path, longitudinal, transverse, and pattern cracking in both non-wheel-path and wheel-path are produced. During the process of local calibration of the Pavement ME Design, PaveVision3D data can be used as the major data collection sources with the following observations:

- IRI data from PaveVision3D Ultra system can be directly used for the local calibration of Pavement ME Design.
- Since PaveVision3D Ultra cannot differentiate where the cracks initiated, it is recommended that the local calibration refinement be confined to total cracking that combines alligator and longitudinal cracks in the wheel-path. As recommended in the AASHTO Local Calibration Guide (AASHTO 2012), to combine percent total lane area fatigue cracks with linear or longitudinal fatigue cracks, the total length of longitudinal cracks should be multiplied by 1-foot and that area divided by the total lane area. When combining alligator and longitudinal cracks, the alligator transfer function should be the one used in the local calibration process for determining the local calibration values.
- Because PaveVision3D Ultra data cannot confirm reflective cracks, it is recommended that the local calibration refinement be confined to total cracking of HMA overlays. In this case, all surface cracks in the wheel path (reflective, alligator, and longitudinal cracks) should be combined. If

all cracks are combined, the alligator and reflection cracking transfer functions can be used in the local calibration process.

- Because PaveVision3D Ultra system only collects total rut depth on pavement surface, it is recommended that the calibration refinement be confined to the total rut depth predicted with the Pavement ME Design.

7.3 Highway Performance Monitoring Systems (HPMS)

The HPMS process is designed to be a cooperative effort between the States and FHWA. State Highway Agencies are primarily responsible for collecting the HPMS data and providing the following types of data to FHWA: Full Extent, Sample Panel, Summary, Estimates, and Metadata (FHWA 2010).

Within the context of the HPMS system, some data elements must be reported for their Full Extent (i.e. system-wide). The Full Extent network consists of the National Highway System (NHS) routes (including intermodal connectors) and all other roads, excluding those functionally classified as minor collectors in rural areas and local roads in any area. Within the extent of all Federal-aid eligible roads, a random selection of roadway sections is used to represent various attributes at a system-wide level for the purposes of assessing the performance and condition of the network. This process helps to reduce any burden that may be imposed on the States to perform data collection to meet their HPMS reporting requirements. These sections of the network are referred to as Sample Panel sections. Moreover, the Sample Panel sections are selected randomly and are intended to give a statistically valid representation of the State's road network. Due to the structure of the HPMS

data model, the States are not required to extract the Sample Panel data items, as long as the data in their submittal covers the Sample Panel. States are encouraged to submit their entire dataset for each data item.

The data items listed in Table 7.5 are to be submitted by the States as part of the Sections dataset, which will be stored as a table in within FHWA's database:

- **Item Number** is the number assigned to each data item;
- **Data Item** identifies the type of attribute data to be reported;
- **Extent** indicates if the data item is required for the Full Extent (FE), Sample Panel (SP) sections, or the Full Extent and Ramp sections (FE+R).

Table 7.5 Pavement Data Items in HPMS (FHWA 2010)

Data Item Type	Item Number	Data Item	Extent	
Pavement	47	International Roughness Index (IRI)	FE*	SP*
	48	Present Serviceability Rating (PSR)		SP*
	49	Surface Type		SP
	50	Rutting		SP
	51	Faulting		SP
	52	Cracking Percent		SP
	53	Cracking Length		SP
	54	Year of Last Improvement		SP
	55	Year of Last Construction		SP
	56	Last Overlay Thickness		SP
	57	Thickness Rigid		SP
	58	Thickness Flexible		SP
	59	Base Type		SP
	60	Base Thickness		SP
	61	Climate Zone		SP
	62	Soil Type		SP
FE = Full Extent for all functional systems (including State and non-State roadways); FE* = Full Extent for some functional systems; SP = Sample Panel Sections; SP* = Some Sample Panel Sections.				

Based on the HPMS data requirements for pavement, PaveVision3D Ultra data collection can be used to prepare data items 47 (IRI), 50 (rutting), 51 (faulting), 52 (crack percentage), 53 (crack length) at full extent. Since PaveVision3D analyzing software, ADA-3D, can generate indicator values for HPMS sample segments based on users input beginning and ending locations, the following observations are made when using PaveVision3D data to meet the HPMS reporting requirements:

- **Item 47**: IRI data from the PaveVision3D Ultra can be directly used for HPMS reporting.
- **Item 50**: Rut depth data rounded to the nearest 0.1 inch from the PaveVision3D Ultra can be directly used for HPMS reporting.
- **Item 51**: PaveVision3D Ultra can measure faulting for each joint between adjacent jointed concrete panels in the direction of travel. The average of faulting values can be used for HPMS reporting.
- **Item 52**: percent area with fatigue type cracking for all severity levels for AC pavements (in wheel path) and percent of slabs with cracking for PCC (jointed and continuous) pavements calculated from PaveVision3D Ultra data can be used to report Crack Percent for HPMS.
- **Item 53**: relative length in feet per mile (ft/mi) of transverse cracking for AC pavements and reflection transverse cracking for composite pavements calculated from PaveVision3D Ultra data can be used to report Crack Length for HPMS.

CHAPTER 8 CONCLUSIONS AND RECOMMENDATIONS

8.1 Conclusions

This project provides rapid survey using PaveVision3D Ultra for approximately 1,280 lane miles of ODOT interstate highways (I-35 and I-40) and SH-51 from I-35 to Sand Springs. With sophisticated ADA software interface, the collected 1mm 3D data can provide highway agencies with automated evaluation of pavement surface including cracking, rutting, roughness, and hydroplaning speed for safety analysis. Particularly, the following tasks have been completed:

- Used PaveVision3D Ultra to collect geographically true and complete pavement surfaces or virtual pavement surfaces with IMU at 1mm resolution for the ODOT interstate network and SH 51 from I-35 to Sand Springs (about 70 centerline miles) at highway speed;
- Using ADA computer software, calculated pavement surface cracking, rutting, roughness in term of IRI, and predicted hydroplaning speed for each 0.1-mile section based on 1mm 3D texture data continuously collected at high speeds using the 3D Ultra technology and cross slope and longitudinal grade from the IMU system;
- Implemented the PELT method to identify change points and dynamically determine homogeneous segments so as to assist DOT effectively using the available 1mm 3D pavement surface data to optimize pavement management decision-making;

- Tested the 1mm 3D technology for automated bridge deck evaluation on two bridges to identify various joint problems, bridge deck surface defects;
- Identified the potential application of 1mm 3D data to meet the needs for Pavement ME Design and HPMS reporting.

8.2 Recommendations

The application of 3D 1mm laser imaging technology for network survey is unprecedented. This innovative technology allows highway agencies to access its options in using the 1mm 3D system and the collected data sets for various design and management purposes.

8.2.1 Pavement Management System (PMS)

Through the project, ODOT have gained experience in applying the latest 3D laser imaging technologies for ODOT pavement network to collect consistent, accurate, and repeatable pavement cracking data for pavement management purposes. PMS is a data driven process that requires high quality cracking, rutting, IRI, and other data to develop rigorous deterioration models for decision making. The new 3D laser imaging technology has been proved to be a vehicle to fulfill the requirements.

8.2.2 Bridge Deck Evaluation

The collected data and analyses can be used to assist bridge engineers in better evaluating bridge deck conditions at a significantly more efficient way without requiring field visit to each individual bridge. The potential to develop a work flow from data collection to producing data for ODOT bridge deck survey forms is also clear. Further efforts are recommended to develop such work flow to minimize field trips for manual surveys and improve staff operational safety at ODOT. In addition, more research is expected to develop customized software to automatically process and report bridge deck data and to establish virtual bridge decks.

8.2.3 Pavement ME Design

Data availability and data quality are two critical implementation hurdles for ODOT, as well as for many other DOTs in their recent efforts in studying Pavement ME Design. The inconsistency of the distress data trend and the low distress values observed on the majority of ODOT highway hinders the comparisons of field monitoring results and Pavement ME Design predictions to be statistically meaningful. The 1mm 3D technology provide the ideal solution to gather time-series distress data with high data quality and at precise location reference for the local calibration and implementation of Pavement ME Design.

8.2.4 Highway Performance Monitoring System (HPMS)

The 2010 version of HPMS requires state agencies to report several important performance data at their "Full Extent" for the purposes of assessing the performance and condition of national highway network. PaveVision3D Ultra data collection can be used to help reduce any burden that may be imposed on ODOT to

perform data collection to meet the new HPMS reporting requirements. IRI, rutting, faulting, cracking (percentage and length) that are included in HPMS can be automatically generated for HPMS reporting.

8.2.5 Pavement Safety Evaluation

The measurement of pavement surface characteristics for safety analysis is a direct application of 3D laser images as the 3D data can represent actual or virtual pavement surfaces with full-lane coverage. This project has established a framework using predicted hydroplaning speed to evaluate pavement surface safety, which will assist ODOT safety engineers in diagnosing and solving safety problems at "black" spots in Oklahoma.

In addition, it has been shown that approximately one quarter of highway fatalities in the United States occur at or near horizontal curves. Contributing factors to these run-off-the-road crashes include excessive vehicle speed, distracted driving, and driver error. At some locations, the deterioration of pavement surface friction may also be a factor, particularly during wet weather. The PaveVision3D technology is able to identify those sites that have deficient surface friction and unsatisfied hydroplaning speed. In an effort to reduce the deaths and injuries that occur along these horizontal curves, the Federal Highway Administration Office of Pavement Technology has initiated the Surface Enhancements At Horizontal Curves (SEAHC) program for the installation and demonstration of friction enhancing treatments at numerous horizontal curves. This technology can help evaluate the effectiveness of the installation of SEAHC surfaces.

REFERENCES

AASHTO (1986). Guide for Design of Pavement Structures. Technical Report, Washington, D.C..

AASHTO (2010). *Guide for the Local Calibration of the Mechanistic-Empirical Pavement Design Guide*. American Association of State Highway and Transportation Officials, Washington, D. C.

AASTHO. (2013a). *Quantifying cracks in asphalt pavement surfaces from collected images utilizing automated methods*. AASHTO Designation PP67-10. Washington, D. C.

AASTHO. (2013b). *Standard practice for determining pavement deformation parameters and cross slope from collected transverse profiles*. AASHTO Designation: PP69-10. American Association of State Highway and Transportation Officials. Washington, D. C.

AASHTO (2013c). *Collecting images of pavement surfaces for distress detection*. AASHTO Designation PP68-10. American Association of State Highway and Transportation Officials. Washington, D. C.

ASTM (2005). Measuring Pavement Macrotexture Properties Using the Circular Track Meter, ASTM E 2157-01.

ASTM (2006). *Measuring Pavement Macrotexture Depth Using a Volumetric Technique*. ASTM E 965-96.

ASTM Standard Practice, (2008). *Standard Practice for Computing International Roughness Index of Roads from Longitudinal Profile Measurements.* ASTM Designation: E 1926-08, ASTM International.

ASTM (2009). *Measuring Pavement Texture Drainage Using an Outflow*. ASTM E 2380-05.

ASTM Standard Practice, (2012). *Standard Terminology Relating to Vehicle-Pavement Systems.* ASTM Designation: E 867-06, ASTM International.

Auger, I. E. and Lawrence, C. E. (1989). Algorithms for the optimal identification of segment neighborhoods. *Bulletin of Mathematical Biology*, 51 (1), pp:39–54.

Burtch, Robert (2002), LIDAR Principles and Applications, presentation at the *2002 IMAGIN Conference*, Traverse City, MI

Chesterton John, Noel Nancekivell, Noel Tunnicliffe (2006). *The use of the Gallaway Formula for Aquaplaning Evaluation in New Zealand*. Transportation and the Pursuit of Excellence NZIHT & Transit NZ 8th Annual Conference.

FHWA (2010). Highway Performance Monitoring System (HPMS). Federal Highway Administration, U.S. Department of Transportation, Washington, D. C.

Gallaway, B. M., et. Al. (1979). *Pavement and Geometric Design Criteria for Minimizing Hydroplaning*. Report No. FHWA-RD-79-31. Federal Highway

Herr B. (2001). Calibration and Operation of Pavement Profile Scanners, *RPUG*, Lake Tahoe, Nevada.

Herr B. (2009). PSI Current Technology Overview, white paper.

Killick, R., Fearnhead, P., and Eckley, I. A. (2012) Optimal detection of changepoints with a linear computational cost. *JASA*, 107(500), pp:1590 – 1598.

Kumar S.Santosh, Kumar Anupam, and T.F. FWA (2009). Analyzing effect of tire groove patterns on hydroplaning speed. *Journal of the Eastern Asian Society for Transportation Studies*, Vol. 8.

McGhee, K.H. (2004). NCHRP Synthesis 334: *Automated Pavement Distress Collection Techniques: A synthesis of highway practice*. Transpiration Research Board, Washington, D.C.

Sayers, M. and Karamihas, S., (1998). *The Little Book of Profiling*. University of Michigan, Ann Arbor,1998.

Simpson, A. (2001). *Characterization of Transverse Profiles*. FHWA-RD-01-024. Fugro-BRE, Inc. Austin, TX.

Scott, A. J. and Knott, M. (1974) A cluster analysis method for grouping means in the analysis of variance. *Biometrics*, 30(3), pp:507–512.

Thomas Fridtjof (2003). Statistical Approach to Road Segmentation. *Journal of Transportation Engineering*, Vol. 129, No. 3, pp: 300-308.

Wang K.C.P. (2004). *Automated Pavement Distress Survey through Stereovision*, NCHRP-IDEA Program Project Final Report, Washington, D.C.

Wang Kelvin C.P. (2011a). Automated Survey of Pavement Distress based on 2D and 3D Laser Images. Report for MBTC DOT 3023, Fayetteville Arkansas.

Wang Kelvin C. P. (2011b). Elements of Automated Survey of Pavements and a 3D Methodology. *Journal of Modern Transportation*, Volume 19, Number 1, pp: 51-57.

Wang K. C. P., Luo Wenting, Lin Li, Qiang Li (2014). Surface Drainage Evaluation for Rigid Pavements Using IMU and 1mm 3D Texture Data. In *Transportation*

Research Record: Journal of the Transportation Research Board (In Press), TRB, National Research Council, Washington, D.C.

Zhang Allen, Kelvin C.P. Wang, Ran Ji, and Qiang Joshua Li (2014). Improved Pavement Cracking Algorithms with 1mm 3D Pavement Surface and Their Performance Measures. Submitted to the Journal of *Computer-Aided Civil and Infrastructure Engineering* for publication consideration, John Wiley & Sons, Inc.

APPENDICIES DETAILED PAVEMENT SURFACE CHARACTERISTICS

In total there are 6 appendices for each of the six roadways (three highways in two directions). In each appendix, route description and detailed surface characteristics including IRI, rutting, fatigue cracking, and predicted hydroplaning speed for each roadway are provided.

Summary of Six Roadways in Appendices

Appendix	Roadway	# Sections (AC & PCC)	Total Length (Miles)
A	I-35 North Bound	15	236.2
B	I-35 South Bound	17	238.6
C	I-40 East Bound	23	333.6
D	I-40 West Bound	20	333.8
E	US-51 East Bound	3	70.9
F	US-51 West Bound	5	71.0